UNIVERSITY KASDI MERBAH-OUARGLA

FACULTY OF MATHEMATICS AND MATTER SCIENCES

DEPARTMENT OF PHYSICS

Order N^o :

Serial N^o :

THESIS OF DOCTORATE

MAJOR: THEORTICAL PHYSICS

By:

MALKI ZOUHIDA

Theoretical Study Of Physical Phenomena Around A ProtoPlanetary Disk

Discussed on: 10 / 01 / 2024

President :	Smail Chihi	Prof	Univ. Ouargla
Examiner :	Said Douis	Prof	Univ. Ouargla
Examiner :	Zineb Korichi	MCA	ENS.Ouargla
Examiner :	Mosbah Difallah	Prof	Univ.El-Oued
Supervisor :	M. T. Meftah	Prof	Univ. Ouargla
Co-supervisor :	E. B. Belghitar	MCA	Univ. Ouargla

2023/2024

Dedications

To my father and dearest mother.

To all my brothers and sisters and as well as my family and friends.

To who makes me smile.

To who gives me courage and helps me to follow my wishes despite the difficulties.

To all my teachers from primary school to the end of this thesis.

To everyone who helped us in completing this work, even if only with advice.

Thank you!

Malki zouhida

Acknowledgements

This research was done at "Kasdi Merbah Ourgla University, Department of Physics, Faculty of Mathematics and Material Sciences", It was a great honor for me to have the chance to complete this thesis in the LRPPS (Laboratory of Radiation and Plasmas and Surface Physics). In the few lines that follow, I would like to thank everyone who has contributed, directly or indirectly, to the completion of this thesis.

First of all, I thank my God for his clemency and mercy, for having given me the strength, the courage, the will and the patience to be able to carry out this modest work.

I would first like to thank Mr. "Mestah, MT", Professor at the University of Kasdi Merbah in Ouargla, who did me the honor of superrising this dissertation, accompanied me in the preparation of this work with great diligence as well as remarkable human qualities, and whose daily presence was a major asset for the realization of this work, both scientifically and morally. I would also like to thank him for the trust and understanding he has always shown towards me. If this work is completed, it is thanks to his help and support. May he be assured of my deep esteem and may he find here the expression of my deep gratitude.

I would especially like to extend my sincere gratitude to Mr. Belghitar, E.B. at the University of Ouargla for his attentive monitoring of my work with calm, his scientific rigor, all of which helped me develop this thesis.

I'd like to thank the examiners, each in his or her own name, for agreeing to look over this work. I am very proud of their jury participation.

Thanks to all my friends both inside and outside of Kasdi Merbah University, as well as all of my colleagues and university employees, particularly teachers. I'd like to thank everyone who has assisted us on our academic journey, particularly our fathers, mothers, siblings, and everyone who has guided and accompanied me over the last few years.

Thank you all!

Malki zouhida

Table of contents

List of Figures

List of Tables

Liste of abbrevations

Abbreviation	Description
AGN	Active galactic nuclei / nucleus
BH	Black hole
CV	Cataclysmic variable
DN(e)	Dwarf nova(e)
HMXB	High-mass X-ray binary
LMXB	Low-mass X-ray binary
MRI	Magneto-Rotational Instability
NS	Neutron Star
RIAF	Radiatively inefficient accretion flow
RLOF	Roche lobe overflow
SED	Spectral energy distribution
SMBH	Supermassive black hole
WD	White dwarf
XRB	X-ray binary
YSO	Young stellar object
DIM	Disk instability model
HAEBE	Herbig Ae/Be stars
TTS	T Tauri Stars
ADAF	Advection dominated accretion flow
GRB	Gamma ray bursts
PPD	Proto-Planetary disk
AU	Astronomical unit
Jy	Jansky (unit of flux density)
μ m	Micrometer, or micron (10^6 meters)
MMSN	Minimum Mass Solar Nebula
Myr	Million years
PMS	Pre-main-sequence
RD	Rotation diagram
VLT	Very Large Telescope
QSO	Quasa-stellar object / Quasar

Physical Constants (SI)

Boltzmann constant	$K_B = 1.38064852 \times 10^{-23}\ \mathrm{m^2 \cdot kg \cdot S^{-2} \cdot k^{-1}}$
Stefan-Boltzmann constant	$\sigma_{\mathrm{SB}} = 5.6703 \times 10^{-8}\ \mathrm{W \cdot m^{-2} \cdot k^{-4}}$
Gravitational constant	$G = 6.67384 \times 10^{-11}\ \mathrm{m^3 \cdot kg^{-1} \cdot S^{-2}}$
Solar mass	$M_\odot = 1.988435 \times 10^{30}\ \mathrm{kg}$
Solar radius	$R_\odot = 6.96 \times 10^{8}\ \mathrm{m}$
Astronomical unit	$\mathrm{Au} = 149.5978 \times 10^{9}\ \mathrm{m}$

Physical Quantities

ΔE	kinetic energy
G	gravitational constant
M	central objects mass
M_{BH}	mass black hole
r	radius, distance from the center
e	dissipated energy/internal energy
P	pressure
T	temperature of the gas
ρ	density
$\mathrm{c_s}$	speed of sound
τ_{visc}	viscous/secular time scale
τ_{acc}	accreting time scale
$\mathrm{v_k}$	keplerian orbital velocity
$\mathrm{v_r}$	radial or ‚drift"velocity
$\mathrm{v_{out}}$	velocity of outflow
Ω_{k}	keplerian angular velocity
Ω	angular velocity
$\dot{\mathrm{M}}$	accretion rate
$\mathrm{M_E}$	eddington accretion rate
F	radiative flux

L_E	eddington luminosity
L_{LB}	boundary layer luminosity
c	speed of light
(r, φ, z)	cylindrical polar coordinates
H(r)	scale height, disks thickness
η_{eff}	efficiency of gravitational energy release
v	velocity
Σ	surface density
v	turbulent viscosity
σ	cross-section
α	α-parameter
q^+	viscous dissipation rate
q^-	radiative loss rate
σ_{SB}	stefan-Boltzmann's constant
σ_{ff}	opacity determined by free-free absorption
σ_T	opacity determined by electron scatterin
F	energy/heat flux
$r*$	stellar radius
r_{out}	outer radius
k	boltzmann's constant
r_i	inner radius of the disk
κ	scattering/absorbing surface area or opacity
$\varphi_R(r)$	roche potential

Abstract

Accretion is one of the mechanisms mainly responsible for the emergence of most things in the universe. Almost all astronomical objects, from planets and stars to entire galaxies, were formed through this process. In general, accreting matter forms a disk around a central object due to the conservation of the materials angular momentum. The first goal of this work is to study accretion disks, mainly protoplanetary disks, because they allow studying a large number of physical processes that determine their development, and they also develop due to viscosity and the transfer of angular momentum by the central star. The second major goal is to provide analytical solutions to the equation for the evolution of a protoplanetary disk and a planet, as well as to understand the effect of angular momentum on surface density distribution without utilizing approximations. Based on the basic equations that govern the temporal evolution of the surface density of the accretion disk, as well as the equation of the co-evolution of the planet and the protoplanetary disk resulting from planet migration due to the interaction of the tides with the disk, the disk is also subject to the planet's tidal torque. The second part of this equation represents the rate at which angular momentum per unit mass is transferred from the planet to the disk. By applying conditions and approximations that determine the surface density behavior more clearly in the two methods in each region, we obtain analytical solutions to the equation for the evolution of a protoplanetary disk and a planet, and the results were consistent with previous results.

Keywords: accretion, protoplanetary disk, surface density, angular momentum.

General Introduction

General introduction

The progressive discovery of the Solar System and the diversity of the planets that compose it has made it possible to place the Earth in a somewhat broader context. The question of the formation of the planets then arose. Noting the quasi-coplanarity of the orbits of the Solar system, Kant (1755) then Laplace (1796) introduced the concept of the primitive solar nebula, the disk of matter from which the planets originated (Boué, G 2010). In the 1940s, the accretion disk paradigm was introduced by (kuiper 1941) , noting that mass transfer between two binary stars in contact could form a "ring" of matter around the accreting star. Subsequently, the concept was taken up and extended by (Prendergast and Burbidge 1968) to explain the characteristics of the binary X Cyg X2 and by (Lynden-Bell 1969) to justify the high luminosity of active galactic nuclei (AGNs). The basic idea of accretion disks was proposed soon after the confirmation of quasars, and its classical picture established at the beginning of the 1970s (Montesinos, M 2012)(Giovannelli, F., & Sabau-Graziati, L 2016). One of the early models considered for compact X-rays sources using accretion disks was due to (Pringle & Rees 1972). The accretion disk model grew in popularity and began to be recognized as the theory capable to describe important energetic emissions observed in the Universe (Alecian, E 2013).

Accretion disks are the generic structures associated with compact objects (considered to be black holes, Neutron stars, white dwarfs) powered by matter accretion onto them (Kazanas, D 2019). The angular momentum of gravitationally-interacting matter forms a centrifugal barrier to the infall of that matter on to its center of mass. For gaseous matter this barrier is believed to give rise to a gravitationally-bound disk structure. If the gas continues to evolve by radiating its angular momentum and falling on to the center of mass, the system is called an accretion disk (Mamatsashvili, G 2009). The accretion disk is a central element to theories of star formation, interacting binaries, and Active Galactic Nuclei (AGN). In star formation, the accretion disk is an intermediate stage between the initial condensation of a diffuse cloud and a fully evolved solar system such as our own. In interacting binaries the transfer of matter from one object to the other is governed by the rate of infall from the accretion disk which is invariably formed. The disk is therefore dynamically important to systems such as Cataclysmic Variables, Type I supernovae and the x-ray luminosity of Black Holes (Giovannelli, F., & Sabau-Graziati, L 2016).

In astrophysics the term accretion is used to describe the process of acquiring matter, typically gaseous, by a massive body (Narayan, R., & Quataert, E. 2005). As a result of the

infall, the gravitational energy is extracted. Its amount is roughly proportional to the ratio of the mass and radius of the attracting object: M/R. It is clear that the more massive and compact the object is, the larger amount of energy may be released. Accretion onto compact objects is therefore an extremely important process in the astrophysical context, as it transforms the gravitational energy into radiation in many of the most luminous classes of objects in the universe (Sadowski, A 2011).

The spherically symmetric (zero angular momentum) accretion on a gravitating body is the simplest case one can imagine. It was first studied by Bondi (1952) and is called the Bondi accretion. It was shown that the solution describing such a process is unique and that the ow becomes transonic crossing the critical (sonic) radius. It is currently accepted that Bondi-type of accretion hardly occurs in the Universe because all potential sources of accreting matter (e.g., gas clouds or stars) have non-zero angular momentum (Sadowski, A. 2011).

Accretion disks appear in many astrophysical objects. Protostellar clouds of molecular gas create protoplanetary disks surrounding newly formed stars. Stars in close compact binary systems transfer mass through accretion disks when they fill their Roche lobe or due to strong stellar winds. Supermassive BHs in AGNs are believed to accrete cold matter from their vicinity. According to the collapsar model, short γ-ray bursts accrete the ejecta at super-critical rates shortly after the outbursts. Other examples of accretion disks in the Universe may also be given. Accretion appears to be involved in most of the high-luminosity phenomena in the universe (Sadowski, A. 2011).

Protoplanetary disks form through the gravitational collapse of their parental molecular cloud cores in a process regulated by the balance of gravitational, magnetic, gas pressure and rotational forces. After the dissipation of the protostellar envelope and the birth of a central star (central stars), the surrounding protoplanetary disk continues to regulate the inward radial transport of matter and the associated angular momentum transport outward, and, therefore, forms a special class of accretion disks (Armitage, P. J. 2011).

Gravitational interactions between a planet and its protoplanetary disk change the planet's orbit, causing it to migrate toward or away from its star. Significant migration will have an effect on the details and efficiency of planet formation (Chambers, J. E. 2009).

Through this work, we seek to theoretically study the evolution of the accretion disk to reach results that are consistent with what astronomical observation produces, so we contribute greatly to the knowledge, analysis, and interpretation of what is behind this observation, and this is through identifying the protoplanetary disks and their evolution, how the process

of planetary migration occurs, and the most important variables that control the evolution of surface density and the change in angular momentum. The purpose of this research is to better understand the processes that lead to star formation, their interaction with the surrounding disk, and how this affects planet formation. In particular, we will focus on studying the interactions between the protoplanetary disk and the planet. Therefore, we decided that our study plan, which we will adopt in our thesis entitled (A theoretical study of the physical phenomena around the protoplanetary disk, which includes a general introduction to present the work and what we aim to achieve and five chapters to conclude with a conclusion, will serve as a summary through which we show the various results reached. We present the approach taken in this thesis, starting with a general introduction to the process of star formation and a comprehensive definition of accretion disks, then explaining the accretion process and what results from it in the universe from different models, but it occurs in the same way regardless of the type of model, with a main focus on protoplanetary disks and the interactions that occur. between the planet and the disk and an explanation of the message structure in detail, which will be discussed in the following sections:
In the first chapter, we focus on the basics of cosmic phenomena in addition to an overview of stars (their formation, evolution, and classifications). We explain accretion physically and the ways matter is transferred between various cosmic phenomena. We also present the most important models of accretion disks present in the universe. In the second chapter, we will focus on the most important model, which is the protoplanetary disk, which we consider the basis of our study. In it, we will present how planets (small and giant) are formed. We will also conduct an extensive study on the migration of planets and their different forms. We focus mainly on the gravitational interactions that occur between the planet and the disk. The gravitational connection with the disk affects the size of the planets orbit and stimulates or inhibits its orbital deviation, causing it to migrate toward or away from its star. In the third chapter, we will focus on the basic factors for studying the evolution of the accretion disk, the most important physical parameters that govern the evolution of a protoplanetary disk, and calculating the surface density using the laws of conservation of mass and angular momentum. We will also explain the behavior of the planet that it exercises in the disk, which is the focus of the comparison that must be reached in our work. In the fourth and fifth chapters, we will rely on two methods to discuss the behavior of surface density in different regions of the protoplanetary disk, where we aim to obtain analytical solutions to the equation for the evolution of a protoplanetary disk and a planet and to know the effect

of angular momentum on the surface density distribution without using any approximations to it based on the equation. The general rule that governs the temporal evolution of the surface density of a viscous accretion disk, based also on the equation of co-evolution of the planet and a protoplanetary disk resulting from the migration of the planet due to tidal interaction with the disk, and the disk is also subject to the tidal torque of the planet, by applying conditions, considerations, assumptions, as well as approximations, the behavior of surface density is determined more clearly by the two methods in each region, and comparing the results obtained theoretically, with other results previously found through numerical calculation, we obtain results consistent with previous results (lin papalouzou 1986), and a general conclusion in which we review what we have achieved with mention some aspirations and horizons that we aspire to in the future.

(Credit NASA/Space Telescope Science Institute)

Chapter 1

Basic Concepts of accretion disks in several cosmic phenomena

Contents

1.1 Introduction

Accretion is a universal phenomenon that takes place in the vast majority of astrophysical objects. The progress of ground-based and space-borne observational facilities has resulted in the great amount of information on various accreting astrophysical objects, collected within the last decades. The accretion is accompanied by the process of extensive energy release that takes place on the surface of an accreting object and in various gaseous envelopes, accretion disk, jets and other elements of the flow pattern (Giovannelli, F., & Sabau-Graziati, L 2016). In this chapter, we will provide a step-by-step approach to the topic, beginning with stars and how they form and develop and ending with compact organisms at the conclusion of their life.

Then we present a general description of the properties of the disks that have been observed surrounding compact bodies, as well as the basic physical mechanisms that control their development. Finally, we provide with prototypes of accretion disks found in the universe.

1.2 The Stars

1.2.1 Formation of stars

Stars form alone and in groups, associations, and clusters (Pudritz 2002 and WardThompson 2002). Recent work suggests that stars form by gravitational collapse of shock compressed density fluctuations generated by the supersonic turbulence generally observed in molecular clouds (Elmegreen 1993 ; Padoan & Nordlund 1999 ; Klessen, Heitsch, & Mac Low 2000 ; Ostriker, Stone, & Gammie 2001 ; Mac Low & Klessen 2003). When the latter is sufficiently massive (mass beyond a critical mass known as the Jeans mass, of the order of a few solar masses, even if it depends on the configuration, the volume etc.), its self-gravity initiates a collapse of the cloud on it self, which little by little fragments into decoupled systems.

At the center of each fragment forms a pre-stellar core as temperature and pressure rise, until the conditions necessary to ignite the fusion of hydrogen are reached. We then obtain a protostar called "class 0".

During cloud collapse, the conservation of angular momentum prevents cloud contraction, especially in the plane perpendicular to the cloud's axis of rotation. This added to the radiation pressure, which has arisen since the formation of the protostar, leads to the formation of a torus around the central star in a few tens of thousands of years. This stage is called "class I".

The gas torus is hot and there fore swollen, mainly from residual gravitational energy, but also from the heating of the central protostar. In a few hundred thousand years, this torus becomes a disk, as blackbody radiation carries energy through the surface. Due to the conservation of angular momentum which prevents rapid contraction in the plane perpendicular to the axis of rotation, the torus flattens as it cools until it forms a disk (Williams et Cieza 2011). About a million years after the protostar formed, the thin disk is formed and the protostar has become a T Tauri star (Class II object). After a few million years (typically 10 million years), the disk wears off and we are in the case of evolved T-Tauri stars or Class III objects. These class names may seem strange, but they come primarily from the study of spectra of young stars which exhibit different characteristics depending on the stage of evolution of the star (Cossou, C.,2013).

Figure 1.1 summarizes the star formation, the different phases and in particular the characteristics of the emission spectrum of these objects.

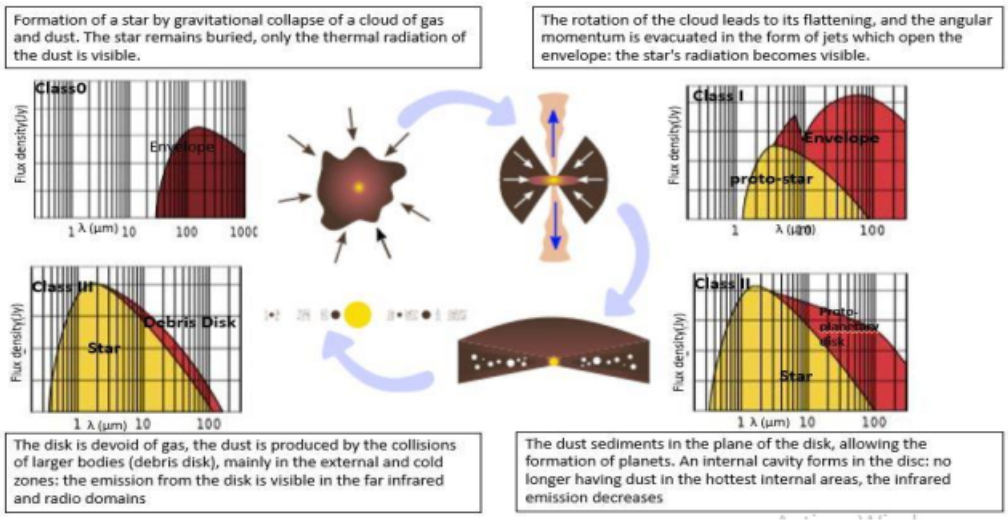

Figure 1.1: Representation of the different stages of evolution of the stellar material [16].

1.2.2 Evolution of stars

The evolution of a star, or stellar evolution, designates all the phenomena ranging from the formation to the death of a star. It can be broken down into several main phases including the formation of the star, its stay on the main sequence and its final phase. During its lifetime, a star emits particles and electromagnetic radiation (part of which in the form of visible radiation) thanks to the energy released by the nuclear fusion reactions that occur in the internal zones of the star. Most of the star's existence is spent on the main sequence, where it burns hydrogen to form helium. Once the core of the star is depleted in hydrogen, it leaves the main sequence to evolve towards its final stage of evolution, leaving a compact object: a white dwarf, a neutron star or even a black hole.

Evolutionary paths of different types of stars. The paths start on the main sequence and end when there is no more nuclear fusion. The mass of a star is the determining factor in its evolution. The more massive a star, the faster it consumes the hydrogen it contains because the temperature is higher there due to the stronger compression of gravity. In the case of stars of a few solar masses, when the core of the star no longer contains enough hydrogen, it becomes a red giant. From then on, the star is doomed to form a planetary nebula, while the core becomes a white dwarf. The most massive stars evolve towards the branches of giants and supergiants and will end up in supernovae (Dommanget, J 1964).

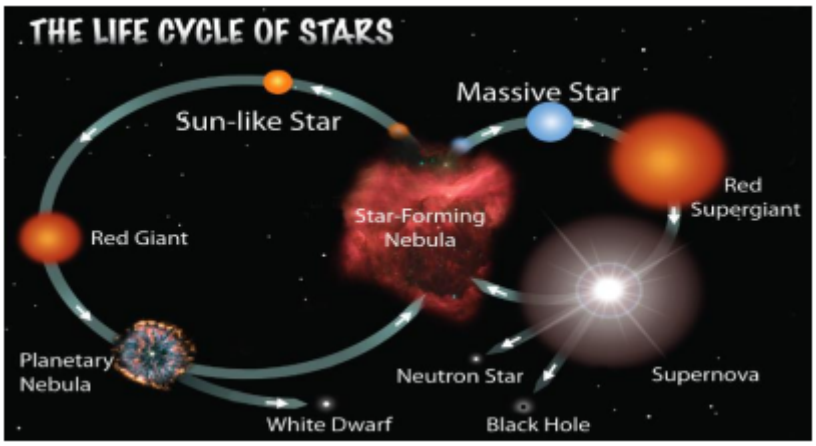

Figure 1.2: the life cycle of stars.

1.2.3 The classification of stars

To classify the stars, we use the Hertzsprung-Russel diagram (or HR diagram), which gives us the spectral type of the stars according to the surface temperature and the luminosity of this one. We can also notice that it gives us the color of the stars as well as their magnitude, between which there is a relationship of proportionality. 90% of the stars are on the diagonal band of the graph, which is called the main sequence. They spend most of their lives there. Stars outside this sequence are generally at the beginning or end of their life, during so-called transitional phases: when they leave the main sequence, they become giants, then white dwarfs (Jung J 1971 ; Mayer & Macák 1973).

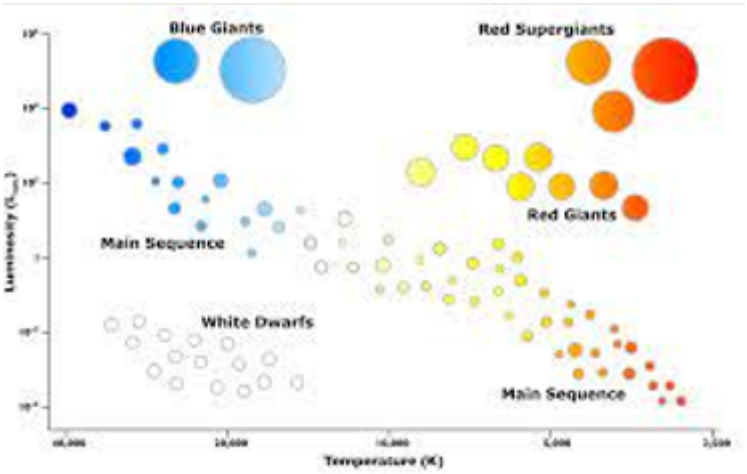

Figure 1.3: the Hertzsprung-Russel diagram (Credit NASA/Space Telescope Science Institute).

The Hertzsprung-Russell (HR) diagram, Shows the power (luminosity) as a function of temperature (spectral class); The "absolute magnitude" ordinate is a logarithmic measure of the

power.

Most stars are on the main sequence Appendix A:

massive stars are hot and have high power (top left), but they are very rare. They have a short life, a few million years. The core is hot enough and dense enough for the elements to fuse down to iron. The iron core formed does not have enough energy for fusion or fission. There is no energy source that keeps the core hot so that it can resist the forces of gravity. These forces will lead to the star's core collapsing in a second, turning it into a sphere of neutrons (or even strange matter), releasing huge amounts of gravitational energy. As a result, the outer layers of the star explode in the form of a supernova. These layers are ejected at speeds of up to 10,000 km/s. while small stars have lower masses, are cool and have low power (bottom right) , In stars with an initial mass less than eight times that of the Sun, the loss of mass will cause the core to shrink to less 1.4 times the mass of the Sun. This type of star has a mass less than 1.44 solar masses.

Giant stars are on (the upper right) of the diagram, they have a power a million times greater than the Sun and live very little. They are so massive that after they remain without energy and their core collapses, their mass is times higher than the mass of the Sun. Gravity exceeds the energy exerted by neutrons. The core continues to collapse until it is so dense that gravitational forces prevent any emission, including light. In this case the star becomes a black hole.

Spectral classification of stars

All series stars, i.e. stars in their basic stage of life, emit a lot of electromagnetic waves, but these waves usually focus at specific parts of the spectrum, and the reason for this is that the larger the stars, the higher their temperature, and they emit electromagnetic waves of high frequencies, and thus their color appears close. It is blue, and because smaller stars are less hot and generate electromagnetic radiation at low frequencies, their color is reddish. Astronomers categorize stars into seven types based on their spectrum (Mora, A., Merín & all 2001):

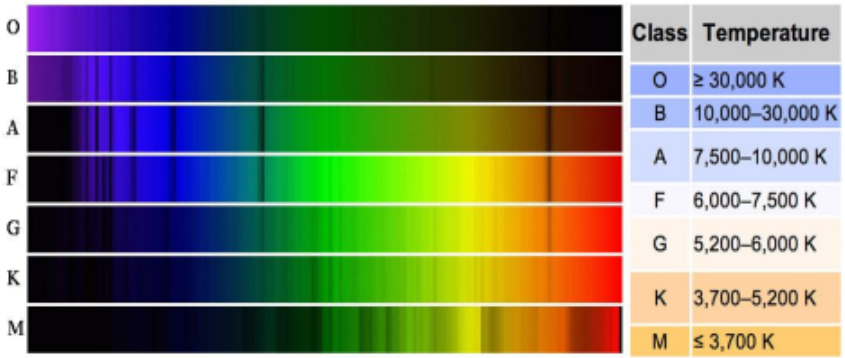

Figure 1.4: Spectral classification of stars (Credit NASA/Space Telescope Science Institute).

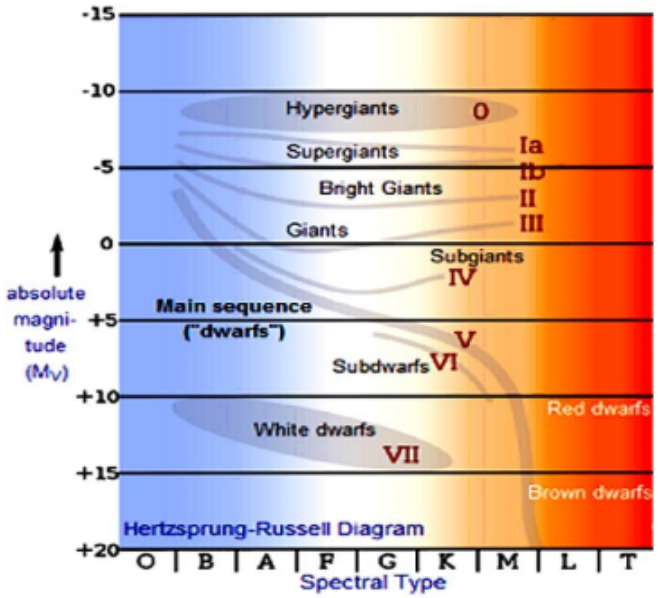

Figure 1.5: Stellar luminosity classes (Credit NASA/Space Telescope Science Institute).

1.3 The compact star (compact object)

In astronomy, the term compact star (or compact object) refers collectively to (white dwarfs, neutron stars, and black holes (Appendix A)). All compact objects have a high mass relative to their radius, which gives them a very high density compared to ordinary atomic matter.

Compact stars are often the extremities of stellar evolution and are in this respect also called stellar remnants. The state and type of a stellar remnant depends primarily on the mass of the star from which it formed. The ambiguous term compact star is often used when the exact nature of the star is not known, but evidence suggests that it has a very small radius compared to ordinary stars. A compact star that is not a black hole can be called a degenerate star (Maurya, S ; Gupta, Y & Ray, S 2016).

1.4 Accretion disk

1.4.1 General description of an accretion disk

A brief history of disk models

The basic idea of accretion disks was proposed soon after the confirmation of quasars, and its classical picture established at the beginning of the 1970s.

When the gas infalls into the compact object, some of the binding gravitational energy of the gas is released due the viscosity present in the accretion flow. The amount of gravitational energy released during the operation is huge. This was first noted by (Zel'Dovich 1964), (Zeldovich & Novikov 1967), and independently (Salpeter 1964). However, they considered an isolated compact object converting gravitational energy into radiation during its collapse. Under the same argumentation that gravitational energy can be converted into radiation by viscous forces, Lynden-Bell proposed in 1969 that the energy source of quasars can be explained by viscous accretion disks (Armijo, M. M., 2012).

The accretion disk model grew in popularity and began to be recognized as the theory capable to describe important energetic emissions observed in the Universe. It was in 1973 that Shakura & Sunyaev proposed a fundamental theory of accretion disks known as the standard accretion disk model or simply the α-disk model. Around the 1980s, different features of accretion disk were explored such as (i) Active disks, especially heated by viscous friction. (ii) Passive disks, essentially heated by the radiation of the central star. The disks can be distinguished according to the mass of the central star (which influences by the power of the radiation, for example) and the state of activity of the disk. This leads to the following observational classes:

(i) The T Tauri Stars (TTS). They are young, low-mass Class II stars. They have a moderate accretion rate of approximately 10^{-9} to $10^{-6} M_{\odot}$ year. The visible flux is generally dominated by that of the star, while the disk is preponderant in the infrared (Bertout et al, 1988).

(ii) The stars FU Orionis (FUOrs), which are considered to be T Tauri having experienced an accretionary burst (Hartmann & Kenyon, 1996). They show high accretion rates of 10^{-5} to $10^{-4} M_{\odot}$ yyear. The flux is dominated by that of the disk at all wavelengths.

(iii) The stars of Herbig Ae/Be(HAe/Be), of greater mass with a spectral type A to B, present lines in emission. Some of them show an excess in infrared, which can be

interpreted as evidence of a disk (Natta et al, 2001).

In 1980, he presented Paczyn'ski & Wiita a Polish doughnut disk consisting in an optically thick torus. And later, when advection were recognized as an important ingredient, the slim disk appeared (Abramowicz 1988), giving a new branch of accretion disk, where the advective energy transport was included in the energy balance, producing super-Eddington accretion rates. The importance of these advective models, called ADAFs (AdvectionDominated-Accretion-Flows) grew up in the 1990s, and were developed by several authors (Narayan & Yi 1994, Abramowicz & Lasota 1995).

All these models showed a good agreement with observations. Accretion disk is now the accepted paradigm for describing a several energetic phenomena either on small scales, like disks around Young stellar object (YSO), or Cataclysmic variable stars (CV) or on large scales, like active galactic nuclei (AGNs) or quasars (Armijo, M. M., 2012).

Standard model: α-disk

The main idea of the αmodel was to describe a geometrically thin non-self gravitating diskby hydrodynamical equations averaged over the disk thickness. Geometrically thin and nonself-gravitating disk means that the scale of height of the disk H (thickness) is much smaller than the radial distance r (i.e., H/r $\ll$ 1) and the mass of the disk Md is much lower than the mass of the central object M_* (i.e., $M_d \ll M_*$) So the disk's gravitational influence is negligible. The most important process governing the accretion of rotating matter is the action of viscous stress within the flow. The goal is to describe the motion of a viscous compressible fluid with variable dynamic viscosity η. Viscous stresses drive accretion by transporting angular momentum outward and mass inward; it's also a way to transform matter's gravitational energy into heat, which is released towards the top and bottom of the disk's surface and radiated away.

The original standard disk model (the α-disk model) also supposes an optically thick accretion disk and a turbulent fluid described by a viscous stress tensor which is proportional to the total pressure. It is then parametrized as

$$\tau_{r\phi} = \alpha\rho c_s^2 = -\alpha \mathrm{P} \tag{1.1}$$

where α is a dimensionless constant, that can be fixed for values between zero (case when accretion is halted) and close to one, and c_s the sound speed of the flow (Armijo, M. M.,

2012).

The main assumptions in the standard disk model can be summarized as follows:

- Gravitation is only determined by the central object (no self-gravity effect).
- The disk is geometrically thin. i.e., $\mathrm{H/r} \ll 1$
- The disk is steady. i.e., $\partial/\partial t \equiv 0$
- The disk is axisymmetric i.e., $\partial/\partial\phi \equiv 0$
- Azimuthal motion dominates over radial motion i.e., $v_\phi \gg$ rr
- Hydrostatic balance is assumed in the vertical direction
- The disk is optically thick in the vertical direction
- Viscous heat dissipation balance radiation output i.e., $\mathrm{Q}^+ = \mathrm{Q}^-$
- The r_ϕ component of the viscous stress tensor is assumed proportional to the pressure i.e., $\tau_{\mathrm{r}\phi} = -\alpha \mathrm{P}$. All other components are zero
- There are no magnetic fields present in the disk

The Composition of the Disk

Accretion disks are composed of gas and dust grains (mainly composed of silicates), the latter having an observed size ranging from tenths of a micrometer to a centimeter, rotating around a central object such as a young star, a white dwarf, a neutron star or a black hole. When the molecular cloud contracts to form a star due to the presence of angular momentum, the contraction will not be fully spherical. While the central protostar grows roughly spherical by18 accreting material from the envelope, the outer part of the cloud tends to be mostly distributed into a disk due to the action of gravity and centrifugal forces. In the presence of rotation, the least energy orbit is circular. The material located in the disk rotates with a Keplerian motion around the central star $V \alpha R^{-1/2}$

The Keplerian angular velocity of a particle orbiting in the disk is given by $\Omega_{\mathrm{K}} = (\mathrm{GM/r^3})^{1/2}$ where G is the universal gravitational constant, M is the mass of the star and r is the distance between the centre of the star and the particle. As a result, the angular velocity decreases outwards, while the specific angular momentum that scales as $h = r^2\Omega$ increases outwards (the specific angular momentum is the angular momentum per unit of mass). If the disk is

viscous, the inner parts that are rotating faster than the outer parts shear past the outer parts. A transport of angular momentum is established from the inner part to the outer part. According to (Lynden-Bell & Pringle, 1974), a simple energybalance shows that a viscous disk can lower its energy by transporting mass towards lower radius and angular momentum towards largr radius. The Keplerian disks (Appendix A) surrounding young stars are therefore very likely accreting mass from the outer parts to the inner parts of the disk, while angular momentum is evacuated towards the outer part of the disk.
However, since the gas in the disk has a non-zero viscosity, the radial layers of the disk "rub" against each other and transform the mechanical energy into heat. The disk material then gradually spirals towards the central object emitting heating radiation. We can therefore see in accretion disks an efficient way to convert gravitational energy into thermal or radiant energy. In practice, 10% of the mass energy of the gas can be converted by accretion around a neutron star, a value which can rise to 40% around a black hole (Pringle 1981). The observable physical amount of radiation produced in accretion disks is luminosity. As photons carry momentum and can therefore exert pressure, there is a maximum possible luminosity at which gravity is able to balance the outward pressure of radiation. The limit for a stable and spherically symmetric accretion flow is given by the Eddington luminosity L_{Edd} .

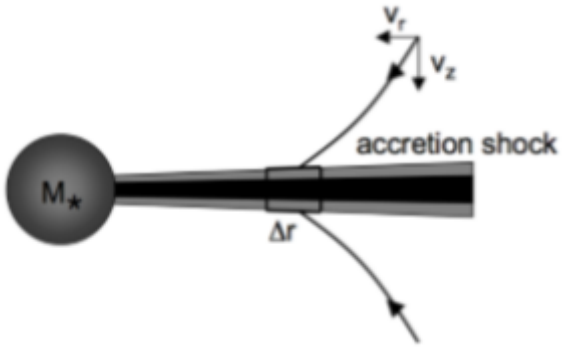

Figure 1.6: Schematic view of disk formation during the collapse of a rotating spherical cloud.

1.4.2 Angular Momentum Transport

In many cases the accreting gas has a non-zero angular momentum and therefore can not be accreted directly. Only if matter transfers its angular momentum to matter further out in the disk, an inward transport of matter is possible. This principle of distributing as much

angular momentum on as little as possible matter is the main definition of accretion (Asmus 2008 ; Balbus & al,2013). The result of this asymmetric behavior is, that almost all the mass of a disk can be accreted, without an external torque removing the angular momentum. Usually disks are subjects to gravitational, magnetorotational (MRI), purely hydrodynamical and convective instabilities that, inturn, cause turbulence in disks which ensures outward transport of angular momentum. This effect of turbulence can be characterized as turbulent viscosity. The dual role of turbulence shall be mentioned. Firstly, it is responsible for outward angular momentum transport, secondly, it provides a channel for conserving gravitational energy, originating in mass falling onto the central object and transformed into thermal energy.

Turbulent viscosity (Shakura-Sunyaev)

Temporal evolution of the disk is governed by the viscous stresses acting on the disk material. These stresses are typically subsumed into a dimensionless parameter α that characterizes the efficiency of angular momentum transport. (Shakura & Sunyaev 1973) developed the most commonly invoked prescription of this kind, proposing a turbulent kinematic viscosity of the form

$$v = \alpha v \ell \tag{1.2}$$

which is the product of the turbulent velocity v and the size ℓ of the largest eddies in the turbulent pattern. As turbulence is quickly dissipated by shocks in a highly supersonic flow, the turbulent velocity is often taken to be roughly equal to the local sound speed of the disk medium, c_s. An upper limit to the size of the largest eddies that form can similarly be argued to be roughly equal to the disk half-thickness H; hence

$$v = \alpha \frac{{c_s}^2}{\Omega} \tag{1.3}$$

where $H = \dfrac{c_s}{\Omega}$, We can now express the viscosity in terms of the disk parameters and hence estimate the efficiency of angular momentum transport and thus mass accretion onto the central star. It is also very obvious to estimate how large α should be to reproduce the observed time scale of disk evolution. The viscous timescale can be expressed as

$$\tau = \frac{r^2}{v} = \left(\frac{h}{r}\right)^{-2} \frac{1}{\alpha\Omega} \tag{1.4}$$

Here, we can fill in 1Myr as the typical evolutionary timescale at 50AU. In addition, we assume that the disks are indeed very thinand h/r $\sim$ 0.05. This yields an α of 0.02 (Dominik, C, 2015; DeSouza, A & Basu, S 2017).

The magnetorotational instability (MRI)

One mechanism that may act as an effective α-viscosity is the magnetorotational instability (MRI). (Balbus & Hawley,1991) have demonstrated that a weak magnetic field can make an otherwise hydrodynamically stable disk become unstable to the MRI. Simulations in ideal magnetohydrodynamics (MHD) find that the nonlinear outcome of MRI can amplify and sustain turbulence that can then lead to angular momentum transport (Brandenburg et al., 1995; Hawley et al., 1996). However, in a largely neutral medium (such as in a protostellar disk) the ionization fraction must be large enough for the neutral-ion collision frequency to be greater than the local epicyclic frequency.

Many studies have been performed to determine in which regions of protostellar disks the MRI may be active (Sano et al., 2000; Fromang et al., 2002; Cleeves et al., 2013). For example, (Igea & Glassgold,1999) find that the MRI can be active at distances greater than 5 AU from the central star, while (Cleeves et al. 2013) finds that the disk midplane is largely inactive to the MRI after accounting for the effect of stellar winds and magnetic mirroring of cosmic rays.

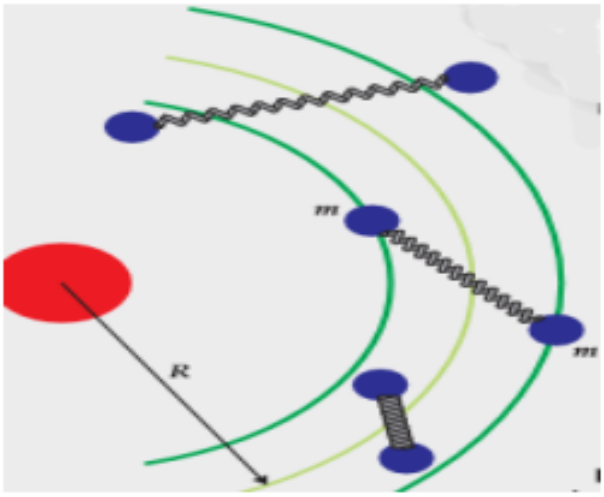

Figure 1.7: Two masses in orbit connected by a weak spring [7], [37].

The spring exerts tension force T resulting in a transfer of angular momentum from the inner

mass mi to the outer mass mo . If the spring is weak, the transfer results in an instability as mi loses angular momentum, drops through more rapidly rotating inner orbits, and moves further ahead. The outer mass mo gains angular momentum, moves through slower outer orbits, and drops further behind. The spring tension increases and the process runs away.

Gravitational instabilities

Gravitational torques may represent an alternative source for angular momentum transport in cold and massive disks. Using self-consistent cooling, (Boley et al. 2006) showed that an α prescription based on the gravitational instability agrees with the (Gammie 2001) description very well, which assumes that the viscous heating is locally balanced by the cooling. (Cossins et al. 2009) have also used smoothed particle hydrodynamics to show that these disks often possess tightly wound spiral arms that can be approximated with a local treatment. Here we consider a perturbation in an otherwise axisymmetric thin disk, which has the form of an annulus of width r and increased local mass Δm (e.g., the formation of a spiral arm). The growth condition for a perturbation depends on whether its self-gravity is greater than the tidal acceleration acting on it. That is,

$$\frac{\mathrm{G}\Delta\mathrm{m}}{\Delta\mathrm{r}^2} \sim \pi\mathrm{G}\Sigma > \frac{GM_*}{r^2}\frac{\Delta\mathrm{r}}{r} \tag{1.5}$$

A natural length scale thus emerges, in excess of which perturbations of this nature are stabilized by their rotation,

$$\Delta\mathrm{r} \sim \pi G\Sigma\left(\frac{GM_*}{r^3}\right)^{-1} = \frac{\pi G\Sigma}{\Omega^2} \tag{1.6}$$

Furthermore, with the assumption of vertical hydrostatic equilibrium, the disk self-gravity is supported by gas pressure in the vertical direction. This additional constraint implies Δr must be at least larger than the disk half-thickness H, $\Delta\mathrm{r} \geq \mathrm{H} = \frac{c_s}{\Omega}$ the "Toomre Q" parameter, (Toomre 1964), originally formulated these arguments, summarizing the instability criterion as:

$$\mathrm{Q} \equiv \frac{c_s\Omega}{\pi G\Sigma} < 1 \tag{1.7}$$

1.5 The physics of accretion

Accretion of matter onto compact objects is perhaps the only mechanism that gives sufficient energy to feed the most luminous objects in the Universe. Examples can be found in different classes of narrow binary systems and nuclei of active galaxies and quasars. How much energy can be produces by accretion, is shown by the following. The energy, ΔE, released by a parcel of mass, Δm, falling from infinity onto an object of mass M and radius R, is given by $\Delta E = \frac{GM\Delta m}{R_*}$. meaning that the power generated by mass accreting at a rate $\dot{M}$ onto this object, We can also characterise the efficiency of any energetic process by relating the energy released to the rest mass energy of the parcel of mass, such that $\Delta E = \eta \Delta mc^2$, where η is the radiative efficiency. Similarly, in terms of luminosity,

$$L = \eta \dot{M} c^2 \tag{1.8}$$

Nuclear fusion is one of the more efficient energetic processes in the universe, with an efficiency of $\eta = 0.007$ for hydrogen fusion. If we rearrange the above equations in terms of η, we find

$$\eta = \frac{G}{c^2}\frac{M}{R} \tag{1.9}$$

the efficiency of accretion is directly related to the compactness, $M/R*$, of the central object R^* where is radius of star Values of compactness and the associated radiative efficiencies for four different compact objects are shown in table 1.1. The compactness for black holes was calculated using the Schwarzschild radius, $r_s = \frac{2GM}{c^2}$, which defines the event horizon of a non-rotating black hole. It is also pertinent to define the gravitational radius $r_G = 1/2r_s$, which can be useful as a characteristic scale for any compact object of mass M. (Matthews, J 2017)

Object	M ($M_\odot$)	R_* ($R_\odot$)	$M_\odot/R_*$ ($M_\odot/R_\odot$)	$\boldsymbol{\eta}$
White Dwarf	0.8	0.01	79.4	1.6×10^{-4}
Neutron Star	1.4	1.4×10^{-5}	10^5	0.2
Black Hole	10	4.2×10^{-6}	2.4×10^5	0.5
SMBH	10^9	4244	2.4×10^5	0.5

Table 1.1: Approximate values of compactness and accretion efficiency for four different compact objects with typical parameters. Here, $R*$ for black holes is set to the event horizon for a Schwarzschild black hole, SMBH stands for supermassive black hole [48].

1.5.1 Spherical Accretion

The simplest geometry one might propose for accretion would be one in which a central mass accretes matter in a spherically symmetric manner. The process of spherical accretion has come to be known as Bondi-Hoyle-Lyttleton accretion (Hoyle & Lyttleton, 1939; Bondi & Hoyle 1944). In particular, Bondi (1952) studied spherically symmetric accretion onto a point mass and derived. the Bondi radius, $\mathrm{r_B} = \frac{\mathrm{GM}}{\mathrm{c^2\ s}}$, where $c_s = c_s\,(r_B)$ is the sound speed as a function of radius.

1.5.2 Accretion Luminosity: The Eddington Limit

The mass M of the central object plays an important role in the nature of the accretion disk, especially when considering the maximum luminosity allowed by the system. This maximum luminosity is called the Eddington limit.

The luminosity that is released around an accreting source cannot be unlimited: with increasing luminosity the radiation pressure increases, until this is so large that all matter that wants to fall onto the compact object is blown away again. The radiation pressure works primarily on electrons (Thomson scattering) and it is given by σ_T F/c, where $\sigma_T = 6.65 \times 10^{-25}$ cm^2 is the Thomson cross section, F the outward flux (in erg s-1 cm^2) and c the speed of light. The radiation pressure pushed up electrons against the gravitational force, at the same time electrons drag the protons with them due to Coulomb interaction, but the force of radiation into protons is negligible next to electrons because the scattering-cross section of protons is $(m_e/m_p)^2 \simeq 25 \times 10^{-8}$ smaller than for electrons.

Under this condition, accretion is only possible if the total gravitational attraction overcomes the radiation outward force. The Eddington limit corresponds to the situation when these quantities are equal. The gravitational force exercised from the central object of mass M to a electron-proton pair is given by $\dfrac{GM\,(m_e + m_p)}{r^2} \simeq \dfrac{Mm_p}{r^2}$, and must be equal to the radiative force over one electron. Then we have

$$\frac{GMm_p}{r^2} = \frac{\sigma_T\ \mathrm{F}}{\mathrm{c}} \tag{1.10}$$

The flux F of the accreting source is related to his luminosity through, $F/L4\pi r^2$. If that quantity becomes zero, the maximum luminosity is reached. This defines the so-called Ed-

dington limit:

$$L_{Edd} = \frac{4\pi G M m_{\rm p} c}{\sigma_T} \simeq 1.26 \times 10^{38}\,(\mathrm{M}/M_{\odot})\,\mathrm{erg}\,s^{-1} \tag{1.11}$$

with an associated Eddington accretion rate of

$$\dot{\mathrm{M}}_{\rm Edd} = \frac{\mathrm{L_{Edd}}}{\eta \mathrm{c}^2} = 4\pi \mathrm{r} \frac{\mathrm{m_p} c}{\sigma_T} = 9 \times 10^{16} \mathrm{g \cdot s^{-1}}\,(r_*/1\mathrm{km}) \tag{1.12}$$

When accretion exceeds this limit, the associated luminosity will exceed L_E, then the outward pressure radiation overtakes gravitational attraction hence; accretion is halted (Armijo, M. M 2012).

1.6 Accretion disks in the universe

Accretion disks are ubiquitous throughout the universe, found rotating about a wide array of different objects including super massive black holes (AGN), white dwarves (dwarf novae), neutron stars / stellar-mass black holes (x-ray binaries), and young stars (circumstellar or protoplanetary disks (PPDs)). While these disks exist across many orders of magnitude in size-scale and energy, they all share a very general common origin: they form as the result of gravitational collapse of a system that has net-angular-momentum. This net-angularmomentum defines an axis about which the resulting system will rotate as the matter in the disk structure accretes inwards towards the central objectAccretion disks are flattened astronomical objects made of rapidly rotating gas which slowly spirals onto a central gravitating body. The gravitational energy of infalling matter extracted in accretion disks powers stellar binaries, active galactic nuclei, proto-planetary disks and some gamma-ray bursts. The black hole accretion in quasars is the most powerful and efficient stationary engine known in the universe.

1.6.1 Accretion Disks in X-ray binaries

Thanks to the efficient conversion of the accreting matter into radiative energy, Xray binaries are the most powerful X-ray emitters in our Galaxy. These systems consist of two interacting objects: a compact object, which can be a BH or a neutron star (NS), and a non-degenerate secondary star (companion star). Owing to gravity, the matter accreted from the companion star falls onto the compact object reaching X-ray energies. At some stages of their evolution, depending on the physical parameters of the binary system, XRBs can

transfer matter through two main processes (Frank et al., 1987):

- **stellar wind** During a particular evolutionary phase of the system the companion star ejects part of its mass in the form of a stellar wind. A fraction of this outflow is captured gravitationally by the compact object;
- **Roche lobes outflow** This can occur both if the star evolves and increase its radius and if the system reduces its dimension. In both cases the system reaches a point where the gravitational attraction of the compact object removes the outer layers of the companion star.

It is known that the mechanism which leads the matter to leave the companion star and to be accreted onto the compact object is determined by the mass of the companion star. Based on this parameter, the X-ray binaries are classified as low-mass or high-mass X-ray binaries (LMXBs and HMXBs, respectively) (Bassi, T 2020).

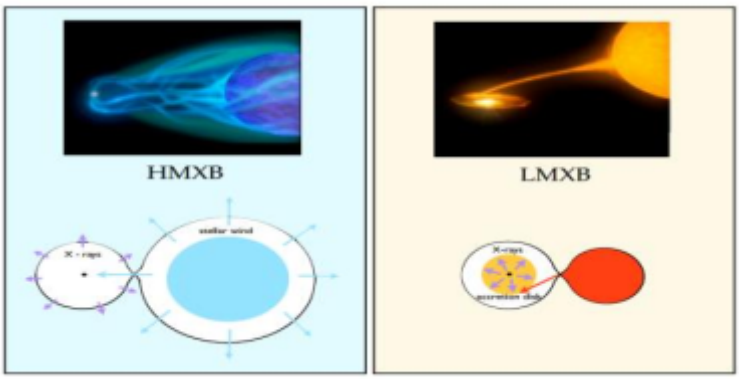

Figure 1.8: schematic view of high mass and low mass X-ray binaries. Each panel shows the accretion modes in the different binary system, respectively by stellar wind and by Roche lobe overflow via an accretion disk [20], [8].

In HMXBs, the companion star is a young massive star ($M > M_{\odot}$) of spectral type O-B. These systems are relatively young objects ($\sim 10^7$ years) and they are mostly distributed near the Galactic plane. The accretion onto the compact object occurs through a strong stellar wind, which may be driven by absorption of UV photons from the companion or X-ray heating. LMXBs, instead, are old systems ($\sim 10^{8-9}$ years) mostly concentrated in the Galactic central region and in globular clusters, in which the donor is a low mass star ($M \leq 1M_{\odot}$). In this case the matter is transferred only through Roche lobe overflow and accreted through an accretion disk.

The HMXB family has two sub-classes, (i) the soft X-ray transients that can contain a NS or a BH and exhibit quasi-periodic outbursts and (ii) the pulsars that contain a NS and emit a bean of radiation along the axis of the magnetic field.
Many, if not all, black hole X-ray binaries go through periods during which they emit relativistic twin jets that propagate along the rotational axis of the compact object. They then look like scaled down quasars and are thus often called microquasars. (Bassi, T 2020)

Roche Lobe-Overflow

Roche lobe overflow is the process whereby one of the stars in a binary system, as a consequence of its evolution, fills its critical potential lobe and starts to transfer matter to the other star. One reason might be the expansion of the star due to nuclear evolution to the point that material can escape its gravitational field through, the inner Lagrange point Li. The other is shrinking of the orbit to the point where the companion star atmosphere overfills its Roche lobe. The dynamics of the matter is then dominated by the gravitational field of the accreting star. the matter flowing from L1 can form an accretion disk. This problem assumes a circular Keplerian orbit for the binary, which indeed is very close to reality in close binaries due to tidal circularization. In particular the potential Φ_R contains both gravity and centrifugal forces; this so-called Roche potential is given by:

$$\Phi_{\mathrm{R}}(\mathrm{r}) = -\frac{\mathrm{GM}_1}{|r - \mathrm{r}_1|} - \frac{\mathrm{GM}_2}{|\mathrm{r} - \mathrm{r}_2|} - \frac{1}{2}(\omega \times \mathrm{r})^2 \tag{1.13}$$

where r_1 and r_2 are the distances to the centre of the stars of masses M_1 and M_2 and ω is the angular velocity of the binary and is a vector normal to the orbital plane. The Roche's potential takes into account the gravitational attraction of each of the two stars as well as the centrifugal force. (Figurel.17) shows some sections of the equipotential surfaces and the surface representing the Roche potential for a binary system. The shape of the equipotential surfaces and the dimension are determined by the masses ratio $q = \mathrm{M}_2/\mathrm{M}_1$ and the binary separation a (Frank et al., 2002 ; Savcheva, A 2006).

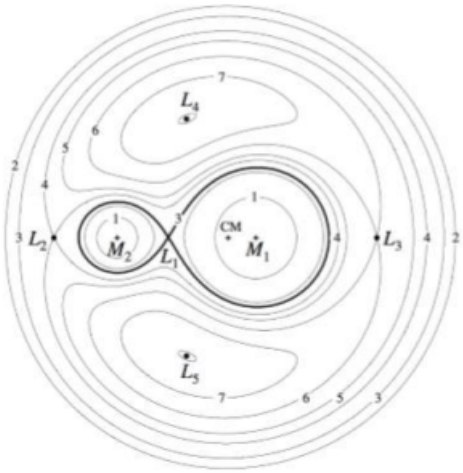

Figure 1.9: The Roche potential in a binary system for $qM = M2/M1 = 0.25$. The Lagrangian points are marked, as are the locations of the individual and system centres of mass [27].

The matter moves inside these surfaces driven by the gravitational force of the nearest star. The largest closed equipotential surface surrounding each star is the Roche lobe. The points where the gravitational and centrifugal forces balance each other out, are called Lagrangian points (L). The point at which the Roche lobes touch each other is the inner Lagrangian point $L1$. During the system evolution one of the two stars may increase in radius up to the point where the gravitational pull of the companion can remove the outer layers of its envelope (Frank et al., 2002). Assuming that one of the two stars has evolved so that its surface has filled its Roche lobe, the pressure gradient or any perturbation push the gas through L1 into the Roche lobe of the second star just causing the accretion process. Then, the mass transfer continues as long as the donor star fills the Roche lobe. We refer to this kind of mass transfer as Roche lobe overflow.

In the context of semi-detached binary systems, the most important equipotential is the dumbbell-shaped region enclosing both masses. Each of these enclosed regions is known as the Roche lobe of the object. A good approximation for the size of the Roche lobe.

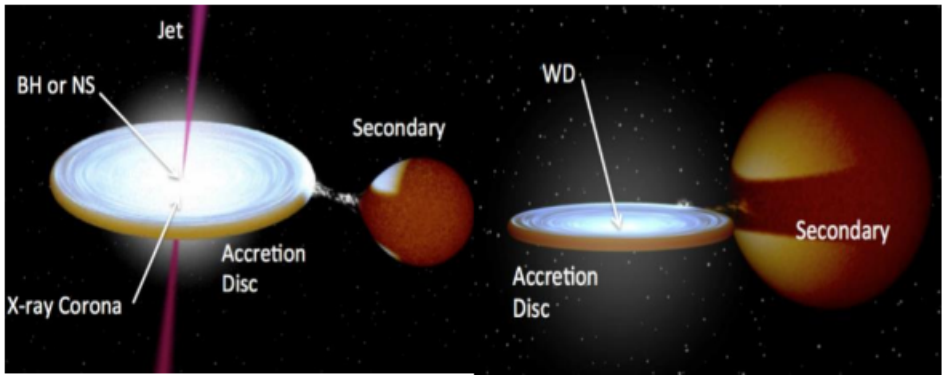

Figure 1.10: a low-mass X-ray binary and cataclysmic variable .(Rob Hynes)(Credit NASA/Space Telescope Science Institute).

1.6.2 Accretion disks in cataclysmic variables (CV_s)

Cataclysmic variables are binary star systems consisting of a white dwarf ("primary") and a normal star ("secondary", or "companion"). Typically, the CVs have sizes comparable to the Earth-Moon system, and orbital periods of a few hours. When the outer layers of the companion overflow the "Roche lobe", the companion loses matter through the first Lagrangian point L1 of the rotating binary system. When the white dwarf is only weakly magnetised, the matter forms an accretion disk around it and eventually reaches its surface. "Dwarf novae" (DN) are CVs that show outbursts lasting for about a week and separated by weeks to months of quiescence. U Gem is the prototype of dwarf novae. (Szkody, P & all 2002) The brightness in the visible light of U Gem increases 100-fold every 120 days or so, and returns to the original level after a week or two. The DN phenomenon is due to a specific accretion disk limit-cycle instability, tidal torques, and fluctuations in the masstransfer rate from the secondary. The geometry of accretion is very different in magnetic CVs, where accretion disks are either truncated or absent and accretion occurs along the magnetic field lines. With respect to the character of the light curves one can distinguish dierent types of CV_s: (Kotko, I & Lasota, J 2012)

1.6.3 Novae

They show very large eruptions which are caused by the thermonuclear explosions of hydrogen1 on the surface of white dwarf when the temperature of accreted material crosses29 reaches the ignition temperature and unstable hydrogen burning set in. The classical novae erupt only once during their observational history while recurrent novae repeat the outburst

at least one more time.

1) **Dwarf Novae**

Their outbursts are of lower amplitude than those in novae and occur much more often. But the crucial difference is that the DN outbursts are the result of the thermal-viscous instability in accretion disk. DN can be further divided into three subgroups depending on the characteristic features observed in their light curves :

a) **U Gem-type**

They show only normal outbursts which show up in a quasi-periodic way. their recurrence times may be as short as few days. Usually they appear every several tens of days. With respect to their duration times normal outbursts may be divided into narrow and wide. The distinction between them follows from the observational comparisons not from the strict deffnition but one can adopt that the narrow are these which last $\sim 1-5$ days while wide ones are longer, up to ~ 20 days.

b) **SU UMa-type**

All SU UMa stars have orbital periods below ~ 2 hr (below the period gap). Their light curves consist of normal outbursts and superoutbursts. Super-outbursts are the eruptions which are usually brighter by $\sim 0.5-1$ than normal outbursts and last times longer (Warner, 1995). The characteristic feature of superoutbursts, which does not appear during normal outbursts, are the low-amplitude short-period light variations called super-humps.

2) **Z Cam-type**

Z Cam stars are DN with very high mass transfer rates which are close to their critical values. In their light curves there are periods of elevated brightness which is lower by ~ 1 mag from the normal outburst maximum. Those periods may last for months or even years and are called standstills. After the standstill Z Cam-type systems returns to its low luminosity state.

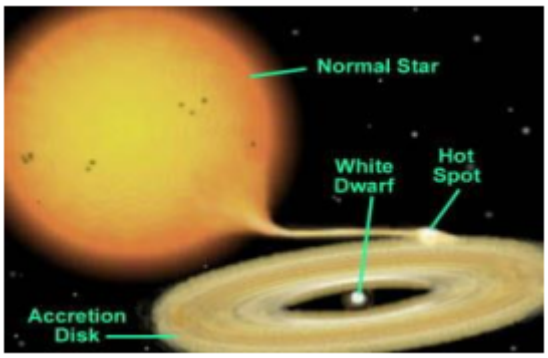

Figure 1.11: The Z Cam-type of white dwarf star (Credit NASA/Space Telescope Science Institute).

1.6.4 Accretion disks in Quasars and other active galactic nuclei (AGN)

Most galaxies have supermassive (millions to billions of solar masses) black holes at their centres (nuclei). In AGN, the black hole accretion produces radiative power that usually outshines its host galaxy. The accretion disk is surrounded by a hot corona which contains clouds of gas. Fast moving clouds close to the disk produce broad lines and slow moving clouds further away from the disk produce narrow lines in the AGN spectra. The observational appearance of an AGN may be affected by the presence of a large outer dust torus.

Classification of active galactic nuclei (Fabian, A 1999)

AGNs have been classified in several ways. Three important classes are:

(i) Seyfert galaxies, which have modest luminosities but tend to be the best studied because they are usually near us;

(ii) quasars, which are brighter than the host galaxy and are particularly numerous at a redshift of when the Universe was about a third of its current age. Quasars are often distant AGNs, with a point-like appearance in optics, with broad emission lines and showing a very pronounced redshift. Their radiation does not generally have a thermal origin, and the luminosity in the radio domain often exceeds that in optics by several orders. of greatness. Their structure shows, in most cases, the presence of jets from which the radio emission originates. Quasars are the most luminous objects known.

(iii) **Blazars**. About 10% of quasars are radio-strong; the rest is radio-silent, but not silent. Radio intensity is usually associated either directly with collimated relativistic flow or jet, or with regions where a jet has collided with surrounding materials. A blazar is seen when our line of sight is close to the direction of a jet.

Figure 1.12: The active galactic nuclei (AGN) (Credit NASA/Space Telescope Science Institute).

1.6.5 Accretion disks in gamma ray bursts (GRBs)

The most energetic explosions seen in the universe are gamma-ray bursts. They are short, collimated flares of low-energy γ-rays with relativistic emission simultaneously also at longer wavelengths (e.g., X-ray flashes, radio jets). Observations indicate that GRBs are cosmological and followed by slowly fading afterglows. The duration of GRB prompt emission can last from 0.01 - 2 seconds (short bursts) up to 2 - 500 seconds (long bursts) and may be explained by merging compact objects or failed supernovae (collapsars), respectively. Afterglows on the other hand are observed and monitored from a couple of days up to several years. All evidence on the origin of the inner engines (i.e., mergers, collapses, pulsars) of GRBs is deduced indirectly. Energetic requirements suggest, however, a similar configuration of the end products: the formation of a solar-mass black hole surrounded by a massive debris disk ($\sim 0.1 M_{\rm sun}$) with a huge accretion rate. The time scale of the burst is determined by the accretion time of this disk. According to these time scales accretion disks in GRBs are most likely hyper-accreting. This means, the temperatures and densities at the required accretion rates are such, that neutrino production is switched on and the electrons are mildly relativistic and degenerate. Generally, GRBs seem to show similarities to radio-loud AGN and galactic microquasars, since all these systems eject strongly collimated, more or less relativistic flows of matter and involve accretion onto a black hole (Piran,T 2005).

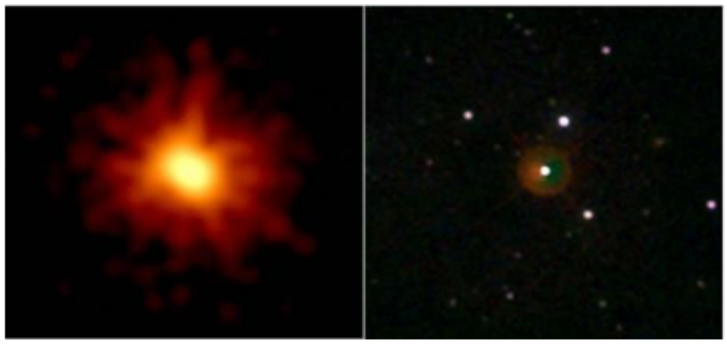

Figure 1.13: The gamma ray bursts (GRBs) (Credit NASA/Space Telescope Science Institute)

1.6.6 Accretion disks in young stellar objects (YSOs)

During star formation, the central part of a dense molecular cloud collapses to a proto-star with a gaseous envelope that finally settles to a rotating proto-planetary accretion disk. Sedimentation and self-gravity in such disks trigger the formation of planets and planetary systems. Proto-stars are heavily embedded in surrounding gas and dust and for this reason visible only in the infrared, millimetre or sub-millimetre wavelength bands. Most of the material that goes into forming a star is accreted through a circumstellar disk and in this process the proto-stellar system drives an energetic bipolar jet and outflow into its surroundings. The least evolved protostars are surrounded by remnant protoplanetary accretion disks.

Based on the spectral energy distribution in the infrared and visible light, YSOs are divided into five classes (0-IV), associated with their evolutionary stages. Class 0 refers to collapsing molecular clouds, proto-planetary disks exist in classes I-III, and class IV contains the zero-age main-sequence star.(Beltrán, M & Wit,W 2016)

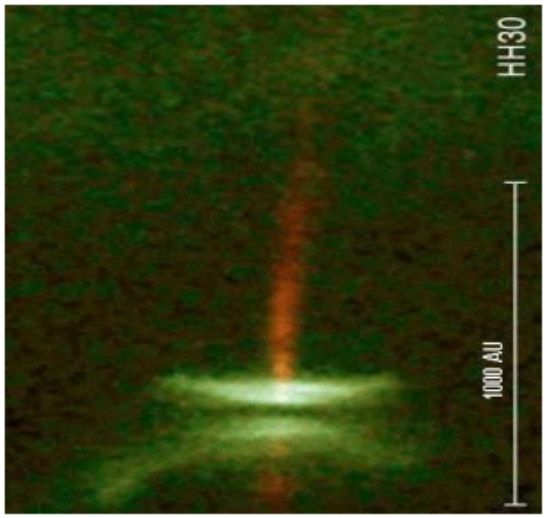

Figure 1.14: The young stellar objects (YSOs) (Credit NASA/Space Telescope Science Institute)

1.6.7 The protoplanetary disks

Protoplanetary disks are the observational manifestation of the initial conditions for planet formation. They can be defined as rotationally supported structures of gas (invariably containing dust) that surround young, normally pre-main-sequence stars. Although most observed disks have inferred masses that are a small fraction of the stellar mass, no meaningful distinction can be drawn between physical processes in protoplanetary disks and those that occur in the earlier, protostellar phase, in which both star and disk are accreting rapidly. Similarly, a common set of processes operate, albeit to varying degrees, in disks around brown dwarfs, Classical T Tauri stars (low-mass pre-main-sequence stars that are actively accreting), and massive stars.

Around low-mass stars, protoplanetary disks are persistent; the typical lifetime of 10^6 years (Haisch, Lada & Lada 2001) equates to thousands of dynamical times at 100 AU. Protoplanetary disks are nearly stable fluid configurations that evolve under the action of relatively slow processes angular momentum transport, mass infall, and disk winds. These agents control both the secular evolution and the eruptive behavior observed in protoplanetary disks, and set the overall environment within which planet formation occurs: the location of the snow line, the mass and time available to form gas giants, the rate of migration, and so forth. Moreover, in most models the evolution of the disk is linked to the presence of turbulence within the disk gas, and the strength and nature of that turbulence controls the growth of solids during the earliest phases of planet formation (Armitage 2010 ; Armitage , P. J 2011).

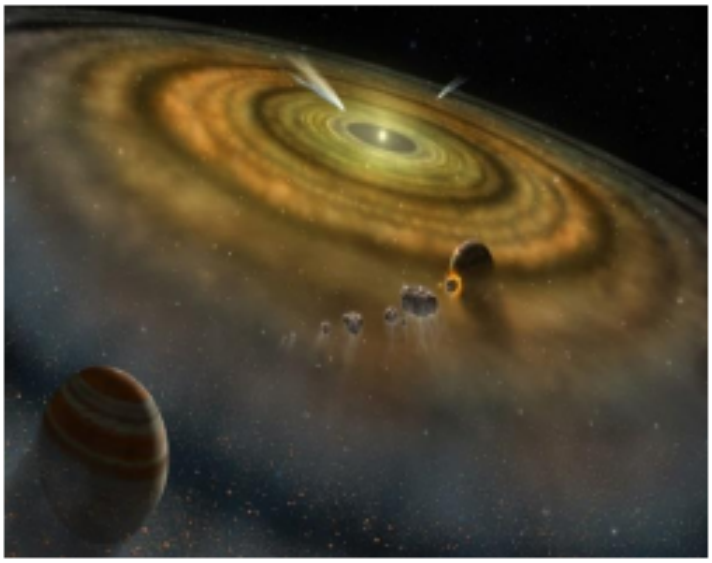

Figure 1.15: The protoplanetary disks (Credit NASA/Space Telescope Science Institute).

Chapter 2

Interactions (disk-planet)

Contents

2.1 Introduction

Circumstellar disks provide the reservoirs of raw material and initial physical conditions for the formation of nascent planetary systems. Studies of their structure and evolution therefore hold the potential to reveal much about the planet formation process in all of its most important stages: the growth of submicron-sized, primordial interstellar grains into larger particles; the agglomeration of these particles into planetesimals; and the growth and orbital evolution of these planetary embryos into the mature systems observed around our own star and dozens of others.

Circumstellar disks pass through several discernible stages on their way to becoming planetary systems. While the terminology describing these disks is a matter of some discussion, we use the following terms to refer to the major stages of evolution of circumstellar disks:

protoplanetary disks retain a substantial and largely primordial reservoir of gas and dust, massive enough to imply planet-forming potential.

transition disks have properties intermediate between protoplanetary and debris disks, exhibiting substantial clearing of gas and dust from the system

debris disks have little or no gas, tenuous dust disks, and dust lifetimes shorter than the age of the system, indicating that the disk is second-generation rather than primordial

This chapter focuses on the first stage of evolution, which necessarily include the epoch of

planetesimal growth and giant planet formation as large planets must form before gas is dissipated from the disk.

Protoplanetary disks around young stars are the birth sights of planetary systems like our own. Disks represent the gaseous dusty matter left after the formation of their central stars. The mass and luminosity of the star, initial disk mass and angular momentum, and gas viscosity govern disk evolution and accretion. Protoplanetary disks are the cosmic nurseries where microscopic dust grains grow into pebbles, planetesimals, and planets.

Gravitational interactions between a planet and its protoplanetary disk change the planets orbit, causing the planet to migrate toward or away from its star. Migration rates are poorly constrained for low-mass bodies but reasonably well understood for giant planets. In both cases, significant migration will affect the details and efficiency of planet formation. If the disk is turbulent, density fluctuations will excite orbital eccentricities and cause orbits to undergo a random walk. Both processes are probably detrimental to planet formation. Planets that forme arlyin the life time of a disk are likely to be lost, whereas late-forming planets will survive and may undergo little migration.

2.2 The standard model of planet formation

At the Global models of planet formation can be thought of as big puzzles. The foundations of the model of formation of the Solar System were laid in the 18th century by the philosopher Emmanuel Kant (1755) then by the scientist Pierre Simon de Laplace (1796). According to this scenario, the planets formed in a rotating disk of gas and dust around the nascent sun (Chambers2004 ; Armitage2007a). Originally, this hypothesis was made to explain the prograde and almost coplanar orbits of all the planets. Today such disks, called protoplanetary disks, have been observed around young stars by the Hubble Space Telescope. These direct observations also make it possible to constrain planetary formation models by analyzing the composition of the disk, its temperature and its lifespan. In particular, the characteristic time of survival of circumstellar disks around young stars is around 10 million years, which means that planets form during this same period of time. We describe the stages and processes of planetary formation as envisioned by the current paradigm. The evolution in a given region of the disk progresses through these stages in order, but different stages may take place concurrently in different regions of the disk.(Boué, G 2010 ; Raymond, S. N & all ,2020)

2.2.1 Protoplanetary Disks

Protoplanetary disks (PPDs) are rotating disks of circumstellar material (gas and dust) that coexist with a nascent star during its formation and evolution resulting in a mature planetary system like the Solar System. Supplying material to both the central protostar and upcoming protoplanets, PPDs dictate the evolution of both. Therefore, studying the planet forming regions in PPDs is crucial to understanding planet formation. The star formation process naturally produces PPDs as illustrated by figure 2.1. Vast nebulae incubate cold gases into dense filamentary structures which condense into warm cores. These cores of concentrated prestellar material are initially shrouded by an optically thick envelope of dust and gas. Under these conditions, the gravitational collapse of infalling materials conserves the net angular momentum of its natal cloud by settling into a rotating disk of dust and gas around the central protostar. The material remains in the disk as a reservoir for both star and planetesimal formation lasting anywhere from $\sim 10^6$ to $> 10^7$ years, thus imposing an upper time limit on the formation of a planetary system (Li et al. 2014).

The structure of PPDs is an observationally tested design which holds for a majority of disks around pre main sequence (PMS) stars. Angular momentum transport and stellar irradiation fundamentally and energetically set the stage for PPD structure and dynamics. Stellar accretion brings circumstellar material inward while photoevaporation depletes the inner disk. Under these conditions, other evolutionary processes also interact with inner disk material: protostellar outflows and jets (Herczeg et al. 2011, Banzatti et al. 2015a) coupled with magnetohydrodynamic (MHD) winds (Ercolano and Pascucci 2017). A PPD will evolve by accreting material on the central star or dynamic clearing by planet growth. The relationship shared between PPDs and planets cannot yet be fully understood without imposing constraints (Sanchez, M. A. 2021).

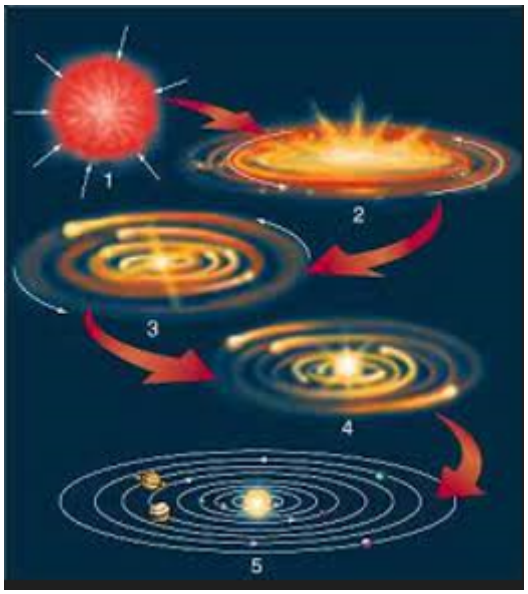

Figure 2.1: Solar System formation [79].

where each stage represents, (a) Nebular cloud collapse initiating star formation. (b) YSO material accretion and accumulation into a disk structure. (c) First stages of planet formation in the PPD. (d) Planetesimals form and grow due to PPD evolution. (e) Complete gas disk dissipation. (f) Final stage of planet formation (Sanchez, M. A. 2021).

Composition

The protoplanetary disk is mainly composed of gas, hydrogen and helium 99% in majority. However, even if the dust represents only about 1% of the mass of the disk, it plays a role at least as important as the gas itself. Functioning as a catalyst for certain reactions (eg the formation of H2), dust is also an essential element of disk chemistry. At short wavelengths, the dust grains dominate the opacity of the disk. At millimeter wave lengths In particular, dust plays an essential role in heating gas. Indeed, it absorbs stellar radiation ($\sim 1\mu$m) and re-emits thermal radiation at longer wavelength. The gas is also heated by the photoelectric effect, produced by the interaction of UV radiation and the surface of the small grains. When the density of the medium is high, the numerous collisions between the grains and the molecules represent the main source of heating of the gas in the molecular layer. Composed mainly of carbon and silicates, the grains of dust are less than 0.1μm in size in the youngest objects and the interstellar medium (Draine, 2003). In the cold regions of the disk, the grains are surrounded by a mantle of ice, resulting from the condensation of gases (Pericaud, J. 2016).

In addition, dust is also responsible for the opacity of the disk, that is to say its ability to let light through or not. A crucial parameter of protoplanetary disk models is the opacity of the disk which represents the absorption of incident radiation by a cell of gas. The latter depends mainly on the chemical composition of the dust except when the temperature becomes sufficiently high for all of the dust to sublimate, generally beyond 1500 K (Pollack et al., 1994), the opacity then being governed by the gas molecules (Cossou, C. 2013).

2.2.2 Formation of the telluric planets of the solar system

The formation of the planets of the solar system, from dust to their current size, would have taken a few tens of millions of years and would have taken place in three major phases (Kallenbach et al. 2000). First, gas and dust of the order of a micrometer form the protoplanetary disk, and accumulate forming planetesimals of kilometer sizes revolving around the proto-sun. Then, these planetesimals come together forming protoplanets. Eventually, these protoplanets collide, forming the current planets of the solar system.

Formation of planetesimals

At the start of the formation of terrestrial planets. Dust grains aggregate together during collisions, forming larger objects ranging in size from millimeters to centimeters (Weidenschilling 2000). These objects form chondrites by heating up in the solar nebula (Chambers 2010). In this nebula, the dust grains agglomerate with the chondrites forming a large cloud which mixes strongly with the gases, and orbits together around the proto-sun (Kallenbach et al. 2000). The movement of the components of this cloud is probably turbulent in the protoplanetary disk. This turbulence influences gravitational instability and in turn limits the direct formation of planetesimals. Despite the influence of turbulence, the particles stick together by collisions forming planetesimals of kilometric sizes. This process occurs rapidly on a timescale of a few thousand years to a few million years (Rubie et al. 2015, Chambers 2010, Laibe et al. 2008, Kallenbach et al. 2000). Mutual gravitational interactions increase between large objects, resulting in the growth of large objects at the expense of small objects. So planetesimals are the result of gravitational instabilities and collisions between particles, which will come together forming protoplanets.

Formation of protoplanets

After the formation of planetesimals, the speed and force of collisions between objects become more important. This speed depends strongly on the size of the particles. Low velocity collision results in coalescence, while high velocity collision promotes some fragmentation (Chambers 2010). While the gravitational field of the object increases monotonically with the size of the object, it is therefore necessary for the fragments to have a high speed to escape. Otherwise, they will regroup with the parent particles. So, with the increase in the size of the object, the fragmentation becomes limited.

However, the formation of planetary embryos from killometer-sized planetesimals in a protoplanetary disk occurs in two consecutive steps. During the first stage, called "Runaway growth", large planetesimals grow faster than small planetesimals and their mass ratio grows exponentially during protoplanet formation (Kokubo and Ida 1995). At this stage of growth, the random relocity of the planetesimals increases by the mutual gravitational interaction which, in turn, gradually changes the orbit of the planetesimals. When the larger bodies of the protoplanetary system become massive enough to control the velocity distribution of the smaller planetesimals, the "Runaway" stage of growth stops (Chambers 2010). Thus, the "Runaway" growth stage of planetesimal-protoplanetary systems results in a large number of planetesimals and a small number of protoplanetaries. Due to the ineffectiveness of dynamic friction and the increased rate of dispersal between planetesimals, the growth phase transitions from "Runaway" to the second "Oligarchic" growth stage. In this growth phase, the protoplanets resulting from the "Runaway" growth phase dominate the neighboring smaller planetesimals. Because of this, the protoplanets and planetesimals in the system begin to interact with each other.

During the growth of the protoplanets during this phase, the dynamic friction decreases and the orbit of the protoplanets moves away from the circular shape, which leads to stopping the "Oligarchic" growth (Chambers 2010). Growth from planetesimals to protoplanets is estimated at around $10^5 - 10^6$ years (Wetherill and Stewart 1993, Kokubo and Ida 2000). At the end of the "oligarchic" stage of growth, the Mars-sized protoplanets move in intersecting orbits, collide and come together to form the planets of the solar system (Agnor et al. 1999, Kokubo and Genda 2010). This growth phase begins by drawing the swarm of smaller planetesimals remaining into the system and forming larger objects. The eccentricities of these embryos increase rapidly due to mutual gravitational disturbances between them, resulting in an overlapping of their orbits which allows impacts between them (Chambers and

Wetherill 1998). These impacts produce oscillations in the eccentricity and inclination which prevent the isolation of the embryos (Qaddah, B. 2019).

2.2.3 Formation of the Giant-Planets

Giant planets might have rocky cores of 10-20 M Earth (Stevenson, D. J. 1982 ; Guillot et al.,2004), that is significantly larger mass than our terrestrial planets. Therefore, the formation and timescale differ very much within and beyond the snowline. terrestrial planet formation is dominated by collisions of rocky objects and lasts presumeably for several million years. Giant planet formation has to end when the gaseous circumstellar disk dissipates (3-5 Myrs), therefore interestingly, gas-giants are believed to form faster than rocky planets. There are two main giant planet formation scenarios: **disk instability and core accretion**.

Giant Planet Formation via Core Accretion

Beyond the ice line, the embryos can probably reach several times the mass of the Earth. From 10 earth masses, the gravity of the embryo is sufficient to retain gas from the disk, and constitute an envelope of hydrogen and helium. For this reason, these planetary embryos are also called hearts (Dutrey, A. 2008).

The accretion of a significant layer of gas takes time: the pressure opposes the collapse of the gas on the core. For several million years, accretion continues slowly: the more the core acquires mass by accumulating solids, the more it is able to retain a large envelope of gas, which cools slowly. The envelope should not be confused with the atmosphere of a planet: it is much larger and less dense. A mini-disk surrounds the planet, through which it accretes gas, like the star. This phase lasts several million years, which may be too long given the lifespan of a disk. It can however be accelerated if the migration allows the solid core to grow faster, by seeking new solids outside its now empty area of influence (ontmerle, T. and all 2006 ; Papaloizou, J. C. B.and all 2007).

If the mass of the envelope reaches about 100 Earth masses, the pressure can no longer sustain it, and the envelope collapses. All the available gas is then absorbed by the planet, which quickly reaches the mass of Jupiter, or even exceeds it. As nothing (or almost) can stop the collapse, we see that the quantity of gas available will determine the final mass of the planet. However, we have seen that the gas density in the protoplanetary disk decreases over time. This could explain Saturn's relatively moderate mass: if it formed later than Jupiter, there was less gas available. In addition, Saturn and Jupiter are enriched in heavy

elements compared to the solar composition (and therefore to the initial proto-solar disk), which could come from the fact that they were formed from a disk that had already lost a good part of its gas (Gomes, R and all 2005).

If the critical mass for collapse is not reached before the disk of gas dissipates completely, the planet will never become a gas giant, but will remain as a large core of rocks and ice of a fifteen times the mass of the Earth, surrounded by a little hydrogen and helium. This is probably what happened for Uranus and Neptune.

We should also mention an alternative to the core accretion model described above: **gravitational instability**. According to this idea, certain parts of the disk collapse in on themselves under the effect of their own gravity, like the molecular cloud which gave birth to the star. The result of this rapid collapse would be a giant planet. However, it seems difficult that the conditions of density and temperature are met in the disk for such a collapse to take place, and it could not explain neither the enrichment of Jupiter and Saturn, nor the existence of Uranus and Neptune. Most planetary scientists agree that gravitational instability probably occurs only rarely, in the most distant parts of the disk, tens or even hundreds (of AU from the star) (Tsiganis, K. and all, 2005).

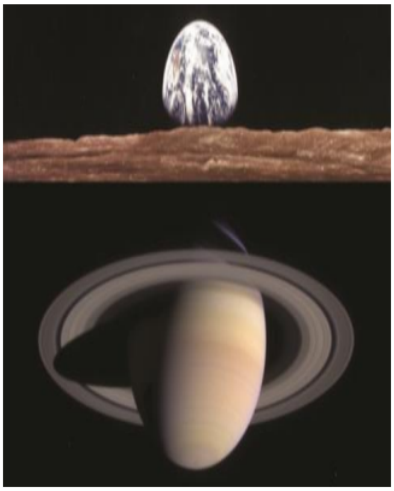

Figure 2.2: It shows two different categories of planets. Terrestrial planets are small and dense while giant planets are large, sparse, and surrounded by many satellites (Credit NASA/Space Telescope Science Institute)

2.3 Planetary migration

A planet embedded in a disk of gas or small particles modifies the distribution of material in its vicinity, causing the planets orbit to change. Gravitational interaction with a disk can

excite or damp a planets orbital eccentricity and can also alter the size of the planets orbit, causing the planet to migrate toward or away from its star. These changes can occur rapidly on timescales much shorter than the time required to form a planet. The phenomenon of planetary migration has been known for decades (Goldreich & Tremaine 1980, Lin & Papaloizou1986).

The direction and rate of migration vary depending on the mass of the planet and the local properties of the gas disk Type-I migration affects Earth-mass planets (with a mass less than about 50M$\oplus$), where the planet-disk interaction can be treated using linear approximations. The resulting migration rate is proportional to the mass of the planet and the surface density of the disk (Ward 1997). Type-II migration affects Jupiter-mass planets. Here, the planet is massive enough to clear an annular gap in the disk a round its orbit, and the planet's motion be comestied to the viscous evolution of the disk (Ward 1997).

2.3.1 Resonant Torques

The total angular momentum exchange between disk and planet can be expressed as the sum of the torques exerted at discrete resonances in the disk. These resonances correspond to the points in the disk where the planet excites waves, which almost invariably take the form of spiral density waves. In general, resonances occur when a characteristic frequency of the planet matches a frequency in the disk. In a circular disk there are two important types of **resonance corotation** and **Lindblad resonances** .

If the angular velocity of planet is $\Omega_{\rm p}$ and the angular velocity of disk Ω(R), the co-rotation resonance is found where

$$\Omega(\mathrm{R}) = \Omega_{\rm p} \tag{2.1}$$

If the disk is Keplerian (i.e., if we neglect gas pressure and self-gravity), then the co-rotation resonance is found at the planet's orbital radius. The condition for Lindblad resonances is similar: where the angular velocity of the gas Ω(R) and that of the angular velocity of planet $\Omega_{\rm p}$ are related by

$$m\left[\Omega(R) - \Omega_p\right] = \pm k(R) \quad m \in Z \tag{2.2}$$

where m is mass of disk $\kappa(R)$ is formally the epicyclic frequency (Papaloizou et al. 2007), but in a Keplerian disk $\kappa(R) = \Omega(R)$ and the Lindblad resonances are found at radii

$$R_L = \left(1 \pm \frac{1}{m}\right)^{2/3} a \tag{2.3}$$

A circular Keplerian disk therefore has a single co-rotation resonance, and a "comb" of Lindblad resonances that "pile up" close to the planet

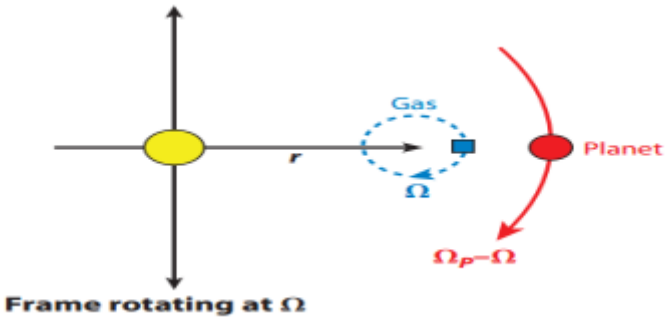

Figure 2.3: Schematic diagram showing the motion of a parcel of gas and a planet in a reference frame rotating at the average orbit al velocity of the gas $\Omega(R)$.

he gas (blue) undergoes small epicycles in the rotating frame owing to the eccentricity of its orbit. The planet (red) moves at an angular velocity of $\Omega_p - \Omega(R)$ in the rotating frame. A corotation resonance occurs when $\Omega(\mathrm{R}) = \Omega_\mathrm{p}$. A Lindblad resonance occurs when the gas undergoes an integer number of epicycles for every passage of the planet.
Spiral density waves are launched at Lindblad resonances, carrying angular momentum away from the planet to other regions of the disk. The disk outside the planet's orbit exerts a negative torque on the planet, where as the disk inside the orbit exerts apositive torque. In general, these torques are not equal. The outer Lindblad resonances lie closer to the planet than do the inner ones, especially when pressure gradients in the disk are taken into account (Papaloizou etal.2007). As a result, the outer torque is stronger, and the planet migrates toward the star. Interactions can also be important at the corotation resonance $\Omega(R) = \Omega_p$ where the gas and planet orbit at thes a merate. Forlow-mass planets, these torques are typically too small to offset the differential Lindblad torque except in regions where there is a strong surface density gradient (Papaloizouetal.2007).

2.3.2 Types of migrations

- **Type I migration**

  Most studies of type-I migration have considered a vertically isothermal disk. Recently, it has become apparent that migration changes substantially when radiative transfer within the disk is taken in to account (Kley & Crida2008, Paardekooper & Mellema

2006). If the opacity of the disk is similar to that of interstellar dust, planets with masses $< 50M\oplus$ are likely to migrate outward owing to increased corotation-torques (Kley &Crida2008). If the opacity is lower, owing to dust coagulation, migration will be inward in the outer disk and outward in the inner disk (Paardekooper & Mellema2006), possibly leading to a favored location for planets to form and survive.

Corotation torques and differential Lindblad torques are both altered in regions where the surface density of the disk changes rapidly with distance from the star. A steep surface density gradient will be present at the inner edge of the disk and also at the inner edge of a dead zone. Outward migration is likely at each of these locations, even if the over all migration trend is inward (Masset et al. 2006b, Morbidelli et al. 2008). This is known as Type I migration and occurs on a short time scale relative to the lifetime of the accretion disk.

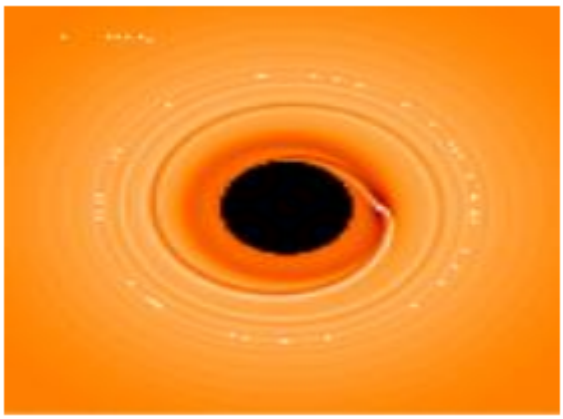

Figure 2.4: shows the first type of migration.

- **Type II migration**

  Type II migration occurs for massive planets with masses comparable to MJ or larger. Because of angular momentum deposition in the disk, those planets open an annular gap in the protoplanetary disk at the location of the planet where the density is significantly reduced. In this case the migration speed is slowed down from the linear rate because of the reduced mass available near the planet. During the migration process the gap created by the planet will have to move with the planet through the disk. Hence, it is often assumed that in an equilibrium situation the gap moves exactly with the viscous accretion velocity of the disk, and that the planet is locked in the middle of the gap to maintain torque equilibrium (Ward 1982, 1997; Lin & Papaloizou 1986).

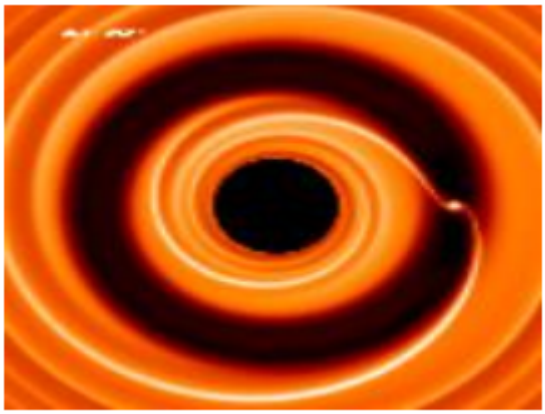

Figure 2.5: shows the second type of migration.

- **Type III migration**

  Between these two regimes, some interesting things happen. Planets with masses comparablento that of Saturn can undergo a third kind of migration in massive disks. In this situation, the planet clears a partial gap in the disk. The remaining gas close to the planet exerts a corotation torque that grows in proportion to the migration speed. This can generate a positive feedback, leading to very rapid inward or outward migration (Masset & Papaloizou2003) Currently, it is unclear whether the conditions needed to generate type-III migration are likely to occur in practice (DAngelo & Lubow2008). Under certain conditions, this mode can lead to rapid inward migration (Masset and Papaloizou 2003). Finally, when the mass of the planet becomes comparable to that of the disk, the inertia of the planet begins to play a role in its migration and retard

the variations in migration, normally governed by the evolution of the gas disk (Crida and Morbidelli 2007).

Figure 2.6: shows the third type of migration.

Chapter 3

Evolution of a protoplanetary disk

Contents

3.1 Introduction

In order to get insight into how viscosity acts to transport angular momentum outwards, following (Lynden-Bell & Pringle 1974, Pringle 1981) and (Frank et al. 2002) , let us start with the simplest model of accretion disk a thin gaseous disk rotating around a central star with considerably larger mass M so that disk self-gravity can be neglected. We adopt cylindrical polar coordinates (r, φ, z) with central star at the origin. The disk lies in the $z = 0$ plane. The thin disk approximation implies that the disk scale height $H = cs/\Omega$, where again cs is the sound speed and Ω is the angular velocity of disk rotation (this expression for H is easily obtained from the vertical hydrostatic equilibrium) is much smaller than the distance from the central star $H/r << 1$.

In protoplanetary disks, for example, this ratio istypically $\mathrm{H/r} \sim 0.05 - 0.1$ and in AGN disks it is even smaller, $\mathrm{H/r} \sim 0.001 - 0.01$, so the condition for thin disk limit is more or less satisfied. Many studies are limited just to this approximation, because it helps to understand basic physical processes and instabilities, which can be then generalized to thick disk. In this case basic hydrodynamic equations are integrated in the vertical direction to

yield two dimensional equations. The disk is then characterized by its surface density Σ, which is a mass per unit surface area of the disk, given by integrating the gas density in the vertical z-direction. The thin disk approximation is equivalent to requiring that the sound speed cs is much less than the rotation velocity $r\Omega(r)$, or the disk flow is strongly supersonic. From this condition one can readily find that the rotation velocity is given by Kepler law (Pringle 1981, Frank et al. 2002):

$$\Omega(r) = \Omega_K(r) = \left(\frac{GM}{r^3}\right)^{1/2}. \tag{3.1}$$

In this case a disk is said to be rotationally supported, i.e., gravity force exerted by the central star is balanced by centrifugal force due to rotation. Because of the thin disk approximation, the pressure gradients tum out to be much smaller than these two forces. The disk being accreting implies that in addition to Keplerian velocity it also possesses radial, or 'drift' velocity vr directed to the central star. As will be clear below, this radial velocity is much smaller than Keplerian velocity so the ordering $v_r \ll c_s \ll r\Omega K$ holds and is directly related to the viscosity parameter v implying that accretion takes place on time scales longer than dynamical time Ω^{-1}

Below is a list of all the variables describing the state of the disk, as well as the equation for the evolution of the accretion disk. Based on the conservation of mass and angular momentum, we then show the behavior of the planet's angular momentum in PPD. Finally, by following the various steps, we solve the evolution equation of a protoplanetary disk.

3.2 Accretion parameters governing disk structure

For deriving the general equations of disk structure, we follow the motion of an annulus of the disk and use the vertically integrated form in all equations, i.e. the surface density Σ instead of the physical density ρ Matter can flow into the annulus and out of it with a velocity v_r. We consider in the following an axisymmetric disk and assume that the surface density can be written in the general form of $\Sigma(r,t)$ which is an integral of the mass density $\rho(r,z)$ over the disk height z.

$$\Sigma(r,t) = \int_{-\infty}^{\infty} \rho(r,z)dz \tag{3.2}$$

The state of the disk at time t and in the vicinity of point r is mainly described by a characteristic temperature T (which is here the temperature at the equatorial plane $z = 0$); its surface density Σ and its local accretion rate dM/dt.

Vertical disk structure

The vertical (z-direction) disk structure is found by solving the equation of hydrostatic equilibrium

$$\frac{1}{\rho_{\rm gas}}\frac{\partial \mathrm{P}}{\partial z} = \frac{\partial}{\partial z}\left(\frac{GM_*}{\sqrt{r^2+z^2}}\right) \tag{3.3}$$

If the disk is vertically thin ($z \ll r$) and the gas temperature does not depend on z (i.e. avertically isothermal disk), The above equation can be integrated to give the vertical density structure,

$$\rho_{\rm gas}(r,z) = \rho_{\rm c}(r) e^{-z^2/\left(2H_{gas}^2\right)} \tag{3.4}$$

where $\rho_{\rm c}(r)$ is the density at the disk midplane.

The half-height of the disk H

The gas scale height is

$$H_{\rm gas} = \sqrt{\frac{KT_c r^3}{(\mu m_p G M_*)}} \tag{3.5}$$

where T_c is the midplane gas temperature. When we deal with the vertical hydrostatic equilibrium of the disk, we find:

$$H = \frac{C_s}{\Omega} \tag{3.6}$$

The angular velocity Ω

Assuming that the orbits of matter particles are circular and obey Kepler's laws, we have

$$\Omega = \left(\frac{GM}{r^3}\right)^{1/2} \tag{3.7}$$

G the gravitaion constant.

The pressure P

The total pressure P is broken down into gas pressure due to particles P_{gas} and radiation pressure due to photons $P_{\rm rad}$ We have:

$$\mathrm{P} = P_{\rm gas} + P_{\rm rad} = \frac{\rho}{\mu m_p} KT + \frac{1}{3} aT^4 \tag{3.8}$$

In these expressions: ρ is the average density in $[\mathrm{gcm}^{-3}]$; T is the gas temperature; k is Boltzmann's constant; m_p the mass of the proton; a is the radiation constant, it is $a = 7.564.10^{-15}$cgs. We have: $\left(\frac{K}{m_p}\right) = 8.31434.10^{7}$cgs

The speed of sound C_s

It is the speed of the adiabatic disturbances of density, we have:

$$C_s = \left(\frac{\Gamma_1 P}{\rho}\right)^{1/2} \tag{3.9}$$

Γ_1 is a quantity which depends on β and which is $5/3$ when $\beta = 1$ and $4/3$ when $\beta = 0$. To simplify, we ignore this constant and we set $\Gamma_1 = 1$.

The pressure indicator β

The parameter β is conventionally defined as the ratio of the gas pressure to the total pressure:

$$\beta = \frac{P_{\rm gas}}{P} \tag{3.10}$$

For $\beta = 1$, the gas pressure dominates and for $\beta = 0$, the radiation pressure.

The viscosity v

v is the kinematic viscosity, of turbulent origin, of the gas in $[\mathrm{cm}^2 S^{-1}]$.

$$v = \frac{2}{3} \alpha \mathrm{C_S H} \tag{3.11}$$

α is a phenomenological parameter whose value is unknown.

The accretion rate dM/dt

It is a local rate which therefore depends on r, it is ppsitive if the matter is accreted.

$$\dot{M} = -2\pi r \Sigma \mathrm{v}_r \tag{3.12}$$

We Consider a geometrically axisymmetric accretion disk whose mass density is $\Sigma(r,t)$. The gas in the disk moves in circular orbits with the local Keplerian velocity

$$v_\varphi(r) = r \cdot \Omega(r) \tag{3.13}$$

where $\Omega(r)$ is the angular velocity at radius r. Circular orbits are considered because a circular orbit at minimum energy for an angular momentum, and because the delay for energy loss (via viscous "friction") is very rapidly than the delay for redistribution of the angular momentum.

To clarify, "energy loss" means the conversion of roughly kinetic energy into random thermal energy (i.e. heat), which then cools via radiative emissions. (i.e. the photons carry energy, which we detect as disk luminosity). The kinetic energy basically, of course, comes from the gravitational potential energy of the gas. In addition to its orbital motion, the mass in the disk also flows slowly in the radial direction with velocity $v_r(r)$. A negative value of vr implies a flux towards the central mass. This should not be confused with the slow deviation of the inward radial velocity, $v_r(r)$ from the highly supersonic azimuthal velocity $v_\varphi(r)$.

3.3 The evolution of accretion disk

In order to determine how a disk evolves, we first consider mass and angular momentum conservation in a thin annulus. We assume that the disk is axisymmetric, with surface density $\Sigma(R)$

3.3.1 Conservation of mass

Accretion is a radial flow of gas, and we denote the radial velocity as $v_R(R)$; by convention, positive v_R is in the outward direction (accretion therefore has $v_R < 0$). We then consider an annulus at radius R with thickness ΔR. The rate of mass flow through the inner edge of the annulus is

$$\dot{M}_{\mathrm{inner}} = 2\pi \mathrm{R}\Sigma(\mathrm{R}) v_{\mathrm{R}}(R) \tag{3.14}$$

and the rate of mass flow through the outer edge of the annulus is

$$\dot{M}_{\rm outer} = 2\pi(\mathrm{R}+\Delta R)\Sigma(\mathrm{R}+\Delta R)v_{\rm R}(R+\Delta R) \tag{3.15}$$

The difference between these two quantities is the rate of change of mass in the annulus, so

$$2\pi \mathrm{R}\Delta \mathrm{R}\frac{\partial \Sigma}{\partial \mathrm{t}} = \dot{M}_{\rm inner} - \dot{M}_{\rm outer} \tag{3.16}$$

and we can substitute to find

$$\mathrm{R}\frac{\partial \Sigma}{\partial \mathrm{t}} = -\frac{(\mathrm{R}+\Delta R)\Sigma(\mathrm{R}+\Delta R)v_{\rm R}(R+\Delta R) - \mathrm{R}\Sigma(\mathrm{R})v_{\rm R}(R)}{\Delta R} \tag{3.17}$$

We can then take the limit $\Delta R \to 0$ to find

$$R\frac{\partial \Sigma}{\partial \mathrm{t}} + \frac{\partial}{\partial \mathrm{R}}\left(\mathrm{R}\Sigma v_{\rm R}\right) = 0 \tag{3.18}$$

which is the equation of mass continuity for a thin disk.

3.3.2 Conservation of angular momentum

If the orbital frequency is $\Omega(r)$ then the angular momentum per unit area is $R^2\Omega\Sigma$, and a similar analysis yields a corresponding equation for the conservation of angular momentum However, in this case we must consider the effects of torques on the annulus, so the equation for angular momentum conservation becomes

$$R\frac{\partial}{\partial t}\left(R^2\Omega\Sigma\right) + \frac{\partial}{\partial R}\left(R^2\Omega R\Sigma v_R\right) = \frac{1}{2\pi}\frac{\partial \mathrm{G}}{\partial \mathrm{R}} \tag{3.19}$$

Here $G(R)$ is the torque: it appears as a radial derivative, as we are interested only in the differential torque across the annulus. (If the torque is constant across the annulus then $\partial G/\partial R = 0$ and there is no net change in the angular momentum.)

At this point we can make little further progress without making some assumptions about the origin of the torque G. The simplest assumption is to assume that the torques are due to an ordinary fluid viscosity. in thatcase, the shearing nature of a Keplerian disk will result in viscous torques between adjacent annuli (as they have different azimuthal

velocities). The viscous torque G is therefore

$$\mathrm{G} = 2\pi \mathrm{R} \cdot \mathrm{R}\nu\Sigma \cdot \frac{\partial \mathrm{G}}{\partial \mathrm{R}} R \tag{3.20}$$

Here ν is the kinematic viscosity. The second term is the viscous force per unit lengh, the first term comes from integrating around the anmulus, and the final factor of R is the lever arm of the torque. The fact that $G \propto d\Omega/dR$ reflects the fact that the viscous torque is only nonzero if the disk has differential rotation. (If Ω is constant, the disk rotates as a solid body and there are no viscous torques between adjacent annuli.)

$$\frac{\partial}{\partial \mathrm{t}}\left(R^2\Omega\Sigma\right) + \frac{1}{R}\frac{\partial}{\partial \mathrm{R}}\left(R^3\Sigma v_{\mathrm{R}}\Omega\right) = \frac{1}{\mathrm{R}}\frac{\partial}{\partial \mathrm{R}}\left(R^3 v\Sigma\frac{\partial\Omega}{\partial \mathrm{R}}\right) \tag{3.21}$$

which is the equation for angular momentum conservation in a viscous accretion disk. We can then combine, we find

$$\frac{\partial\Sigma}{\partial \mathrm{t}} = -\frac{1}{R}\frac{\partial}{\partial \mathrm{R}}\left[\frac{1}{\dfrac{\partial}{\partial R}\left(R^2\Omega\right)}\frac{\partial}{\partial \mathrm{R}}\left(R^3\nu\Sigma\frac{\partial\Omega}{\partial \mathrm{R}}\right)\right] \tag{3.22}$$

3.4 Evolution equation of protoplanetary disk

The two equations (conservation of mass equation) (3.18) and (conservation of angular momentum equation) (3.21) can be combined to give a single equation for the evolution of surface density.(Appendex B)

This is the general equation governing the evolution of a viscous accretion disk with an arbitrary rotation profile $\Omega(R)$ If we further assume that the disk is in Keplerian rotation we can substitute $\Omega = \sqrt{GM_*/R^3}$ and find

$$\frac{\partial\Sigma}{\partial \mathrm{t}} = \frac{3}{R}\frac{\partial}{\partial \mathrm{R}}\left[R^{1/2}\frac{\partial}{\partial \mathrm{R}}\left(\nu\Sigma R^{1/2}\right)\right] \tag{3.23}$$

This equation is one of the key equations in the theory of accretion disks, its temporal evolution being determined only by the kinematic viscosity ν. In general, ν is a function of the local variables in the disk, which are Σ, r and t. Thus, this equation is a nonlinear diffusion equation for Σ and the viscous evolution of accretion disks depends on the behavior

of the viscosity ν.

We present models of giantplanet migration in evolving protoplanetary disks, where the disks evolve to viscous transport of angular momentum by the central star. Planets migrate due to tidal interaction with the disk(in the Type II migration regime), and the disk is also subject to tidal torques from planets. The equation that describes the coupled evolution of a protoplanetary disk and planet (Lin & Papaloizou 1986) is

$$\frac{\partial \Sigma}{\partial t} = \frac{1}{R}\frac{\partial}{\partial R}\left[3R^{1/2}\frac{\partial}{\partial R}\left(\nu\Sigma R^{1/2}\right) - \frac{2\Lambda\Sigma R^{3/2}}{(GM)^{1/2}}\right] \tag{3.24}$$

Where $\Sigma(R,t)$ is the disk surface density, t is time, R is cylindrical radius, ν is the kinematic viscosity, and M is the stellar mass. The first term on the right hand side describes ordinary viscous evolution of the disk (Lynden-Bell & Pringle 1974; Pringle 1981), and The second term describe show the disk responds to the planejary torque.

Here Λ is the injection rate of angular momentum per unit mass into the disk. Following (Trilling et al. 1998; Armitage et al 2002), for a planet of mass $M_p = kM_*$, k is the ratio between the mass M_p of planet and that of the star, the shape of the torque distribution in the two regions:

$$\Lambda(R) = \begin{cases} \dfrac{-k^2 GM_*}{2R}\left(\dfrac{R}{\Delta_p}\right)^4 : & R < a \\ \dfrac{k^2 GM_*}{2R}\left(\dfrac{a}{\Delta_\rho}\right)^4 : & R > a \end{cases} \tag{3.25}$$

where

$$\Delta_p = \max(H, |R-a|)$$

(Δp) is equal to the greater of H and $|R-a|$ whereas H is the scale-height of the disk.

The prediction of the direction of migration by an analytical calculation is a bit difficult because a precise calculation of the torque (torque) is necessary. But in our case we are talking about massive planets, and we consider a geometrically stationary thin disk, with a viscosity in the form $\eta = s.r^n, \quad n < 2$.

The rotating accretion disk is axisymmetric around a star of mass M_*. The specific angular momentum transfer rate from the planet, of mass $M_p = kM_*$ to the disk is given by $\Lambda(r)$.

To better understand angular momentum behavior, we consider the following steps. For computational convenience, we introduced a set of dimensionless variables such that the cylindrical radius $x = R/a$ and the torque $l(x) = \frac{a^{3/2}}{\sqrt{GM}}\Lambda(R)$ and for the following application, we take $a = 2.5H$

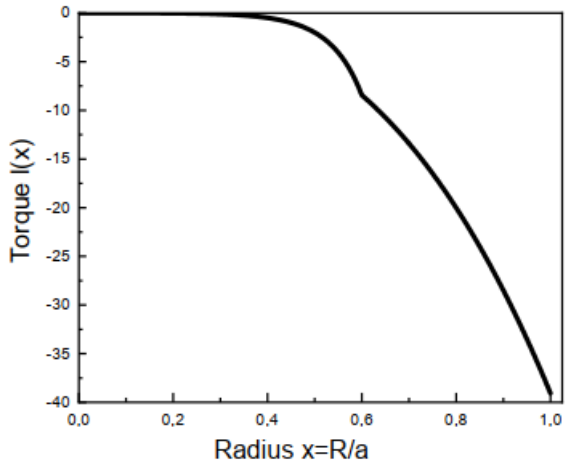

Figure 3.1: The torque in the region 1.

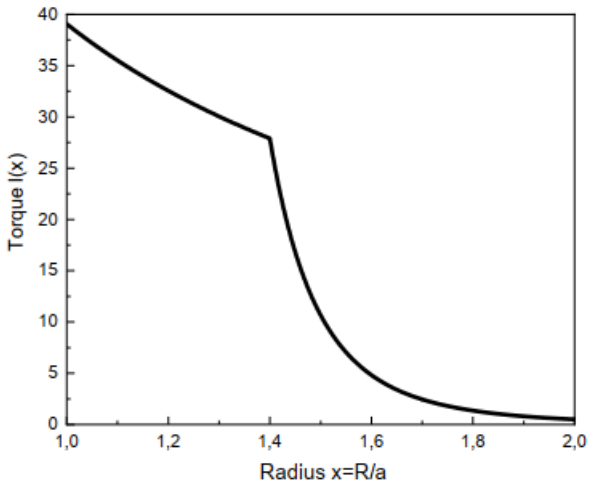

Figure 3.2: The torque in the region 2.

Torque describes the movement of a planet during it revolves around the star, and knowing the stress that occurs to the planet from the side of the star and how this stress affects the change of its orbit and its movement (approaching or moving away from the star) We notice the following through the curve of angular momentum changes in terms of :

- In the first region ($0 \leq x \leq 1$), the angular momentum is initially zero and gradually increases until it the minimum value ($x = 1$), after which the angular momentum increases at both ends until it reaches a maximum and a minimum value at the planet.
- In the second region ($1 \leq x \leq 2$), the angular momentum gradually decreases until it is negligible far from the planet.

3.5 Solution the evolution equation for a ppd

To find the equation for the evolution of the surface density for a PPd, we will limit ourselves to the steady state and start with equation (3.24)

$$\underbrace{R.\frac{\partial}{\partial t}\Sigma(R.t)}_{1} = \underbrace{\frac{\partial}{\partial R}\left[3R^{1/2}\frac{\partial}{\partial R}\left(\eta.\Sigma.R^{1/2}\right)\right]}_{2} - \underbrace{\frac{2}{(GM)^{1/2}}\frac{\partial}{\partial R}\left[\Lambda.\Sigma.R^{3/2}\right]}_{3}$$

we've got

$$\Sigma(R.t) = \varphi(R).\exp(-\lambda t) \tag{3.26}$$

Performing the derivatives with respect to R we find

The first side:

$$\frac{\partial}{\partial t}\Sigma(R.t) = -\lambda.\varphi(R).\exp(-\lambda t) \tag{3.27}$$

where λ is a constant.

The second side :

$$\begin{aligned} 3\frac{\partial}{\partial R}\left[R^{1/2}\frac{\partial}{\partial R}\left(\eta.\Sigma.R^{1/2}\right)\right] &= 3\frac{\partial}{\partial R}\left[\eta'.\varphi(R).R + \eta.\varphi'(R).R + \frac{1}{2}\eta.\varphi(R)\right]\exp(-\lambda t) \\ &= 3\Big[\eta''.\varphi(R).R + \eta'\left(\varphi'(R).R + \varphi(R)\right) + \eta'.\varphi'(R).R \\ &\quad + \eta\left(\varphi''(R).R + \varphi'(R)\right) + \frac{1}{2}\left(\eta'.\varphi(R) + \eta.\varphi'(R)\right)\Big]\exp(-\lambda t) \end{aligned} \tag{3.28}$$

The third side :

$$\begin{aligned} -\frac{2}{(GM)^{1/2}}\frac{\partial}{\partial R}\left[\Lambda.\Sigma.R^{3/2}\right] &= -\frac{2}{(GM)^{1/2}}\left[\Lambda'\varphi(R).R^{3/2} + \Lambda\left(\varphi'(R).R^{3/2} + \frac{3}{2}\varphi(R).R^{1/2}\right)\right]\exp(-\lambda t) \\ &= -\frac{2}{(GM)^{1/2}}\left[\Lambda'\varphi(R).R^{3/2} + \Lambda.\varphi'(R).R^{3/2} + \frac{3}{2}.\Lambda.\varphi(R).R^{1/2}\right]\exp(-\lambda t) \end{aligned} \tag{3.29}$$

Substituting equations (3.27), (3.28), and (3.29) into equation

$$
\begin{aligned}
-\lambda.R.\varphi(R).\exp(-\lambda t) = 3\Bigg[&\eta''.\varphi(R).R + \eta'\Big(\varphi'(R).R + \varphi(R)\Big) + \eta'.\varphi'(R).R \\
&+ \eta\Big(\varphi''(R).R + \varphi'(R)\Big) + \frac{1}{2}\Big(\eta'.\varphi(R) + \eta.\varphi'(R)\Big)\Bigg]\exp(-\lambda t)\frac{2}{\Big(GM\Big)^{1/2}} \\
&\Big[\Lambda'\varphi(R).R^{3/2} + \Lambda.\varphi'(R).R^{3/2} + \frac{3}{2}.\Lambda.\varphi(R).R^{1/2}\Big]\exp(-\lambda t) \qquad (3.30)
\end{aligned}
$$

$$
\begin{aligned}
0 = {} & 3\eta''.\varphi(R).R^2 + \frac{9}{2}\eta'.R\varphi(R) + 6\eta'\varphi'(R).R^2 + \frac{9}{2}\eta R\varphi'(R) \\
& + 3\eta.\varphi''(R).R^2 - \frac{2}{\Big(GM\Big)^{1/2}}\Lambda'\varphi(R).R^{5/2} \\
& - \frac{2}{\Big(GM\Big)^{1/2}}\Lambda.\varphi'(R).R^{5/2} - \frac{3}{\Big(GM\Big)^{1/2}}\Lambda.\varphi(R).R^{3/2} + \lambda.R^2.\varphi(R) \\
0 = {} & \frac{3\eta''}{3\eta.}.\varphi(R).R^2 + \frac{9\eta'}{2.3\eta.}.R\varphi(R) + \frac{6\eta'}{3\eta.}\varphi'(R).R^2 \\
& + \frac{9}{2.3\eta}\eta R\varphi'(R) + \varphi''(R).R^2 - \frac{2}{\Big(GM\Big)^{1/2}3\eta.}\Lambda'\varphi(R).R^{5/2} \\
& - \frac{2}{\Big(GM\Big)^{1/2}3\eta.}\Lambda.\varphi'(R).R^{5/2} - \frac{3}{\Big(GM\Big)^{1/2}3\eta.}\Lambda.\varphi(R).R^{3/2} + \frac{\lambda.}{3\eta.}R^2\varphi(R) \\
0 = {} & R^2\varphi''(R) + \Big[\frac{3}{2} + \frac{2\eta'}{\eta}R - \frac{2\Lambda}{\sqrt{GM}3\eta}R^{3/2}\Big]R\varphi'(R) \\
& + \Big[-\frac{\Lambda}{\sqrt{GM}\eta}R^{3/2} - \frac{2}{\sqrt{GM}3\eta.}\Lambda'.R^{5/2} + \frac{3\eta'}{2\eta}R + \frac{\eta''}{\eta}R^2 + \frac{\lambda.}{3\eta.}R^2\Big]\varphi(R) \\
0 = {} & \varphi''(R) + \Big[\frac{3}{2R} + \frac{2\eta'}{\eta} - \frac{2\Lambda}{\sqrt{GM}3\eta}R^{1/2}\Big]\varphi'(R) \\
& + \Big[-\frac{\Lambda}{\sqrt{R}\sqrt{GM}\eta} - \frac{2}{\sqrt{GM}3\eta.}\Lambda'.R^{1/2} + \frac{3\eta'}{2\eta R} + \frac{\eta''}{\eta} + \frac{\lambda}{3\eta}\Big]\varphi(R) \qquad (3.31)
\end{aligned}
$$

or again, by posing

$$
R = ax, \quad \varphi(R) \to u(x), \quad \eta(R) \to \nu(x) \qquad (3.32)
$$

Where $\eta(R) = SR^n$

We find

$$\begin{aligned}
0 &= \frac{d^2\varphi(R)}{dR^2} + \left[\frac{3}{2R} + \frac{2\eta'}{\eta} - \frac{2\Lambda}{\sqrt{GM}3\eta}R^{1/2}\right]\frac{d\varphi(R)}{dR} \\
&\quad + \left[-\frac{\Lambda}{\sqrt{R}\sqrt{GM}\eta} - \frac{2}{\sqrt{GM}3\eta.}\frac{d\Lambda}{dR}.R^{1/2} + \frac{3}{2R}\frac{d\eta}{\eta dR} + \frac{d^2\eta}{\eta dR^2} + \frac{\lambda}{3\eta}\right]\varphi(R) \\
0 &= \frac{d^2u(x)}{a^2dx^2} + \left[\frac{3}{2ax} + \frac{2d\nu}{a\nu dx} - \frac{2\Lambda\sqrt{a}}{\sqrt{GM}3\nu}x^{1/2}\right]\frac{du(x)}{adx} \\
&\quad + \left[-\frac{\Lambda}{\sqrt{a}\sqrt{x}\sqrt{GM}\nu} - \frac{2}{\sqrt{GM}3\nu.}\frac{d\Lambda}{adx}\sqrt{a}\sqrt{x} + \frac{3d\nu}{2a^2x\nu dx} + \frac{d^2\nu}{a^2\nu dx^2} + \frac{\lambda}{3\nu}\right] \\
&\quad u(x)
\end{aligned} \tag{3.33}$$

multiply by a^2

$$\begin{aligned}
0 &= \frac{d^2u(x)}{dx^2} + \left[\frac{3a}{2x} + \frac{2ad\nu}{\nu dx} - \frac{2\Lambda a^2\sqrt{a}}{\sqrt{GM}3\nu}x^{1/2}\right]\frac{du(x)}{adx} \\
&\quad + \left[-\frac{\Lambda a^2}{\sqrt{a}\sqrt{x}\sqrt{GM}\nu} - \frac{2a^2}{\sqrt{GM}3\nu.}\frac{d\Lambda}{adx}\sqrt{a}\sqrt{x} + \frac{3a^2d\nu}{2a^2x\nu dx} + \frac{a^2d^2\nu}{a^2\nu dx^2} + \frac{\lambda a^2}{3\nu}\right]u(x) \\
0 &= \frac{d^2u(x)}{dx^2} + \left[\frac{3}{2x} + \frac{2d\nu}{\nu dx} - \frac{2\Lambda a\sqrt{a}}{\sqrt{GM}3\nu}x^{1/2}\right]\frac{du(x)}{dx} \\
&\quad + \left[\frac{3}{2x\nu}\frac{d\nu}{dx} + \frac{d^2\nu}{\nu dx^2} - \frac{\Lambda a^{3/2}}{\sqrt{x}\sqrt{GM}\nu} - \frac{2a^{3/2}\sqrt{x}}{\sqrt{GM}3\nu.}\frac{d\Lambda}{dx} + \frac{\lambda a^2}{3\nu}\right]u(x) \\
0 &= \frac{d^2u(x)}{dx^2} + \left[\frac{3}{2x} + 2\frac{\nu'}{\nu} - \frac{2\Lambda a\sqrt{a}}{\sqrt{GM}3\nu}x^{1/2}\right]\frac{du(x)}{dx} \\
&\quad + \left[\frac{3}{2x}\frac{\nu'}{\nu} + \frac{\nu''}{\nu} - \frac{2a^{3/2}\sqrt{x}}{\sqrt{GM}3\nu.}\frac{d\Lambda}{dx} - \frac{\Lambda a^{3/2}}{\sqrt{x}\sqrt{GM}\nu} + \frac{\lambda a^2}{3\nu}\right]u(x)
\end{aligned} \tag{3.34}$$

we put

$$l(x) = \frac{\Lambda a^{3/2}}{(GM)^{1/2}} \tag{3.35}$$

$$\underline{\lambda} = \lambda a^2 \tag{3.36}$$

We get

$$\begin{aligned}
0 &= \frac{u''(x)}{u(x)} + \left(\frac{3}{2x} + 2\frac{\nu'(x)}{\nu(x)} - \frac{2\sqrt{x}}{3\nu(x)}l\ (x)\right)\frac{u'(x)}{u(x)} \\
&\quad + \left(\frac{3}{2x}\frac{\nu'(x)}{\nu(x)} + \frac{\nu''(x)}{\nu(x)} - \frac{2\sqrt{x}}{3\nu(x)}l\ '(x) - \frac{l\ (x)}{\sqrt{x}.\nu(x)} + \frac{\underline{\lambda}}{3\nu(x)}\right)
\end{aligned} \tag{3.37}$$

3.6 Conclusion

Based on the basic equations (conservation of mass - conservation of angular momentum) and as a result of the tidal interaction that occurs between the disk and the planet, the disk is also subject to the tidal torque of the planet. We obtain the equation for the co-evolution of the planet and the protoplanetary disk. The second term of this equation contains a rate factor. Transfer of angular momentum. After deriving both sides of the equation and changing the variable, we obtain the general solution to the differential equation for the evolution of a protoplanetary disk and a planet.

Chapter 4

Discussion of the surface density behavior in a(PPD):the first method

Contents

4.1 Introduction

The general approach involves studying the evolution of the protoplanetary disk and planet. We will first find the general solution of the differential equation (3.37) .which will lead us to the analytical solution of the surface density evolution.

$$\begin{aligned} 0 \;=\; & \frac{u''(x)}{u(x)} + \left(\frac{3}{2x} + 2\frac{\nu'(x)}{\nu(x)} - \frac{2\sqrt{x}}{3\nu(x)} l\,(x) \right) \frac{u'(x)}{u(x)} + \\ & \left(\frac{3}{2x}\frac{\nu'(x)}{\nu(x)} + \frac{\nu''(x)}{\nu(x)} - \frac{2\sqrt{x}}{3\nu(x)} l\,'(x) - \frac{l\,(x)}{\sqrt{x}.\nu(x)} + \frac{\underline{\lambda}}{3\nu(x)} \right) \end{aligned}$$

The equation (3.37) has a generic form as

$$0 = u''(x) + f_1(x)u'(x) + f_0(x)u(x) \tag{4.1}$$

where $f_0(x)$ and $f_1(x)$ are respectively given by

$$f_0(x) = \frac{3}{2x}\frac{\nu'}{\nu} + \frac{\nu''}{\nu} - \frac{l\ (x)}{\sqrt{x}.\nu} - \frac{2\sqrt{x}}{3\nu}l\ '(x) + \frac{\lambda}{3\nu} \tag{4.2}$$

$$f_1(x) = \frac{3}{2x} + 2\frac{\nu'}{\nu} - \frac{2\sqrt{x}}{3\nu(x)}l\ (x) \tag{4.3}$$

In order to solve the equation (4.1) we put the change

$$u(x) = \frac{w\ (x)}{q\ (x)} \tag{4.4}$$

After simplifications, it is traight forward and easy to get

$$\frac{w''(x)}{w\ (x)} + \left(f_1(x) - \frac{2q'(x)}{q\ (x)}\right)\frac{w'(x)}{w\ (x)} + \left[f_0(x) - \frac{q''(x)}{q\ (x)} + 2\left(\frac{q'(x)}{q\ (x)}\right)^2 - f_1(x)\frac{q'(x)}{q\ (x)}\right] = 0 \tag{4.5}$$

By using

$$f_1(x) - 2\frac{q'(x)}{q\ (x)} = \frac{g}{x} \tag{4.6}$$

where g is a constant to be determined later. When we replace f_1 in the last equation, we can find $q(x)$, that is to say

$$q\ (x) = \exp\left(\frac{1}{2}\int^x f_1\ (\theta)\, d\ \theta - \frac{g}{2}\ln(x)\right) \tag{4.7}$$

$$q'(x) = \left(\frac{f_1(x)}{2} - \frac{g}{2x}\right) q\ (x) \tag{4.8}$$

$$q''(x) = \left[\frac{f\ '(x)}{2} + \frac{g}{2x^2} + \left(\frac{f_1(x)}{2} - \frac{g}{2x}\right)^2\right] q\ (x) \tag{4.9}$$

then the equation (4.5) transforms to

$$0 = w''(x) + \frac{g}{x}w'(x) + G\ (x)w\ (x) \tag{4.10}$$

where g is a free transformation parameter that we will use for our convenience later and

$$G\ (x) = f_0(x) - \frac{q''(x)}{q\ (x)} + 2\left(\frac{q'(x)}{q\ (x)}\right)^2 - f_1(x)\ \frac{q'(x)}{q\ (x)} \tag{4.11}$$

or equivalently, after using the above expressions (4.7), (4.8), (4.9)

$$G\ (x) = f_0(x) - \frac{{f_1}'(x)}{2} - \frac{{f_1}^2(x)}{4} + \frac{g\ (g-2)}{4\ x^2} \tag{4.12}$$

We substitute the expressions of $f_0(x)$ and $f_1(x)$and ${f_1}'(x)$given above, we find

$$G\ (x) = \frac{3}{16x^2} + \frac{\lambda}{3\nu} - \frac{l\ (x)}{3\sqrt{x}\ \nu} - \frac{\sqrt{x}}{3\nu}\frac{d}{d\ x}l\ (x) - \frac{x}{9\nu^2}l^{\ 2}(x) + \frac{\sqrt{x}}{3}\frac{\nu'}{\nu}l\ (x) + \frac{g\ (g-2)}{4x^2} \tag{4.13}$$

where the viscosity $\nu(x) = sx^{\beta}$ and replace $\underline{\lambda}/(3s)$ by k^2

$$G\ (x) = \frac{3}{16x^2} + \frac{K^2}{x^{\beta}} + \frac{g\ (g-2)}{4x^2} - \frac{1}{3sx^{\beta-1/2}}\frac{d}{dx}l\ (x) - \frac{l^{\ 2}(x)}{9s^2x^{2\beta+1/2}} + \frac{(\beta-1)\ l\ (x)}{3sx^{\beta+1/2}} \tag{4.14}$$

Now, to solve the above differential equation (4.11), we discard the terms containing the torque $l(x)$ and its derivative in (4.12), that is to say

$$0 = \frac{d}{dx}l\ (x) + \frac{l^{\ 2}(x)}{3sx^{\beta-1/2}} - \frac{(\beta-1)}{x}l\ (x) \tag{4.15}$$

This constraint has a twist advantage: the first is to have a freely expression of the torque $l(x)$ that responds to the physical situation in our consideration. The second advantage is a purely mathematical issue that allows as to have analytically the solution of the differential equation (4.11). Indeed,wehave from the constraint (4.15):

$$l\ (x) = \frac{3Sx^{\beta-1}}{3CS + 2\sqrt{x}} \tag{4.16}$$

And

$$G\ (x) = \frac{3}{16\ x^2} + \frac{K^2}{x^{\beta}} + \frac{g(g-2)}{4x^2} \tag{4.17}$$

leading to get a simplified differential equation that governs $\omega(x)$ which is a Bessel's equation

$$0 = w''(x) + \frac{g}{x}w'(x) + \left(\frac{3}{16\ x^2} + \frac{K^2}{x^{\beta}} + \frac{4g(g-2)}{16x^2}\right)w\ (x) \tag{4.18}$$

$$0 = \omega''(x) + \frac{g}{x}\omega'(x) + (\frac{K^2}{x^\beta} + \frac{3+4g(g-2)}{16x^2})\omega(x) \tag{4.19}$$

$$x^2\omega''(x) + gx\omega'(x) + (k^2x^{2-B} + \frac{3+4g(g-2)}{16})\omega(x) = 0 \tag{4.20}$$

Its general solution is a linear combinaison of Bessel functions

$$w\ (x) = x^{\frac{1}{2}(1-g)}\left[C_1(k)J_p(ky) + C_2(k)Y_p(ky)\right] \tag{4.21}$$

We get

$$\begin{aligned} u(x) &= \frac{w(x)}{q(x)} = x^{(1-g)/2}\exp(-\frac{1}{2}\int^x f\ _1(z)dz + \frac{g}{2}\ln(x))\left(C_1(k)J_\nu(ky) + C_2(k)Y_\nu(ky)\right) \\ u(x) &= \frac{x^{-\frac{3}{4}-\beta}}{3CS^2}\left(\frac{2}{3}x + cs\sqrt{x}\right)w\ (x) \\ u(x) &= \frac{w\ (x)}{q(x)} = \frac{x^{-\frac{5}{4}}}{3CS}l^{-1}(x).x^{1/2(1-g)}\left[C_1(k)J_p(ky) + C_2(k)Y_p(ky)\right] \end{aligned} \tag{4.22}$$

where k is an arbitrary mode of solution and $\beta = 3/2$ and $y = \frac{1}{1-\beta/2}X^{1-\beta/2} = 4x^{1/4}$, $p = \frac{1}{2(2-\beta)} = 1$ and $J_p(ky)$, $Y_p(ky)$ are the well known Bessel's functions. The general solution is the summation over all possible modes k, that is to say

$$\Sigma(x,t) = \frac{x^{-\frac{5}{4}+\frac{1}{2}(1-g)}}{3C\ S\ l\ (x)}\int_0^\infty \left[C_1(k)J_1(ky) + C_2(k)Y_1(ky)\right]\exp(-3sk^2t)dk \tag{4.23}$$

we will discuss the behavior of surface density in a protoplanetary disk. We made appropriate considerations for each area ($x < 1$) and ($x < 1$) in order to better understand the surface density behavior.

4.2 Calculation of surface density in the region ($x < 1$)

Starting with the general solution of the equation for the evolution of a protoplanetary disk and a planet,

$$\Sigma(x,t) = F\ (x)\int_0^\infty \left[C_1(k)J_1(ky) + C_2(k)Y_1(Ky)\right]\exp(-3Sk^2t)dk \tag{4.24}$$

and beacause $Y_1(k\ y)$ diverge at zero, we discard it from the solution (4.2) Then in region $x < 1$ we have

$$\Sigma(x,t) = \frac{x^{-5/4}}{3CS} l^{-1}(x).x^{1/2(1-g)} \int_0^\infty C_1(k) J_1(ky)\ \exp(-3Sk^2t)dk \tag{4.25}$$

At initial time $t = 0$, we have (knowing that $y = 4x^{1/4}$)

$$\begin{aligned} \Sigma(x,0) &= \frac{x^{-5/4}}{3CS} l^{-1}(x).x^{1/2(1-g)} \int_0^\infty C_1(k) J_1(4\ k\ x^{1/4})\ dk \\ 3CS.\ l\ (x)\ .x^{5/4}\ .x^{1/2(g-1)}\ .\Sigma(x,0) &= \int_0^\infty C_1(k).k^{-1} J_1(4\ k\ x^{1/4})\ kdk \end{aligned} \tag{4.26}$$

we put $g = -3/2$, then

$$3CS.\ l\ (x)\ .\Sigma(x,0) = \int_0^\infty C_1(k).k^{-1} J_1(4\ k\ x^{1/4})\ kdk \tag{4.27}$$

or equivalently by substituting x by y

$x = \left(\frac{y}{4}\right)^4$

$$3CS.\ l\ ((\frac{y}{4})^4)\ .\Sigma\left((\frac{y}{4})^4, 0\right) = \int_0^\infty C_1(k).k^{-1} J_1(k\ y)\ kdk \tag{4.28}$$

If we consider at the initial time that the surface density is sharped at $x = 1/2$, that is to say

$$\Sigma(x,0) = \Sigma_0 \delta(x - 1/2) \tag{4.29}$$

then

$$3CS.\ l\ ((\frac{y}{4})^4)\ .\delta\left((\frac{y}{4})^4 - \frac{1}{2}\right) = \int_0^\infty C_1(k).k^{-1} J_1(k\ y)\ kdk \tag{4.30}$$

By applying the inverse Hankel transform, we can extract the coefficient $C_1(k)$ as

$$\begin{aligned} C_1(k).k^{-1} &= 3CS\int_0^4 l\ ((\frac{y}{4})^4)\ \delta\left((\frac{y}{4})^4-\frac{1}{2}\right)J_1(k\ y)\ y\ dy \\ \delta\left((\frac{y}{4})^4-\frac{1}{2}\right) &= 2^{3/4}\ \delta\left(y-4(\frac{1}{2})^{1/4}\right) \end{aligned} \tag{4.31}$$

After integrating over y and using the properties of delta Dirac function, we get

$$C_1(k).k^{-1} = 3.2^{3/4}\ CS.l\ \left(\frac{1}{2}\right).J_1(4k\ \left(\frac{1}{2}\right)^{1/4}).4\left(\frac{1}{2}\right)^{1/4} \tag{4.32}$$

$$C_1(k).k^{-1} = \mathbb{Q}\ CS.l\ \left(\frac{1}{2}\right).J_1(4k\ \left(\frac{1}{2}\right)^{1/4}) \tag{4.33}$$

Then the surface density, for $x<1$, becomes

$$\begin{aligned} \Sigma\,(x,t) &= \int_0^\infty \frac{x^{-5/4}}{3CS}l^{-1}(x).x^{1/2(1-g)}\ C_1(k)J_1(4\ k\ x^{1/4})\ \exp\left(-3Sk^2t\right)\ dk \\ \Sigma\,(x,t) &= \frac{1}{3CS}l^{-1}(x)\int_0^\infty C_1(k)J_1(4\ k\ x^{1/4})\ \exp\left(-3Sk^2t\right)\ dk \end{aligned} \tag{4.34}$$

After replacing $C_1(k)$ by its expression, we obtain

$$\begin{aligned} \Sigma\,(x,t) &= \mathbb{Q}.CS\frac{1}{3CS}l^{-1}(x)\int_0^\infty l\ \left(\frac{1}{2}\right)J_1(4k\ \left(\frac{1}{2}\right)^{1/4}).J_1(4\ k\ x^{1/4})\ \exp\left(-3Sk^2t\right)\ kdk \\ \Sigma\,(x,t) &= \frac{\mathbb{Q}\ l\left(\frac{1}{2}\right)}{3\ l\ (x)}\int_0^\infty J_1(4k\ \left(\frac{1}{2}\right)^{1/4})J_1(4\ k\ x^{1/4})\ \exp\left(-3Sk^2t\right)\ kdk \end{aligned} \tag{4.35}$$

or by using the formula (Tanaka, T. (2011)):

$$\int_0^\infty J_\upsilon\left(ky'\right).J_\upsilon\left(ky\right)\exp(-3sk^2t).k.dk = \frac{1}{6st}\exp\left(-\frac{y^2+y'^2}{12st}\right)I_p\left(\frac{yy'}{6st}\right) \tag{4.36}$$

$$\Sigma(x,t) = \frac{\mathbb{Q}\ l\left(\frac{1}{2}\right)}{3\ l\ (x)} \frac{1}{6St} \exp\left(-16\frac{(x)^{\frac{1}{2}} + (\frac{1}{2})^{\frac{1}{2}}}{12St\ (x)}\right)\ I_1\left(16\frac{(x)^{\frac{1}{4}}(\frac{1}{2})^{\frac{1}{4}}}{6St\ (x)}\right) \tag{4.37}$$

$$\Sigma(x,t) = \frac{\mathbb{Q}\ l\left(\frac{1}{2}\right)}{3\ l\ (x)} \frac{1}{6St\ (x)} \exp\left(-16\frac{\sqrt{x} + (\frac{1}{2})^{\frac{1}{2}}}{12St\ (x)}\right) I_1\left(16\frac{(x)^{\frac{1}{4}}(\frac{1}{2})^{\frac{1}{4}}}{6St\ (x)}\right) \tag{4.38}$$

we put:

$$\tau = \frac{3St}{\sqrt{x}}(2-\beta)^2 = \frac{3St}{4\sqrt{x}} \tag{4.39}$$

$$t\ (x) = \frac{4\sqrt{x}}{3S}\ \tau \tag{4.40}$$

$$3St = 4\sqrt{x}\ \tau \tag{4.41}$$

and by using the expression of the torque $l(x)$,we get a more simplified expression, for $x < 1$, of the surface density

$$l\ (x) = \frac{3S\sqrt{x}}{3CS + 2\sqrt{x}} \tag{4.42}$$

$$l\ (\frac{1}{2}) = \frac{3S\sqrt{1/2}}{3CS + 2\sqrt{1/2}} \tag{4.43}$$

$$\frac{l\ (\frac{1}{2})}{l\ (x)} = \frac{\sqrt{1/2}}{\sqrt{x}} \frac{3CS + 2\sqrt{x}}{3CS + 2\sqrt{1/2}} \tag{4.44}$$

$$= \frac{\sqrt{1/2}}{\left(3CS + 2\sqrt{1/2}\right)} \frac{3CS + 2\sqrt{x}}{\sqrt{x}} \tag{4.45}$$

So

$$\Sigma(x,t) = \frac{\mathbb{Q}\ l\left(\frac{1}{2}\right)}{3\ l\ (x)} . \frac{1}{6St\ (x)} \exp\left(-4\frac{\sqrt{x} + (\frac{1}{2})^{\frac{1}{2}}}{3St\ (x)}\right) I_1\left(8\frac{(x)^{\frac{1}{4}}(\frac{1}{2})^{\frac{1}{4}}}{3St\ (x)}\right) \tag{4.46}$$

$$\Sigma(x,\tau) = \frac{\mathbb{Q}}{6} \frac{l\left(\frac{1}{2}\right)}{l\ (x)} . \frac{1}{4\sqrt{x}\ \tau} \exp\left(-\frac{1+\sqrt{2x}}{\tau\sqrt{2x}}\right) I_1\left(2^{\frac{3}{4}} \frac{1}{\tau . x^{\frac{1}{4}}}\right) \tag{4.47}$$

our model stands on a choice of the constant$C$ and S,such that the torque $l(x)$ ful fills an acceptable behaviour

$$CS = -2/3 \tag{4.48}$$

$$S = 4/15 \tag{4.49}$$

that is to say the torque $l(x)$ has the following expression

$$l\ (x) = \frac{3S\sqrt{x}}{3CS + 2\sqrt{x}} = \frac{4\sqrt{x}}{5(-2 + 2\sqrt{x})} \tag{4.50}$$

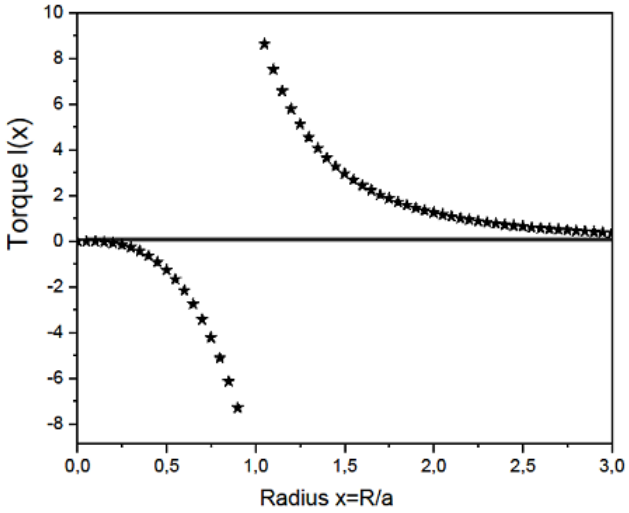

Figure 4.1: The torque in the two regions.

shows the angular momentum behavior in the disk in the two regions $(x < 1)$ and$(x > 1)$. identical to the angular momentum behavior used in previous studies (Lin and Papaloizeau 1986) and explained in Chapter Three (fig 3.1 and fig 3.2). We observe that the angular momentum reaches its peak at the planet $(x = 1)$ and vanishes at the edges of the disk away from the planet.

The surface density in the region$(x < 1)$ is given by

$$\begin{aligned}
\Sigma\,(x,\tau) &= \frac{\mathbb{Q}}{24}\frac{1}{(\sqrt{2}-1)}\frac{1-\sqrt{x}}{x}\frac{1}{\tau}\exp\left(-\frac{1+\sqrt{2x}}{\tau\sqrt{2x}}\right) I_1\left(2^{\frac{3}{4}}\frac{1}{\tau.x^{\frac{1}{4}}}\right) \\
\Sigma\,(x,\tau) &= W_0\frac{(1-\sqrt{x})}{x}\frac{1}{\tau}\exp\left(-\frac{1+\sqrt{2x}}{\tau\sqrt{2x}}\right) I_1\left(2^{\frac{3}{4}}\frac{1}{\tau.x^{\frac{1}{4}}}\right) \\
\frac{\Sigma\,(x,\tau)}{W_0} &= \frac{(1-\sqrt{x})}{x}\frac{1}{\tau}\exp\left(-\frac{1+\sqrt{2x}}{\tau\sqrt{2x}}\right) I_1\left(2^{\frac{3}{4}}\frac{1}{\tau.x^{\frac{1}{4}}}\right)
\end{aligned} \tag{4.51}$$

where W_0 is the contstant

$$\begin{aligned} \tau &= 0.016 \\ \frac{\Sigma(x,\tau)}{W_0} &= 62.5\frac{(1-\sqrt{x})}{x}\exp\left(-62.5\frac{1+\sqrt{2x}}{\sqrt{2x}}\right) I_1\left(\frac{105.11}{x^{\frac{1}{4}}}\right) \end{aligned} \tag{4.52}$$

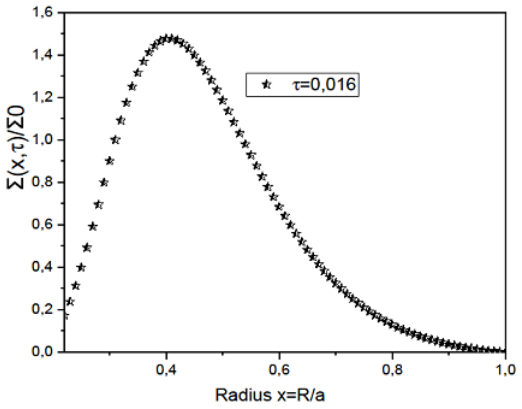

Figure 4.2: The surface density for $x < 1$; At $(\tau = 0.016)$.

$$\begin{aligned} \tau &= 0.032 \\ \frac{\Sigma(x,\tau)}{W_0} &= 31.25\frac{(1-\sqrt{x})}{x}\exp\left(-31.25\frac{1+\sqrt{2x}}{\sqrt{2x}}\right) I_1\left(\frac{52.56}{x^{\frac{1}{4}}}\right) \end{aligned} \tag{4.53}$$

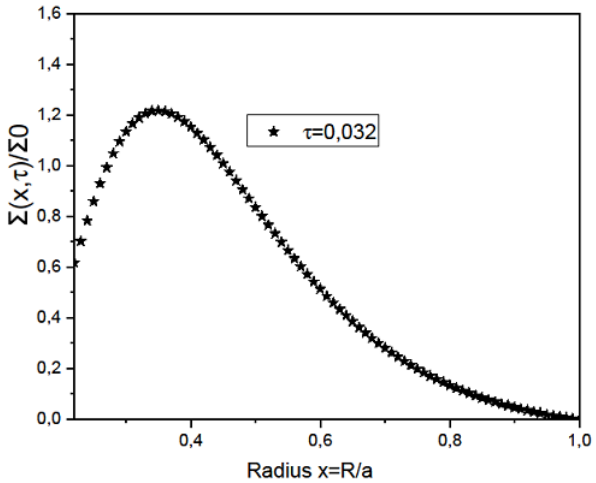

Figure 4.3: The surface density for $x < 1$; At $(\tau = 0.032)$.

$$\begin{aligned} \tau &= 0.064 \\ \frac{\Sigma(x,\tau)}{W_0} &= 15.625\frac{(1-\sqrt{x})}{x}\exp\left(-15.625\frac{1+\sqrt{2x}}{\sqrt{2x}}\right) I_1\left(\frac{26.278}{x^{\frac{1}{4}}}\right) \end{aligned} \tag{4.54}$$

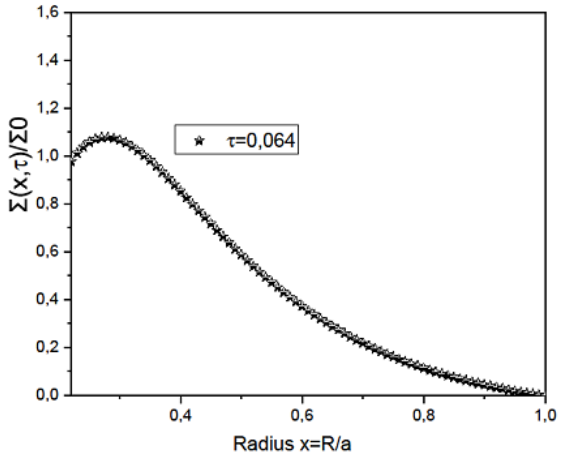

Figure 4.4: The surface density for $x < 1$; At $(\tau = 0.064)$.

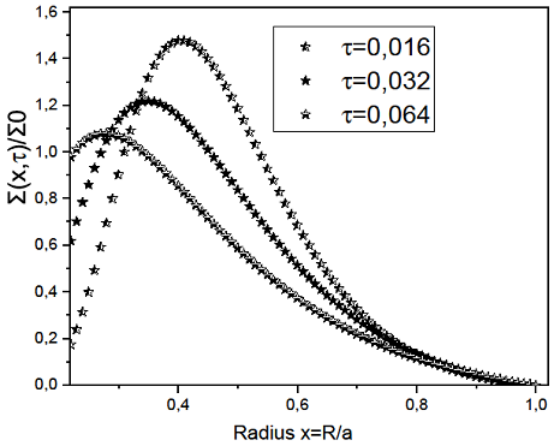

Figure 4.5: The surface density for $x < 1$; At $(\tau = 0.016, 0.032, 0.064)$.

These curves show the evolution of surface density as a function of $x = R/a$. We notice that the surface density has different peaks at various periods of time ($\tau = 0.016, \tau = 0.032, \tau = 0.064$). Surface density is more pronounced at peak $x = 1/2$.

4.3 Calculation of surface density in the region ($x > 1$)

We restart from the general solution (4.1).with as before in the above subsection ($g = -3/2, CS = -2/3$)

we take the modes of k

$$\begin{aligned}\frac{\Sigma(x,t)}{F(x)} &= \int_0^\infty [C_1(k)J_1(ky(x)) + C_2(k)Y_1(ky(x))]\exp(-3Sk^2t)dk \\ F(x) &= \frac{x^{-\frac{5}{4}}}{3CS}l^{-1}(x).x^{\frac{1}{2}(1-g)}, \quad \text{were} \\ F(x) &= -\frac{1}{2l\ (x)}\end{aligned} \tag{4.55}$$

Using the boundary condition at $x = 1$:$\Sigma(x = 1, t) = 0$ then

$$\begin{aligned}0 &= [C_1(k)J_1(ky(1)) + C_2(k)Y_1(ky(1))] \\ C_2(k) &= -\frac{J_1(ky(1))}{Y_1(ky(1))}C_1(k) \\ \frac{C_1(k)}{Y_1(ky(1))} &= -\frac{C_2(k)}{J_1(ky(1))}\end{aligned} \tag{4.56}$$

then

$$\frac{\Sigma(x,t)}{F(x)} = \int_0^\infty \frac{C_1(k)}{Y_1(ky(1))}[Y_1(ky(1))J_1(ky) - J_1(ky(1))Y_1(ky)]\exp(-3Sk^2t)dk \tag{4.57}$$

then, after using that $x = x(y) = (\frac{y}{4})^4$ and we assimilate the constant $\frac{C_1(k)}{Y_1(ky(1))}$ to a novel constant$C(k)$, the equation (4.57) becomes

$$\frac{\Sigma(x,t)}{F(x)} \equiv \int_0^\infty \frac{C(k)}{k}[Y_1(ky(1))J_1(ky) - J_1(ky(1))Y_1(ky)]\exp(-3Sk^2t)kdk \tag{4.58}$$

$$\begin{aligned}\frac{\Sigma(x\,(y),t)}{F(x\,(y))} \equiv \int_0^\infty &\frac{C(k)\,(J_1^2(ky(1)) + Y_1^2(ky(1)))}{k} \\ &\frac{[Y_1(ky(1))J_1(ky) - J_1(ky(1))Y_1(ky)]}{J_1^2(ky(1)) + Y_1^2(ky(1))}\exp(-3Sk^2t)kdk\end{aligned} \tag{4.59}$$

$$\begin{aligned} \text{where} \quad U(k) &= J_1^2(ky(1)) + Y_1^2(ky(1)) \\ \frac{\Sigma(x(y),t)}{F(x(y))} &\equiv \int_0^\infty \frac{C(k)U(k)}{k} \frac{[Y_1(ky(1))J_1(ky) - J_1(ky(1))Y_1(ky)]}{U(k)} \\ & \quad \exp(-3Sk^2t)kdk \end{aligned} \tag{4.60}$$

At $t = 0$, this expression becomes

$$\frac{\Sigma(x(y),0)}{F(x(y))} \equiv M(y) = \int_0^\infty \frac{C(k)U(k)}{k} \frac{[Y_1(ky(1))J_1(ky) - J_1(ky(1))Y_1(ky)]}{U(k)} kdk \tag{4.61}$$

By using the inverse Weber transform, we obtain

$$\frac{C(k)\left(J_1^2(ky(1)) + Y_1^2(ky(1))\right)}{k} = \int_1^\infty M(y)\left[Y_1(ky(1))J_1(ky) - J_1(ky(1))Y_1(ky)\right] ydy \tag{4.62}$$

$$\frac{C(k)}{k} = \int_1^\infty M(y)\left[\frac{[Y_1(ky(1))J_1(ky) - J_1(ky(1))Y_1(ky)]}{(J_1^2(ky(1)) + Y_1^2(ky(1)))}\right] ydy \tag{4.63}$$

or equivalently, following the definition of $M(y)$

$$\frac{C(k)}{k} = \int_1^\infty \frac{\Sigma(x(y),0)}{F(x(y))}\left[\frac{Y_1(ky(1))J_1(ky) - J_1(ky(1))Y_1(ky)}{(J_1^2(ky(1)) + Y_1^2(ky(1)))}\right] ydy \tag{4.64}$$

We assume that the surface density is more pronouced at initial time at the location $x = 3/2$

$$\Sigma(\left(\frac{y}{4}\right)^4, 0) = \Sigma_0 \delta\left(\left(\frac{y}{4}\right)^4 - \frac{3}{2}\right) \tag{4.65}$$

and that

$$\delta\left(\left(\frac{y}{4}\right)^4 - \frac{3}{2}\right) = 2^{3/4}\delta\left(y - 4\left(\frac{3}{2}\right)^{1/4}\right) \tag{4.66}$$

$$\begin{aligned} \frac{C(k)}{k} &= \frac{\Sigma_0.}{F(\frac{3}{2})}\left[\frac{Y_1(ky(1))J_1(k4\left(\frac{3}{2}\right)^{1/4}) - J_1(ky(1))Y_1(k4\left(\frac{3}{2}\right)^{1/4})}{(J_1^2(ky(1)) + Y_1^2(ky(1)))}\right].2^{3/4}.4.\left(\frac{3}{2}\right)^{1/4} \\ \frac{C(k)}{k} &= A\frac{Y_1(ky(1))J_1(k4\left(\frac{3}{2}\right)^{1/4}) - J_1(ky(1))Y_1(4\left(\frac{3}{2}\right)^{1/4}k)}{(J_1^2(ky(1)) + Y_1^2(ky(1)))} \end{aligned} \tag{4.67}$$

then, knowing that $y(1) = 4$, we obtain

$$\frac{C(k)}{k} = A\frac{Y_1(4k)J_1(4\left(\frac{3}{2}\right)^{1/4}k) - J_1(4k)Y_1(4\left(\frac{3}{2}\right)^{1/4}k)}{J_1^2(4k) + Y_1^2(4k)} \tag{4.68}$$

Now we replace the last coefficient $C(k)/k$ in the formula (4.58)

$$y(x) = 4x^{1/4} \tag{4.69}$$

$$\begin{aligned}
\frac{\Sigma(x,t)}{F(x)} &\equiv \int_0^\infty \frac{C(k)}{k}\left[Y_1(4k)J_1(4kx^{1/4}) - J_1(4k)Y_1(4kx^{1/4})\right]\exp(-3Sk^2t)kdk \\
\frac{\Sigma(x,t)}{F(x)} &\equiv \int_0^\infty A\left[\frac{Y_1(4k)J_1(4\left(\frac{3}{2}\right)^{1/4}k) - J_1(4k)Y_1(4\left(\frac{3}{2}\right)^{1/4}k)}{J_1^2(4k) + Y_1^2(4k)}\right] \\
&\quad \left[Y_1(4k)J_1(4kx^{1/4}) - J_1(4k)Y_1(4kx^{1/4})\right]\exp(-3Sk^2t)kdk
\end{aligned} \tag{4.70}$$

$$\begin{aligned}
\text{where} \quad : \quad A &= \frac{\Sigma_0}{F(\frac{3}{2})}.2^{3/4}.4.\left(\frac{3}{2}\right)^{1/4} \\
\frac{\Sigma(x,t)}{\Sigma_0} &= \int_0^\infty \frac{F(x)}{F(\frac{3}{2})}.2^{3/4}.4.\left(\frac{3}{2}\right)^{1/4}.\left[\frac{Y_1(k)J_1(\left(\frac{3}{2}\right)^{1/4}k) - J_1(k)Y_1(\left(\frac{3}{2}\right)^{1/4}k)}{J_1^2(k) + Y_1^2(k)}\right] \\
&\quad \left[Y_1(k)J_1(kx^{1/4}) - J_1(k)Y_1(kx^{1/4})\right]\exp(-3Sk^2t)kdk
\end{aligned} \tag{4.71}$$

$$\begin{aligned}
\frac{\Sigma(x,t)}{\Omega_0} &= \int_0^\infty \frac{F(x)}{F(\frac{3}{2})}\left[\frac{Y_1(k)J_1(\left(\frac{3}{2}\right)^{1/4}k) - J_1(k)Y_1(\left(\frac{3}{2}\right)^{1/4}k)}{J_1^2(k) + Y_1^2(k)}\right] \\
&\quad \left[Y_1(k)J_1(kx^{1/4}) - J_1(k)Y_1(kx^{1/4})\right]\exp(-3Sk^2t)kdk
\end{aligned} \tag{4.72}$$

where Ω_0 is the constant

With

$$F\ (x) = \frac{x^{\frac{-5}{4}}}{3CS}l^{-1}(x).x^{\frac{1}{2}(1-g)} \tag{4.73}$$

If we take $g = -\frac{3}{2}$,than

$$\begin{aligned} F\ (x) &= \frac{1}{3CS} l^{-1}(x) \\ F\ (\frac{3}{2}) &= \frac{1}{3CS} l^{-1}(\frac{3}{2}) \end{aligned} \tag{4.74}$$

with as before

$$l\ (x) = \frac{3Sx^{\beta-1}}{3CS + 2\sqrt{x}} \tag{4.75}$$

then (for $\beta = \frac{3}{2}, 3CS = -2$)

$$\frac{F\ (x)}{F\ (\frac{3}{2})} = \frac{l\ (\frac{3}{2})}{l\ (x)} = \frac{\sqrt{\frac{3}{2}}}{\sqrt{x}} \frac{3CS + 2\sqrt{x}}{3CS + 2\sqrt{\frac{3}{2}}} = \frac{\sqrt{\frac{3}{2}}}{\left(\sqrt{\frac{3}{2}} - 1\right)} \frac{\sqrt{x} - 1}{\sqrt{x}} \tag{4.76}$$

we obtain the following expression of the surface density in the region $x > 1$

$$\begin{aligned} \frac{\Sigma(x,t)}{\Omega_0} &= \frac{\sqrt{\frac{3}{2}}}{\left(\sqrt{\frac{3}{2}} - 1\right)} \frac{\sqrt{x} - 1}{\sqrt{x}} \int_0^\infty \left[\frac{Y_1(k) J_1(\left(\frac{3}{2}\right)^{1/4} k) - J_1(k) Y_1(\left(\frac{3}{2}\right)^{1/4} k)}{J_1^2(k) + Y_1^2(k)} \right] \\ &\left[Y_1(k) J_1(kx^{1/4}) - J_1(k) Y_1(kx^{1/4}) \right] \exp(-3Sk^2 t) k dk \end{aligned} \tag{4.77}$$

$$\begin{aligned} \frac{\Sigma(x,\tau)}{\widehat{\Omega}_0} &= \frac{\sqrt{x} - 1}{\sqrt{x}} \int_0^\infty \left[\frac{Y_1(k) J_1(\left(\frac{3}{2}\right)^{1/4} k) - J_1(k) Y_1(\left(\frac{3}{2}\right)^{1/4} k)}{J_1^2(k) + Y_1^2(k)} \right] \\ &\left[Y_1(k) J_1(kx^{1/4}) - J_1(k) Y_1(kx^{1/4}) \right] \exp(-4\sqrt{x}.\tau.k^2) k dk \end{aligned} \tag{4.78}$$

$$\tau = 0.016$$

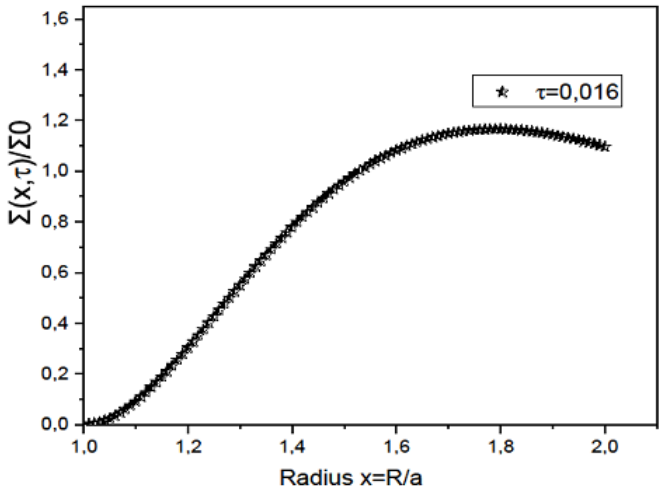

Figure 4.6: The surface density for $x > 1$; At $(\tau = 0.016)$.

$$\tau = 0.032$$

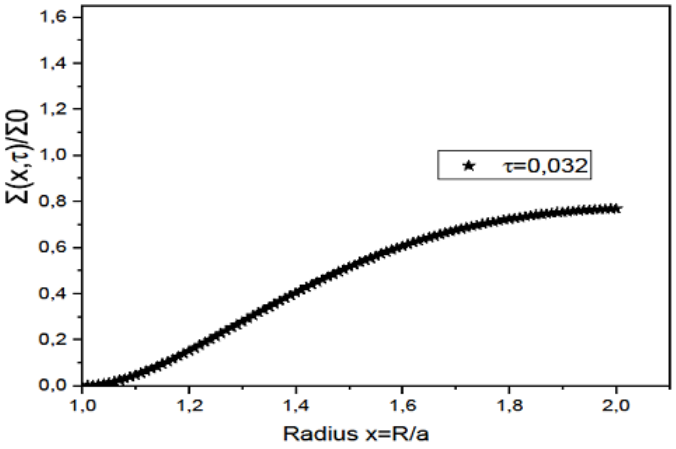

Figure 4.7: The surface density for $x > 1$; At $(\tau = 0.032)$.

$$\tau = 0.064$$

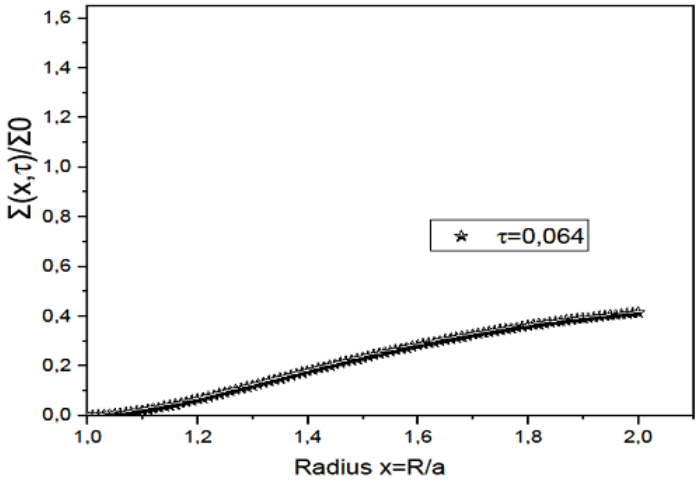

Figure 4.8: The surface density for $x > 1$; At $(\tau = 0.064)$.

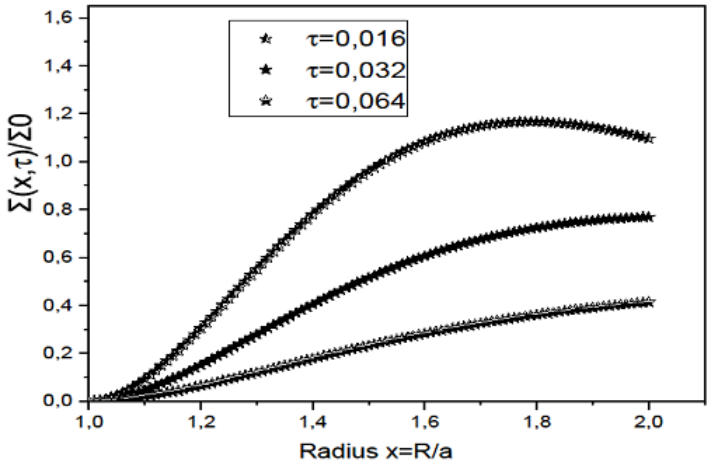

Figure 4.9: The surface density for $x > 1$; At $(\tau = 0.016, 0.032, 0.064)$.

These curves show the evolution of surface density as a function of $x = R/a$. We notice that the surface density has different peaks at various periods of time $(\tau = 0.016, \tau = 0.032, \tau = 0.064)$. Surface density is more pronounced at peak $x = 3/2$.

4.4 Results and discussion

The dynamic interactions of stellars companions and planet are the importante among of the many processes responsible for the formation of protoplanetary disks, and the gravitational interaction between the disk and the planet results in the exchange of angular momentum and planet migration.

Figures (4.5) and (4.9) show how surface density changes near and far from the planet.

In the region ($x < 1$) we find that the surface density increases at the site ($x = 1/2$), and as the time increases, the surface density decreases and decreases near the planet (Fig 4.5) When the density of the protoplanetary disk surface decreases, the planet creates a large gap as its mass increases and becomes gigantic and massive, the viscosity is also low in this case, and a standard migration of (the second type) occurs. While the angular momentum increases until it reaches a maximum and minimum value at ($x = 1$) in (Fig 4.1).

Our results are consistent with an approximation of (Lin and Papaloizeau 1986).

In the region ($x > 1$). the surface density behavior away from the planet is greater and more pronounced at position ($x = 3/2$). In this case, the viscosity is large, and the gap becomes less exhaustive and less resistant to gas, resulting in a separation of migration with respect to disk development (Fig 4.9), while angular momentum decreases at the disk's ends away from the planet (Fig 4.1).

We demonstrated in both regions how planetary torque affects the surface density of the disk by finding an analytical solution to the evolution equation of the disk and an embedded protoplanet. And the results were satisfactory when compared to the previous results (Lin and Papaloizeau 1986).

4.5 Conclusion

The planets are subject to a different torque that can cause them to migrate, and this torque is caused by the gravitational interaction between the planet and the density waves that power the Lindblad resonance in the disk.When the planet's mass is sufficient, it will create a gap in the disk. The formation of the gap terminates the accumulation process, which is crucial in determining the system's behavior, and we have described the behavior of the surface density as the cause of the effect of planetary torque. The surface density of the disk on the planet decreases until it is absent. while the angular momentum increases and decreases in the ends of the disk away from the planet.

We obtain the surface density of the protoplanetary disk by assuming that at the initial time ($t = 0$), the surface density is more pronounced at a boundary value ($x = 1/2$) in the region ($x < 1$) and at the value ($x = 3/2$) in the region($x > 1$) and by applying the inverse Hankel transform and Weber transform and using the Dirac delta properties as well as an appropriate torque that achieves an acceptable behavior. Finally, we obtain the surface density in both regions at the times $\tau = (0.016; 0.032; 0.064)$. When compared to (Lin and Papaloizeau 1986), the results were satisfactory.

Chapter 5

Discussion of the surface density behavior in a (PPD): the second method

Contents

5.1 Introduction

We will find the analytical solution in two regions based on the differential equation for the evolution of a protoplanetary disk (3.37). At the initial time ($t = 0$), the surface density in the region ($x < 1$) becomes $\Sigma(x.t = 0) = u_I$, and the surface density in the region ($x > 1$) becomes $\Sigma(x.t = 0) = u_{II}$.In order to find these solutions, we will rely on changes and transformations that are specific to each region.

5.2 Calculation of surface density

from the equation (3.37):

$$\begin{aligned} 0 &= \frac{u''(x)}{u(x)} + \left(\frac{3}{2x} + 2\frac{v'(x)}{v(x)} - \frac{2\sqrt{x}}{3v(x)}l(x)\right)\frac{u'(x)}{u(x)} \\ &\quad + \frac{3}{2x}\frac{v'(x)}{v(x)} + \frac{v''(x)}{v(x)} - \frac{l(x)}{\sqrt{x}v(x)} - \frac{2\sqrt{x}}{3v(x)}l'(x) + \frac{\lambda}{3v(x)} \end{aligned}$$

We know

$$\begin{aligned} \underline{\lambda} &= \lambda a^2, \quad v(x) = sx^{\beta}, \quad s = S.a^{\beta} \quad , \beta \prec 2 \\ \frac{\underline{\lambda}}{3v(x)} &= \frac{\lambda a^2}{3Sa^{\beta}x^{\beta}} = \frac{\lambda}{3v(x)}, \beta - 2 \prec 2 \end{aligned}$$

And so we write

$$\begin{aligned} 0 &= \frac{u''(x)}{u(x)} + \left(\frac{3}{2x} + 2\frac{v'(x)}{v(x)} - \frac{2\sqrt{x}}{3v(x)} l(x) \right) \frac{u'(x)}{u(x)} \\ &+ \frac{3}{2x}\frac{v'(x)}{v(x)} + \frac{v''(x)}{v(x)} - \frac{l(x)}{\sqrt{x}v(x)} - \frac{2\sqrt{x}}{3v(x)} l'(x) + \frac{\lambda}{3v(x)} \end{aligned} \tag{5.1}$$

5.2.1 In the region $(R < a)$, $(x < 1)$

The equation (5.1) has a generic form as

$$0 = u''(x) + f_1(x)u'(x) + f_0(x)u(x) \tag{5.2}$$

where $f_0(x)$ and $f_1(x)$ are respectively given by

$$f_0 = \frac{3}{2x}\frac{v'(x)}{v(x)} + \frac{v''(x)}{v(x)} - \frac{l(x)}{\sqrt{x}v(x)} - \frac{2\sqrt{x}}{3v(x)} l'(x) + \frac{\lambda}{3v(x)} \tag{5.3}$$

$$f_1 = \frac{3}{2x} + 2\frac{v'(x)}{v(x)} - \frac{2\sqrt{x}}{3v(x)} l(x) \tag{5.4}$$

To solve the equation (5.2) put the change

$$u(x) = \frac{\omega(x)}{q(x)} \tag{5.5}$$

After simplifications, it is traightforward and aisy to get

$$0 = \frac{\omega''(x)}{\omega(x)} + \left(f_1(x) - \frac{2q'(x)}{q(x)} \right) \frac{\omega'(x)}{\omega(x)} + \left[f_0(x) - \frac{q''(x)}{q(x)} + 2\left(\frac{q'(x)}{q(x)} \right)^2 - f_1(x)\frac{q'(x)}{q(x)} \right] \tag{5.6}$$

By using

$$f_1(x) - \frac{2q'(x)}{q(x)} = \frac{g}{x} \tag{5.7}$$

where g is a constant to be determined later. When we replace f_1 in the last equation, we can find $q(x)$, that is to say

$$q(x) = \exp\left(\frac{1}{2}\int^x f_1(\theta)d\theta - \frac{g}{2}\ln(x)\right) \tag{5.8}$$

$$q'(x) = \left(\frac{f_1(x)}{2} - \frac{g}{2x}\right) q(x) \tag{5.9}$$

$$q''(x) = \left[\left(\frac{f_1'(x)}{2} + \frac{g}{2x^2}\right) + \left(\frac{f_1(x)}{2} - \frac{g}{2x}\right)^2\right] q(x) \tag{5.10}$$

then the equation (5.6) transforms to

$$0 = \omega''(x) + \frac{g}{x}\omega'(x) + \left[f_0(x) - \frac{q''(x)}{q(x)} + 2\left(\frac{q'(x)}{q(x)}\right)^2 - f_1(x)\frac{q'(x)}{q(x)}\right]\omega(x) = 0 \tag{5.11}$$

$$0 = \omega''(x) + \frac{g}{x}\omega'(x) + G(x)\omega(x) \tag{5.12}$$

where g is a free transformation parameter that we will use for our convenience later and

$$G(x) = f_0(x) - \frac{q''(x)}{q(x)} + 2\left(\frac{q'(x)}{q(x)}\right)^2 - f_1(x)\frac{q'(x)}{q(x)} \tag{5.13}$$

or equivalently, after using the formula (5.7), (5.8) we find

$$G(x) = f_0(x) - \frac{f_1'(x)}{2} - \frac{f_1^2(x)}{4} + \frac{g(g-2)}{4x^2} \tag{5.14}$$

substitute the expressions of $f_0(x)$ and $f_1(x)$ and $f_1'(x)$ given above, we find

$$G(x) = \frac{3}{16x^2} + \frac{\lambda}{3v(x)} - \frac{l(x)}{3\sqrt{x}v(x)} - \frac{\sqrt{x}}{3v(x)}\frac{d}{dx}l(x) - \frac{x}{9v^2(x)}l^2(x) + \frac{\sqrt{x}}{3}\frac{v'(x)}{v^2(x)}l(x) + \frac{g(g-2)}{4x^2} \tag{5.15}$$

Replace now the viscosity $v(x)$ by Sx^β then:

$$G(x) = \frac{3}{16x^2} + \frac{\lambda}{3Sx^\beta} + \frac{g(g-2)}{4x^2} - \frac{1}{3Sx^{\beta-1/2}}\frac{d}{dx}l(x) - \frac{1}{9S^2x^{2\beta-1}}l^2(x) + \frac{(\beta-1)}{3Sx^{\beta+1/2}}l(x) \tag{5.16}$$

Now, to solve the above differential equation (5.11), we discard the terms containing the torque $l(x)$ in (5.15), that is to say:

$$0 = \frac{d}{dx}l(x) + \frac{l^2(x)}{3Sx^{\beta-\frac{1}{2}}} - \frac{(\beta-1)}{x}l(x) \tag{5.17}$$

Indeed, we have from the constraint (5.17)

$$l(x) = \frac{3Sx^{\beta-1}}{3CS + 2\sqrt{x}} \tag{5.18}$$

and

$$G(x) = \frac{3}{16x^2} + \frac{\lambda}{3Sx^{\beta}} + \frac{g(g-1)}{4x^2} \tag{5.19}$$

leading to get a simplified differential equation

$$0 = \omega^{''}(x) + \frac{g}{x}\omega^{'}(x)\left(\frac{3}{16x^2} + \frac{\lambda}{3Sx^{\beta}} + \frac{g(g-1)}{4x^2}\right)\omega(x) \tag{5.20}$$

For lightrning we put

$$\frac{\lambda}{3S} = \lambda_s \tag{5.21}$$

$$\frac{4g(g-2)+3}{16} = \Gamma \tag{5.22}$$

we get

$$0 = \omega^{''}(x) + \frac{g}{x}\omega^{'}(x) + \left(\frac{\Gamma}{x^2} + \frac{\lambda_s}{x^{\beta}}\right)\omega(x) \tag{5.23}$$

whose general solution is

$$\omega_I(x) = x^{\frac{1-g}{2}}\left(C_1 J_p\left(\frac{2\sqrt{\lambda_s}}{2-\beta}x^{\frac{1-\beta}{2}}\right) + C_2 Y_p\left(\frac{2\sqrt{\lambda_s}}{2-\beta}x^{\frac{1-\beta}{2}}\right)\right) \tag{5.24}$$

$$p = \frac{\sqrt{(1-g)^2 - 4\Gamma}}{2-\beta} \tag{5.25}$$

and $J_p(X)$ and $Y_p(X)$ are the well known Bessel's functions. Then the solution of the surface density in the regionI $(x < 1)$ is $u_I(x) = \omega(x)/q(x)$ or

$$u_I(x) = x^{\frac{1-s}{2}} \exp\left(-\frac{1}{2}\int^x f_1(z)dz + \frac{g}{2}\ln(x)\right)\left(C_1 J_p\left(\frac{2\sqrt{\lambda_s}}{2-\beta}x^{1-\beta/2}\right) + C_2 Y_p\left(\frac{2\sqrt{\lambda_s}}{2-\beta}x^{1-\beta/2}\right)\right) \tag{5.26}$$

or after replacing $f_1(z)$ by its expression (5.1) and the torque by its expression (5.16), we find:

$$\begin{aligned} u_I(x) &= x^{\frac{1-s}{2}}\left(C_1 J_p\left(\frac{2\sqrt{\lambda_s}}{2-\beta}x^{1-\beta/2}\right) + C_2 Y_p\left(\frac{2\sqrt{\lambda_s}}{2-\beta}x^{1-\beta/2}\right)\right) \\ &\quad \exp\left(-\frac{1}{2}\int^x\left(\frac{3}{2x} + 2\frac{v'(x)}{v(x)} - \frac{2\sqrt{x}}{3v(x)}l(x)\right)dx\right) \end{aligned} \tag{5.27}$$

or

$$u_I(x) = C_1\frac{x^{\frac{-3}{4}-\beta}}{3cs^2}\left(J_p\left(\frac{2\sqrt{\lambda_s}}{2-\beta}x^{1-\beta/2}\right) + \frac{C_2}{C_1}Y_p\left(\frac{2\sqrt{\lambda_s}}{2-\beta}x^{1-\beta/2}\right)\right)\left(\frac{2}{3}x + cs\sqrt{x}\right) \tag{5.28}$$

As application make the following considerations

$$\begin{aligned} p &= \frac{\sqrt{(1-g)^2-4\Gamma}}{2-\beta} = 1, \sqrt{(1-g)^2-4\Gamma} = \frac{4}{3}, \frac{C_2}{C_1} = -\frac{1}{10}; \frac{C_1}{S} = 300 \\ S &= \frac{4}{15}; CS = -\frac{2}{3}; \beta = \frac{2}{3}; \frac{2\sqrt{\lambda_s}}{2-\beta} = 9; \sqrt{\lambda_s} = 6 \end{aligned} \tag{5.29}$$

The torque leading to the solution then becomes

$$\begin{aligned} l(x) &= \frac{3Sx^{\beta-1}}{3CS + 2\sqrt{x}} = \frac{3}{2}\frac{Sx^{-1/3}}{\sqrt{x}-1} \\ l(x) &= \frac{2}{5}\frac{x^{-1/3}}{\sqrt{x}-1} \end{aligned} \tag{5.30}$$

which is the torque that we have obtained and presented it in (figure 5.1) leading to the solution

$$\Sigma(x.t=0) = u_I(x) \tag{5.31}$$

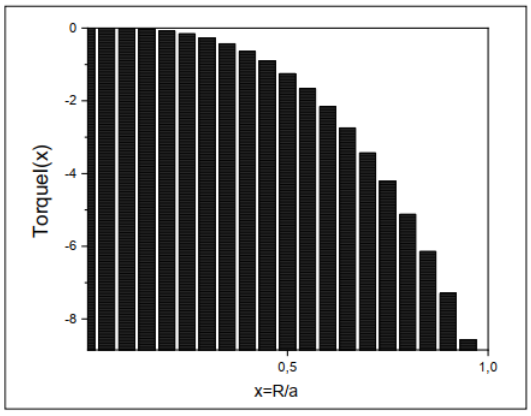

Figure 5.1: the torque $l(x)$ in region I.

$$u_I(x) = -100.x^{\frac{-17}{12}}(x - \sqrt{x})\left(J(1, 9x^{\frac{2}{3}} - \frac{Y(1, 9x^{\frac{2}{3}})}{10}\right) \tag{5.32}$$

which is the surface density in our model that we have obtained and presented it in (figure 5.2)

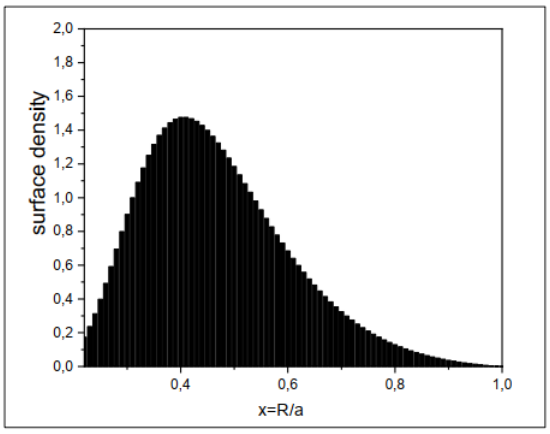

Figure 5.2: The surface density in region I.

5.2.2 In the region $(R > a)$,$(x > 1)$

The equation (5.1) has a generic form as

$$0 = f_2(x)u''(x) + f_1(x)u'(x) + f_0(x)u(x) \tag{5.33}$$

where

$$f_0(x) = \frac{3}{2x}\frac{v'(x)}{v(x)} + \frac{v''(x)}{v(x)} - \frac{l(x)}{\sqrt{x}\eta(x)} - \frac{2\sqrt{x}}{3v(x)}l'(x) + \frac{1}{3v(x)} \tag{5.34}$$

$$f_1(x) = \frac{3}{2x} + 2\frac{v'(x)}{\eta(x)} - \frac{2\sqrt{x}}{3v(x)}l(x) \tag{5.35}$$

$$f_2(x) = 1 \tag{5.36}$$

To solve the equation (5.32) put the change

$$u(x) = \omega(x)\exp\left(\frac{1}{2}\int^x \frac{f_1(x')}{f_2(x')}dx'\right) \tag{5.37}$$

we will transform this equation as

$$0 = \omega''(x) + F(x)\omega(x) \tag{5.38}$$

such as

$$F(x) = \frac{f_0(x)}{f_2(x)} - \frac{1}{4}\left(\frac{f_1(x)}{f_2(x)}\right)^2 - \frac{1}{2}\left(\frac{f_1(x)}{f_2(x)}\right)' \tag{5.39}$$

that is to say

$$F(x) = \frac{3}{16x^2} - \frac{l(x)}{3\sqrt{x}v(x)} - \frac{\sqrt{x}}{3v(x)}l'(x) + \frac{\lambda}{3v(x)} - \frac{x}{9v^2(x)}l^2(x) + \frac{v'(x)\sqrt{x}}{3v^2(x)}l(x) \tag{5.40}$$

By replacing the viscosity $v(x) = Sx^\beta$ in the last expression of $F(x)$, we find

$$F(x) = \frac{3}{16x^2} - \frac{1}{3Sx^{\beta-1/2}}l'(x) + \frac{\lambda}{3Sx^\beta} - \frac{1}{9S^2x^{2\beta-1}}l^2(x) + \frac{(\beta-1)}{3S\cdot x^{\beta+1/2}}l(x) \tag{5.41}$$

By using the same constraint on $l(x)$ as in the region II

$$0 = \frac{1}{x^{\beta-1/2}}l'(x) + \frac{1}{3Sx^{2\beta-1}}l^2(x) - \frac{(\beta-1)}{S\cdot x^{\beta+1/2}}l(x) \tag{5.42}$$

We multiply by $(x^{\beta-1/2})$,We get it

$$0 = l'(x) + \frac{1}{3Sx^{\beta-1/2}}l^2(x) - \frac{(\beta-1)}{x}l(x) \tag{5.43}$$

we find that

$$l(x) = \frac{3Sx^{\beta}}{2x^{3/2} + 3CSx} \tag{5.44}$$

In this regionII, if we take $\beta = 5/4, S = 2/3$ and $C = -0.97$, the corresponding torque expression is

$$l(x) = \frac{2x^{5/4}}{2x^{3/2} - 1.94x} \tag{5.45}$$

The torque from our model, which correspond to regionII is presented in the($Fig5.3$)

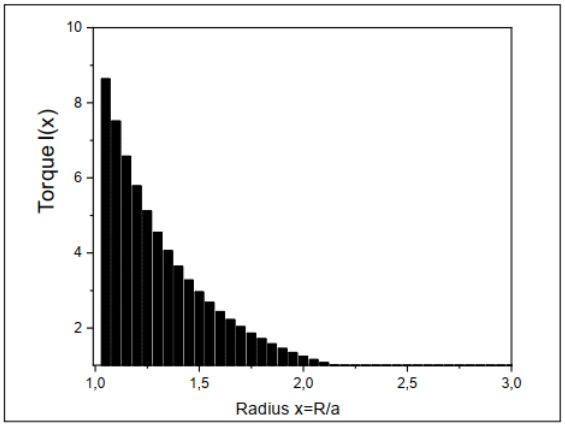

Figure 5.3: The torque $l(x)$ in region II.

The solution in regionII is then given by

$$\omega_{II}(x) = \sqrt{\frac{R}{a}}\left(K_1 J_{\frac{2}{3}}\left(\frac{4\lambda\sqrt{2}}{3}(x)^{3/8}\right) + K_2 Y_{2/3}\left(\frac{4\lambda\sqrt{2}}{3}(x)^{3/8}\right)\right) \tag{5.46}$$

the global solution is then given by

$$u_{II}(x) = \omega_{II}(x)\exp\left(-\frac{1}{2}\int^{x}\left(\frac{3}{2t} + 2\frac{v'(t)}{v(t)} - \frac{2\sqrt{t}}{3v(t)}l(t)\right)dt\right) \tag{5.47}$$

or

$$\begin{aligned} u_{II}(x) &= \omega_{II}(x)\exp\left(\frac{3}{4}\log\left(\frac{1}{x}\right) + \log\left(\frac{1}{v\,(x)}\right) + \frac{1}{3}\int\frac{\sqrt{t}}{v(t)}l(t)dt\right) \\ &= \omega_{II}(x)\exp\left(\frac{3}{4}\log\left(\frac{1}{x}\right) + \log\left(\frac{1}{v\,(x)}\right) + \int\frac{1}{2t - 1.94\sqrt{t}}dt)\right) \\ &= \omega_{II}(x)\exp\left(\log\left(\frac{1}{x^{3/4}}\right) + \log\left(\frac{1}{v\,(x)}\right) + \log(1 - 1.0309\sqrt{x})\right) \end{aligned} \tag{5.48}$$

we find the solution in this (region 2)

$$u_{II}(x) = \frac{3}{2}\left(\frac{1-1.0309\sqrt{x}}{x^{3/2}}\right)\left(K_1 J_{\frac{2}{3}}\left(\frac{4\lambda\sqrt{2}}{3}x^{3/8}\right) + K_2 Y_{2/3}\left(\frac{4\lambda\sqrt{2}}{3}x^{3/8}\right)\right) \tag{5.49}$$

the constants K_1 and K_2 must satisfy the boundary conditions

$$u_{II}(1) = 0 \tag{5.50}$$

$$K_1 J_{\frac{2}{3}}\left(\frac{4\lambda\sqrt{2}}{3}\right) = -K_2 Y_{2/3}\left(\frac{4\lambda\sqrt{2}}{3}\right) \tag{5.51}$$

$$u_{II}(x) = \frac{3}{2}K_1\left(\frac{1-1.0309\sqrt{x}}{x^{3/2}}\right) J_{\frac{2}{3}}\left(\frac{4\lambda\sqrt{2}}{3}\right)\left(\frac{J_{\frac{2}{3}}\left(\frac{4\lambda\sqrt{2}}{3}x^{3/8}\right)}{J_{\frac{2}{3}}\left(\frac{4\lambda\sqrt{2}}{3}\right)} - \frac{Y_{2/3}\left(\frac{4\lambda\sqrt{2}}{3}x^{3/8}\right)}{Y_{2/3}\left(\frac{4\lambda\sqrt{2}}{3}\right)}\right) \tag{5.52}$$

where

$$\Sigma(x.t=0) = u_{II}(x) \tag{5.53}$$

If we take $\lambda = \frac{5}{6}K^2$ we obtain

$$u_{II}(x) = \frac{3}{2}K_1 J_{\frac{2}{3}}\left(\frac{10\sqrt{2}}{9}K^2\right)\left(\frac{1-1.0309\sqrt{x}}{x^{3/2}}\right)\left(\frac{J_{\frac{2}{3}}\left(\frac{10\sqrt{2}}{9}K^2x^{3/8}\right)}{J_{\frac{2}{3}}\left(\frac{10\sqrt{2}}{9}K^2\right)} - \frac{Y_{2/3}\left(\frac{10\sqrt{2}}{9}K^2x^{3/8}\right)}{Y_{2/3}\left(\frac{10\sqrt{2}}{9}K^2\right)}\right) \tag{5.54}$$

such that $J_{\frac{2}{3}}\left(\frac{10\sqrt{2}}{9}\right) = 0.63209$ For The mode $K = 1$ and for $K_1 < 0$, the surface density from our model, which correspond to regionII is presented in the figure 5.2.

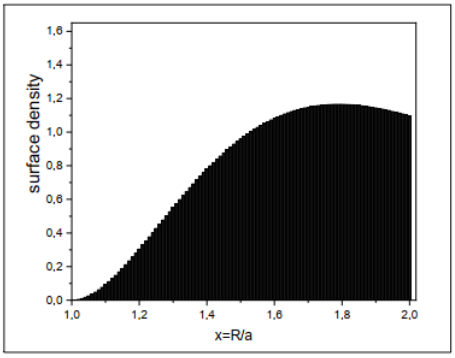

Figure 5.4: The surface density in region II.

5.3 Results and discussions

Figs (5.2) and (5.4). show the behavior of the surface density , this expected behavior followed by the formation of a planet at$(R = a)$ inside the disk. Through these curves, the density is verylow near the planet $(R = a)$, and it has a significant value away from the planet, while the angular momentum reaches its maximum when $(x = 1)$. That is when it is close to the planet as shown by the (figures (5.1) and (5.3)).

The gap is dened as the region in which the surface density is less than of what it would be if there were no planet in the disk. This figure from our results correspond the approximation of (Lin and Papaloizeau 1986). The disks evolve as a result of the viscous transport of angular momentum, which is represented by the shapes (fig5.1) and (fig 5.3) of each region, which are identical to the angular momentum used in our studies (see Chapter Three, Figures(3.1) and (3.2)). As in previous studies (Lin and Papaloizeau 1986).

5.4 Conclusion

The surface density of the protoplanetary disk was obtained using a set of changes and transformations shown in each region, we found similar solutions in previous studies (Lin and Papaloizeau 1986). What distinguishes our work is the solution of the surface density equation for the protoplanetary disk without using an angular momentum approximation. What the figures show in both regions demonstrates the validity of our work.

General conclusion

General conclusion

In our work, we aim to study the theory and reach conclusions that are consistent with what astronomical observation reveals by employing physical theories to explain cosmic phenomena. We make significant contributions to providing more accurate results for accretion processes. The latter is one of the most common processes in astrophysics, the term scientists use to describe the flow of matter toward a gravitational object or toward the center of mass of an extended system, and is responsible for the formation of many of the structures we see around us.

Galaxies formed early in the universe as gas flowed in toward the center of gravitational potential wells established by dark matter. Stars form inside galaxies even today as gas clouds collapse and fragment under their own self-gravity and then grow by accreting surrounding gas. Planets form as gas and rocks coalesce in the debris surrounding a new star. Perhaps the most spectacular observational manifestations of accretion occur, however, when the central object is a black hole. The accretion is accompanied by the process of extensive energy release that takes place on the surface of an accreting object and in various gaseous envelopes, accretion disk, jets and other elements of the flow pattern.

The results presented in this thesis attempt to provide some answers on the properties of accretion disks, their geometries and their structures, more precisely the accretion processes of protoplanetary disks.

As a result, we presented in the first part basic concepts of accretion disks in many cosmic phenomena that can exist in various physical and astronomical systems.

The second chapter included protoplanetary disks around young stars are the birth sights of planetary systems like our own. We showed that protoplanetary disks are also accretion disks that are constantly feeding gas to their host stars. This process requires gas in the disk to lose angular momentum, which is done through the outward angular momentum transport caused by disk turbulence. The realization that disk-planet interactions lead to the exchange of angular momentum between the planet and disk, leading to the possibility of planetary migration and the shaping of the disk. Increased computing power, advances in computational techniques, and continually developing observational advances over the last several decades have allowed astronomers and physicists to develop increasingly sophisticated models of planet formation. In the third chapter, we addressed the fundamental parameters for studying the evolution of the accretion disk and calculating the surface density based on mass and angular moment conservation laws, as well as solving the differential equation for

the surface density of a protoplanetary disk. We discussed the behavior of surface density in different regions of the protoplanetary disk in Chapters 4 and 5, and the analytical results obtained were consistent with previous numerical results (lin paplouzou 1986).
What we have achieved in this work is a good starting point that prompted us to provide suggestions and ideas that can open many horizons for future research work, including:

- Recalculating the surface density, if we assume that the surface density is more pronounced at the initial time at the location $x = 2/5$, $x = 8/5$. In the area ($x < 1$ and $x > 1$).
- The effects of magnetic fields on disk formation and evolution.
- Accretion disk treatment based on the heat and energy conservation equations.

Appendix A

The main sequence of stars

During the main sequence phase, the star is in hydrostatic equilibrium, it undergoes two forces which oppose each other and keep it in equilibrium:

- on the one hand, the thermonuclear reactions which take place in the heart of the star, which exert a radiative pressure which tends to make it increase in volume, which involves a reduction in the temperature of the star.
- on the other hand the forces of gravity, which tend to make it contract and therefore to increase the temperature of the star again.

These two forces in balance, maintain the nuclear reactions in the center of the star and prevent any runaway of the heart of the star
When the core of the star reaches a temperature of the order of a million degrees, it becomes the seat of thermonuclear reactions (fusion of deuterium, lithium and beryllium). At around 7 to 8 million degrees, the temperature is high enough for the hydrogen nuclei in the plasma, the most common, to start fusing to give essentially helium 4He, following a nuclear fusion reaction called the proton-proton cycle , with an overall efficiency equal to $64,000$ GJ.kg-1 (per kg of hydrogen).
If the temperature exceeds 18 million degrees, another chain of reactions becomes predominant: the carbon-nitrogen-oxygen cycle, or CNO cycle, the efficiency of which is much more temperature-dependent than the proton-proton cycle. In the Sun, 2.5% of the energy is generated by this cycle. But in more massive stars, the predominance of the CNO cycle has major consequences on their structure.
Because the temperature and pressure conditions which allow the fusion of hydrogen are only found in the core of stars, and because there is no convection between this core and the envelope of the star (to bring new fuel to the core), the core is enriched in fusion products (helium), which will slow down the fusion reactions. These fusion products are not waste

because they will serve as nuclear fuel later. In fact, in the case of the Sun, only about 10% of its hydrogen mass fuses into helium during the main sequence. Knowing that the Sun's luminosity is 3.9×10^{26}W and its mass is 1.99×10^{30}kg, we can deduce that the lifetime of a star like the Sun is about 10 billion d years on the main sequence. However, this lifespan is highly dependent on the nuclear reactions that take place within the star: massive stars, which contain much more hydrogen than the Sun, paradoxically have a much shorter main sequence lifespan.

As it lives on the main sequence, the star must contract slightly to counter the effect of the enrichment of its core in fusion products (the number of nuclei decreasing). This leads to a slight increase over time in its luminosity.

The Black holes

Black holes have a mass of at least a few solar masses. They are born as a result of the gravitational collapse of the remnant of massive stars (about ten solar masses and more, initially). Indeed, when the combustion by the thermonuclear reactions in the heart of the massive star ends, for lack of fuel, a supernova occurs. The latter can leave behind a heart that continues to rapidly crumble.

Region of the Universe in irreversible gravitational collapse, whose gravitational field is so intense that nothing, not even light, can come out of it. This region has a spherical boundary called the horizon, or surface of the black hole, which light can pass through without being able to exit. Thus, this region appears black. Such a field can be created by a body of high density and of relatively small mass, equal to or less than that of the Sun, compressed in a very small volume, or else by a body of low density and of very large mass.

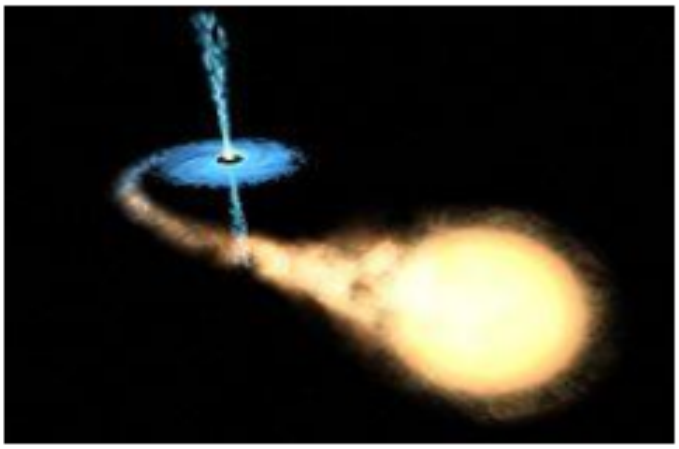

Figure 5.5: A binary system black hole and a star.

A black hole forms from a star when it, at the end of its life, becomes a supernova. Either when its degeneracy pressure, which usually occurs very slowly, can no longer balance the gravitational force proportionally increasing the mass of the nucleus. The latter then goes from about ten thousand degrees to more than 800 million degrees. Its temperature increases more than 80,000 times. When the nucleus is emptied of its energy, gravitation no longer encounters obstacles. The nucleus then begins to compress again, to crush by its own weight. Its gravitational force becomes so strong that the star will not stop at the stage of a neutron star.

Thus the star can only collapse on itself, no more pressure can stop this catastrophic fall. All the mass of the nucleus of the supernova is concentrated in the central point where the density becomes infinite. A black hole is born. The stringy buoy that can be seen circling the black hole is the gaseous remnant of the supernova. This material will eventually be sucked into the black hole. And during the birth of a black hole lets escape along the axis of rotation of the black hole two beams packed with energy: these are the gamma-ray bursts.

- **Supermassive black holes:**

  Supermassive black holes have a mass between a few million and a few billion solar masses. They are found at the center of galaxies and their presence sometimes causes the appearance of jets and X-rays. The nuclei of galaxies which are thus brighter than a simple superposition of stars are then called active nuclei of galaxies (Volonteri, M 2010).

- **Intermediate black holes:**

  Intermediate black holes are newly discovered objects and have a mass between 100 and 10,000 solar masses. In the 1970s, intermediate-mass black holes were thought to form in the cores of globular clusters, but there were no observations to support this hypothesis. Observations in the 2000s showed the existence of ultra-bright X-ray sources. These intermediate black holes could also result from the collapse of population III stars: they are hypothetical populations of very massive stars (thousands of solar masses) which would have formed at the beginning of the Universe, made up of the most lighter: hydrogen or helium (Coleman Miller, M & Colbert, E. 2004).

- **primordial black holes:**

  Primordial black holes, also called micro black holes or quantum black holes, are said to be very small in size. They would have formed during the Big Bang (hence the

name primordial black hole), following the gravitational collapse of small overdensities in the primordial universe (Khlopov, M. Y 2010).

The Neutron star

A neutron star is a star composed primarily of neutrons held together by gravitational forces. Such objects are the compact residue resulting from the gravitational collapse of the core of a massive star when it has exhausted its nuclear fuel, hence their name. This collapse is accompanied by an explosion of the outer layers of the star, which are completely dislocated and returned to the interstellar medium, a phenomenon called supernova. The compact residue is a star only in name: it is no longer the site of nuclear reactions and its structure is radically different from that of an ordinary star. Its density is indeed extraordinarily high, of the order of 1015 grams (or one billion tons) per cubic centimeter, and its mass falls within a very narrow range, around 1.4 times the mass of the Sun, corresponding to what is called the Chandrasekhar mass. This mass occupies a very small volume, with a radius of only about 10 to 20 kilometers. At their birth, neutron stars have a very high rotation speed, several tens of revolutions per second. They also have a very intense magnetic field, up to 10^{11} Tesla. A neutron star located in a binary system can tear material from its companion star and give rise to a pulsed or continuous emission in the field of X and gamma rays. Isolated and without its pulsed emission, a neutron star is much more difficult to detect because only the thermal emission from its surface is possibly detectable (Yakovlev,D & Pethick, C 2004).

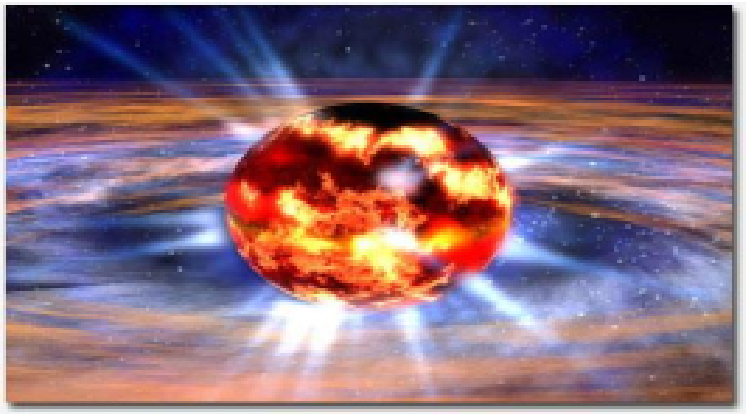

Figure 5.6: The Neutron star.

The white dwarf

A white dwarf, also called a degenerate dwarf, is a remnant of a stellar core composed mostly of electron-degenerate matter. A white dwarf is very dense: its mass is comparable to that of the Sun, while its volume is comparable to that of the Earth. The low luminosity of a white dwarf comes from the emission of stored thermal energy; no fusion takes place in a white dwarf. White dwarfs are thought to be the final evolutionary state of stars that are not high enough in mass to become a neutron star, about 10 solar masses. This includes over 97% of the other stars in the Milky Way (Fontaine, G ;2001).

After the hydrogen-fusion period of a main-sequence star of low or supporting mass ends, such a star will grow to a red giant during which time it melts helium for carbon and oxygen in its nucleus by the triple-alpha process. If a red giant has insufficient mass to generate the core temperatures needed to fuse carbon (about 1 billion K), an inert mass of carbon and oxygen accumulates in its center. Once such a star has shed its outer layers and formed a planetary nebula, it will leave behind a core, which is the remnant of the white dwarf. Usually, white dwarfs are composed of carbon and oxygen (CO white dwarf). If the mass of the progenitor is between 8 and 10.5 solar masses (M $\odot$), the core temperature will be sufficient to fuse carbon but not neon, in which case an oxygen-neon-magnesium white dwarf (ONeMg or ONe) can form. Very low mass stars will not be able to fuse helium, therefore a helium white dwarf can form by loss of mass in binary systems. A white dwarf is very hot when it forms, but since it has no energy source, it will gradually cool down as it radiates its energy. This means that its radiance, which initially has a high color temperature, will decrease and redden over time. Over a very long period, a white dwarf will cool and its matter will begin to crystallize, starting with the core. The star's low temperature means that it will no longer emit significant heat or light and will become a cold black dwarf. Because the time it takes for a white dwarf to reach this state is calculated to be longer than the current age of the universe (about 13.8 billion years).

Figure 5.7: The white dwarf star.

The binary stars

A binary star is a star system made up of two stars orbiting their center of mass. For each star, the other is its companion star. Recent research suggests that a large percentage of stars are part of systems with at least two stars. Binary star systems are very important in astrophysics because observing their mutual orbits allows their mass to be determined. The masses of many individual stars can then be determined by extrapolations made from observed binaries.

Binary stars are not the same as optical double stars, which appear to be close together when viewed from Earth but cannot be held appreciably by gravity. Binary stars can either be distinguished optically (visual binaries) or by indirect techniques, such as spectroscopy. Systems consisting of more than two components, known as multiple stars. Components of binary star systems can exchange mass, bringing their evolution to stages that single stars cannot (Mathieu, R. D 1994).

Classifications by methods of observation

Binary stars are classified into four types according to their observable properties :

Visual binaries

A visual binary star is a binary star for which the angular separation between the two components is large enough to allow them to be observed as a double star in a telescope. The brightness of the two stars is also an important factor, as bright stars are more difficult to separate due to their brightness than dimmer ones are. The brightest star in a visual

binary is the primary star, and the dimmer is considered the secondary (Fleming, T, Gioia, I & Maccacaro 1989).

Spectroscopic binaries

A spectroscopic binary star is a binary star in which the separation between stars is usually very small, and the orbital velocity very high. Unless the plane of the orbit happens to be perpendicular to the line of sight, the orbital velocities will have components in the line of sight and the observed radial velocity of the system varies periodically. In some spectroscopic binaries, spectral lines from both stars are visible and the lines are alternately14 double and single. Such a system is known as a doubled spectroscopic binary (often referred to as "SB2"). In other systems, the spectrum of only one of the stars is seen and the lines in the spectrum periodically shift blue, then red and back. These stars are known as spectroscopic single-lined binaries ("SB1").

Eclipsing binaries

An eclipsing binary star is a binary star in which the orbital plane of the two stars lies so close to the observer's line of sight that the components experience mutual eclipses. In case the binary is also a spectroscopic binary and the parallax of the system is known, the binary is very valuable for stellar analysis.
Eclipsing binaries are variable stars, not because the light of individual components vary, but because of eclipses. The light curve of an eclipsing binary is characterized by periods of nearly constant light, with periodic drops in intensity. If one of the stars is larger than the other, one will be obscured by a total eclipse while the other will be obscured by an annular eclipse.

Astrometric binaries

An astrometric binary star is a binary star for which only one of the component stars can be observed visually. The position of the visible star is detected and measured carefully to have an oscillation, due to the influence of the gravity of its counterpart. Generally, this type of measurement cannot be performed on nearby stars.

Classifications by system configuration

Another classification is based on the distance of stars, relative to their dimensions:

Detached binaries stars

Detached binaries are a kind of binary stars where each component is in its Roche lobe, i.e. the area where the gravitational pull of the star itself is greater than that of the other component. The stars have no major effect on each other, and essentially evolve separately. Most binaries belong to this class.

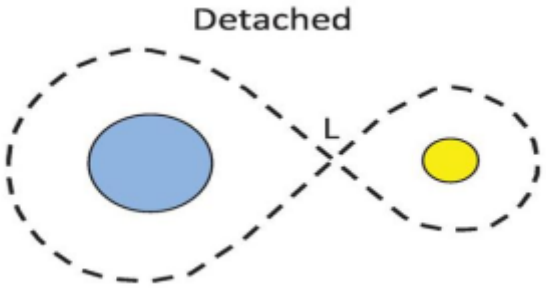

Figure 5.8: Detached binaries stars.

Semi-detached Binary Stars

These are called semi-detached binaries, where one of the rock components fills the lobe of the binary star and the other does not. Gas from the surface of the lobe (donor) Roche filler is transferred to the other, accreting star. Mass transfer dominates the evolution of the system. In many cases, the incoming gas makes an accretion disk around the accretor. Examples of this type are Binary X and Cataclysmic Variable Stars.

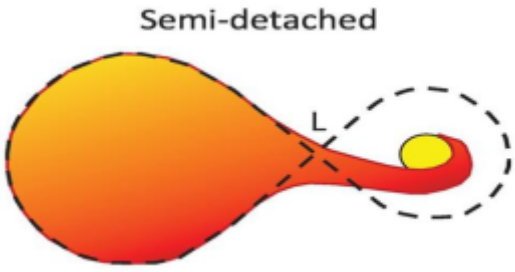

Figure 5.9: Semi-detached Binary Stars.

A contact binary stars

A contact binary is a type of binary star in which both components of the binary fill their Roche lobes. The upper part of the stellar atmospheres forms a common envelope that surrounds the two stars. As the friction of the envelope brakes orbital motion, the stars may eventually merge (Mochnacki, S. W 1981).

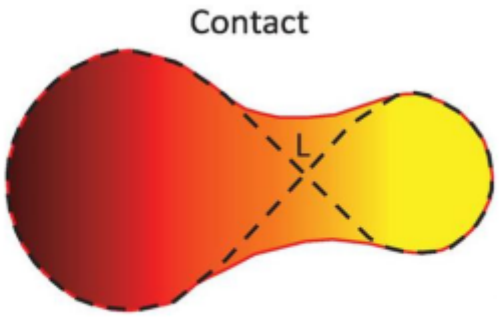

Figure 5.10: A contact binary star.

Keplerian disks

Disks around compact objects (white dwarfs, neutron stars, and black holes) are of particular interest. They are often extremely luminous; indeed, manifested as quasars at the centers of massive galaxies, they are some of the brightest objects in the universe. The dual requirements of copious dissipational heating and outward angular momentum transport suggest that the gas in the disks is highly turbulent.

It is assumed that the disk is very thin and resides in the equatorial plane of the system, as dened by the axis of rotation of the central star, and that the mass (M_*) of the latter is much greater than that of the central. star disk, and therefore the gravitational field $\alpha GM_*/r^2$ For a typical TTauri + disk star system, we have $M_* \approx M_\odot$ and the mass of the disk $\sim 10^{-2}M_\odot$, so the approximation is justifiable. This geometric configuration is illustrated in the following (Figure 1.13) which shows the system (star + disk) seen from the edge.

Assuming a stationary configuration (∂/∂t) and working in cylindrical coordinates (s, φ, z) with the $-z$ axis aligned with the axis of rotation, (in this paragraph s means the same thing as r) we assumes that the fluid elements orbit on circular paths, ie, $u = u_\varphi(s, z)\tilde{e}_\varphi$ and the disk is very thin (in the sense that its thickness h $\ll$ r).

We can formulate the dynamics only in the equatorial plane by assuming invariance in

z in the disk itself, which means that u_φ only depends on s, and $(\partial/\partial t) = 0$. In such a situation the dynamics limit to the s component of Euler's equation, which in the absence of an angular component reduces to an expression of balance between gravity and centrifugal force:

$$\frac{GM_*}{s^2} = \frac{u_\varphi^2}{s} \equiv \Omega_s^2$$

from where we immediately derive the variation of the angular velocity as a function of the cylindrical radius s :

$$\Omega_s = \left(\frac{GM_*}{s^8}\right)^{1/2}, \left[\text{rad}s^{-1}\right]$$

This profile is plotted in the following (figure 1.13) The $s^{-3/2}$ dependence is obviously the one characterizing the Keplerian orbits. A concept that will become important later is that of the radius of corotation, i.e. the radius (r_c) for which the angular speed of rotation of the disk is equal to that of the central star :

$$\Omega\left(r_c\right) = \Omega_* \rightarrow r_c = \left(\frac{GM_*}{\Omega^2}\right)^{1/3}$$

The position of this co-rotation ray is indicated in red on the following (figure 5.1) **(Paul Charbonneau 2015)**. The angular velocity of the disk is $\Omega > \Omega_*$ for $s < r_s$ and conversely $\Omega < \Omega_*$ for $s > r_s$

In general, the central star rotates much more slowly than the edge of the disk with which it makes contact, and the radius of co-rotation is therefore found to be several r^* from the star.

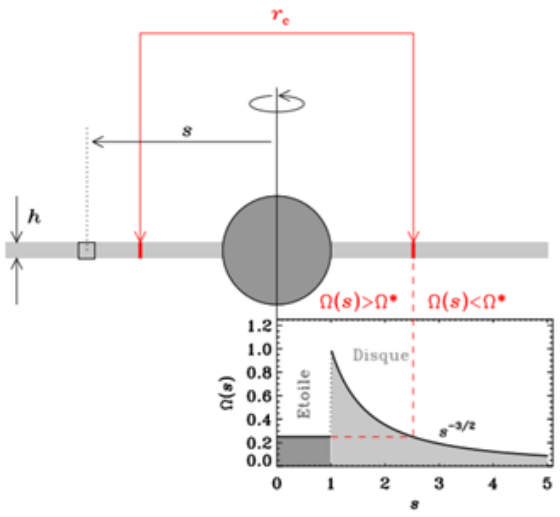

Figure A.1: Geometry of the Keplerian disk, seen here from the edge.

The central star of radius r^* and mass M^* rotates at angular velocity Ω^*. A disk of thickness h occupies the equatorial plane, the rotational speed of the plasma being determined by the balance between gravity and centrifugal force. If the mass of the disk is much smaller than that of the central object, the angular velocity in the disk varies in $s^{-3/2}$. At the co-rotation radius r_c, the angular velocity of the disk is equal to that of the star (red lines).

Appendix B

Conservation of mass equation

$$\frac{\partial \Sigma}{\partial t} + \frac{1}{R}\frac{\partial}{\partial R}(R\Sigma\nu_{_R}) = 0 \qquad (B.1)$$

Conservation of angular momentum equation

$$\frac{\partial}{\partial t}\left(R^2\Omega\Sigma\right) = -\frac{1}{R}\frac{\partial}{\partial R}(R^3\Sigma\nu_{_R}\Omega) + \frac{1}{R}\frac{\partial}{\partial R}(R^3\upsilon\Sigma\frac{\partial\Omega}{\partial R}) \qquad (B.2)$$

The two equations (conservation of mass equation) and (conservation of angular momentum equation) can be combined to give a single equation for the evolution of surface density.

From equation $(B.1)$

$$\frac{\partial \Sigma}{\partial t} = -\frac{1}{R}\frac{\partial}{\partial R}(R\Sigma\nu_{_R})$$

we put

$$h = R^2\Omega = R^2\sqrt{\frac{GM}{R^3}} = \sqrt{GMR}$$

becomes the equation $(B.2)$

$$\frac{\partial}{\partial t}(h\Sigma) = -\frac{1}{R}\frac{\partial}{\partial R}(R\Sigma\nu_{_R}h) + \frac{1}{R}\frac{\partial}{\partial R}(R^3\upsilon\Sigma\frac{\partial\Omega}{\partial R})$$

$$h\frac{\partial\Sigma}{\partial t} = -\frac{1}{R}\left[h\frac{\partial}{\partial R}(R\Sigma\nu_{_R}) + R\Sigma\nu_{_R}\frac{\partial h}{\partial R}\right] - \frac{3\sqrt{GM}}{2R}\frac{\partial}{\partial R}\left(R^3\upsilon\Sigma R^{\frac{-5}{2}}\right)$$

We swear on h

$$\underbrace{\frac{\partial \Sigma}{\partial t}} = \underbrace{-\frac{1}{R}\frac{\partial}{\partial R}\left(R\Sigma\nu_{_R}\right)} - \frac{R\Sigma\nu_{_R}}{Rh}\left(\frac{1}{2}\sqrt{GM}R^{\frac{-1}{2}}\right) - \frac{3\sqrt{GM}}{2hR}\frac{\partial}{\partial R}\left(R^3\upsilon\Sigma R^{-3}R^{\frac{1}{2}}\right)$$

$$\underbrace{\frac{\partial \Sigma}{\partial t} + \frac{1}{R}\frac{\partial}{\partial R}\left(R\Sigma\nu_{_R}\right)} = 0$$

$$0 = -\frac{R\Sigma\nu_{_R}\sqrt{GM}}{2Rh}R^{\frac{-1}{2}} - \frac{3\sqrt{GM}}{2hR}\frac{\partial}{\partial R}\left(\upsilon\Sigma R^{\frac{1}{2}}\right)$$

multiply in$\left(\frac{2Rh}{\sqrt{GM}}\right)$:

$$R\Sigma\nu_{_R}R^{\frac{-1}{2}} = -3\frac{\partial}{\partial R}\left(\upsilon\Sigma R^{\frac{1}{2}}\right)$$

multiply in$\left(\sqrt{R}\right)$:

$$R\Sigma\nu_{_R} = -3\sqrt{R}\frac{\partial}{\partial R}\left(\upsilon\Sigma R^{\frac{1}{2}}\right)$$

We substitute in the equation$(B.1)$:

$$\frac{\partial \Sigma}{\partial t} = -\frac{1}{R}\left(-3\sqrt{R}\frac{\partial}{\partial R}(\upsilon\Sigma R^{\frac{1}{2}})\right)$$

$$\frac{\partial \Sigma}{\partial t} = \frac{3}{R}\left(\sqrt{R}\frac{\partial}{\partial R}(\upsilon\Sigma R^{\frac{1}{2}})\right)$$

Bibliography

[1] Abramowicz, M.A. et al., Astrophysical Journal, 1988, 332, 646 658.

[2] Armijo, M. M., 2012, Accretion disk theory (No. arXiv: 1203.6851).

[3] Armitage, P. J. (2011). Dynamics of protoplanetary disks. Annual Review of Astronomy and Astrophysics, 49, 195-236.

[4] Armitage, P.J. 2010. Astrophysics of Planet Formation, Cambridge, UK: Cambridge University Press. 294 pp.

[5] Asmus, Daniel (2008). Der Innere Rand von Akkretionsscheiben um Schwarze Löcher. MA thesis. Christian-Albrechts-Universität zu Kiel.

[6] Balbus, S. A., & Hawley, J. F.,1991,The Astrophysical Journal, 376, 214-233.

[7] Balbus, S. A., & Hawley, J. F.,1998, 70(1), 1.

[8] Bassi, T.,2020, Accretion and ejection in transient black hole binaries: the case of GRS 1716- 249 (Doctoral dissertation, Université Paul Sabatier-Toulouse III; Università degli studi (Palerme, Italie)).

[9] Beltrán, M. T., & de Wit, W. J.,2016,. The Astronomy and Astrophysics Review, 24(1), 1-68.

[10] Bertout, C., Basri, G., & Bouvier, J., 1988, Astrophysical Journal, 330, 350.

[11] Boley, A. C., Mejía, A. C., Durisen, R. H., Cai, K., Pickett, M. K., & DAlessio, P.,2006, The Astrophysical Journal, 651(1), 517.

[12] Bondi, H., & Hoyle, F.,1944,. Monthly Notices of the Royal Astronomical Society, 104(5), 273- 282.

[13] Brandenburg, A., Nordlund, A., Stein, R. F., & Torkelsson, U.,1995, The Astrophysical Journal, 446, 741.

[14] Cleeves, L. I., Adams, F. C., Bergin, E. A., & Visser, R.,2013, The Astrophysical Journal, 777(1), 28.

[15] Cossins, P., Lodato, G., & Clarke, C. J,2009, Monthly Notices of the Royal Astronomical Society, 393(4),1157-1173.

[16] Cossou, C.,2013, Effet de la structure du disque sur la formation et la migration des DeSouza, A. L., & Basu, S.,2017, 51, 113-121.

[17] Dominik, C.,2015, 102, p. 00002.

[18] Dommanget, J.,1964,. 80, 315.

[19] Dullemond, C. P.,Dominik, C., & Natta,A., 2001, ApJ, 560, 957.

[20] Egron E., 2013, PhD thesis, Universitat di Catania

[21] Elmegreen, B. G.1993,ApJ,419, L29

[22] Fabian, A. C.,1999, 96(9), 4749-4751.35

[23] Fleming, T. A., Gioia, I. M., & Maccacaro, T. (1989). X-ray-selected candidates for the RS CVn and W UMa classes of binary stars. The Astronomical Journal, 98, 692-698.

[24] Fleming, T. A., Gioia, I. M., & Maccacaro, T.,1989,. The Astronomical Journal, 98, 692-698.

[25] Fontaine, G., Brassard, P., & Bergeron, P.,2001, 113(782), 409.

[26] Frank, E. H., & Grodzinsky, A. J.,1987, Journal of biomechanics, 20(6), 629-639.

[27] Frank, M.,2002, 40(1), 1-1. Fromang, S., Terquem, C., & Balbus, S. A.,2002, Monthly Notices of the Royal Astronomical Society, 329(1), 18-28.

[28] Szkody, P., Anderson, S. F., Agüeros, M., Covarrubias, R., Bentz, M., Hawley, S., ... & York, D. G. (2002). Cataclysmic variables from the sloan digital sky survey. I. The first results. The Astronomical Journal, 123(1), 430.

[29] Gammie, C. F.,2001, The Astrophysical Journal, 553(1), 174.

[30] Haisch KE Jr., Lada EA, Lada CJ 2001. Ap. J. Lett. 553:153

[31] Hartmann, L., & Kenyon, S. J.,1996, Annual Review of Astronomy and Astrophysics, 34(1), 207- 240.

[32] Hawley, J. F., Gammie, C. F., & Balbus, S. A.,1996, The Astrophysical Journal, 464, 690.

[33] Hibino, T., Hashimoto, A., Inoue, T., Tokuno, J. I., Yoshida, S. I., & Sano, M.,2000,288(5473), 2031-2033.

[34] Hoyle, F., & Lyttleton, R. A.,1939, 405-415

[35] Igea, J., & Glassgold, A. E. (1999). X-ray ionization of the disks of young stellar objects. The Astrophysical Journal, 518(2), 848.

[36] Jaroszynski, M., Abramowicz, M. A., & Paczynski, B.,1980, Acta Astronomica, 30, 1-34.

[37] Ji, H., & Balbus, S. (2013). Angular momentum transport in astrophysics and in the lab. Physics Today, 66(8), 27-33.

[38] Jung, J.,1971, Astronomy and Astrophysics, 11, 351.

[39] Khlopov, M. Y.,2010, Research in Astronomy and Astrophysics, 10(6), 495.

[40] Klessen, R. S., Heitsch, F., & Mac Low, M.-M. 2000, ApJ, 535, 887

[41] Kotko, I., & Lasota, J. P.,2012, Astronomy & Astrophysics, 545, A115.

[42] Lin, D. N., & Papaloizou, J. (1986). On the tidal interaction between protoplanets and the protoplanetary disk. III-Orbital migration of protoplanets. Astrophysical Journal, Part 1 (ISSN 0004-637X), vol. 309, Oct. 15, 1986, p. 846-857., 309, 846-857.

[43] Lynden-Bell, D., Nature, 1969, 223, 690694.

[44] Lynden-Bell, D., Pringle, J.E, 1974, MNRAS, 168, 603.

[45] Lynden-Bell, D.,2002, Monthly Notices of the Royal Astronomical Society, 334(4), 787-796.

[46] Mac Low, M.-M., & Klessen, R. S. 2003, Rev. Mod. Phys., submitted (astro-ph/0301093)

[47] Mathieu, R. D.,1994, Annual Review of Astronomy and Astrophysics, 32(1), 465-530.

[48] Matthews, J.,2017, Disc Winds Matter: Modelling Accretion and Outflows on All Scales. Springer

[49] Maurya, S. K., Gupta, Y. K., Dayanandan, B., & Ray, S.,2016,. The European Physical Journal C, 76(5), 1-9.

[50] Mayer, P., & Macák, P.,1973, 24, 50.

[51] Mochnacki, S. W.,1981, The Astrophysical Journal, 245, 650-670.

[52] Mora, A., Merín, B., Solano, E., Montesinos, B., De Winter, D., Eiroa, C., ... & Wesselius, P. R.,2001, Astronomy & Astrophysics, 378(1), 116-131.

[53] Narayan, R. & Yi I., L13L16, 1994, The Astrophysical Journal, 428, 1.

[54] Norton, A. A., Charbonneau, P., & Passos, D.,2015, 251-283 .

[55] Ostriker,E. C., Stone,J.M., & Gammie,C. F.2001, ApJ,546, 980

[56] Padoan,P., & Nordlund, A.1999, ApJ,526, 279

[57] Piran, T.,2005, 76(4), 1143.

[58] planètes (Doctoral dissertation, Université Sciences et Technologies-Bordeaux I).

[59] Pringle, J. E., 1981, ARA & A, 19, 137.

[60] Pudritz,R.2002, Science,295,68

[61] Salpeter, E.E., Astrophysical Journal, 1964,140, 796800.

[62] Savcheva, A. S.,2006,. Magnetically torqued thin accretion disks (Doctoral dissertation, Massachusetts Institute of Technology)

[63] Shakura, N. I., Sunyaev, R. A., 1973, A & A, 24, 337-355.

[64] Szkody, P., Anderson, S. F., Agüeros, M., Covarrubias, R., Bentz, M., Hawley, S., ... & York, D.

[65] Toomre, A.,1964, The Astrophysical Journal, 139, 1217-1238.

[66] Volonteri, M.,2010, The Astronomy and Astrophysics Review, 18(3), 279-315. Coleman Miller, M., & Colbert, E. J.,2004, International Journal of Modern Physics D, 13(01), 1-64.

[67] Ward-Thompson,D. 2002,Science,295, 76

[68] Warner, E. J., & Quinn, T. P.,1995, 73(1), 146-153.

[69] Wyatt, M. C.,2008, Astron. Astrophys., 46, 339-383.

[70] Wyatt, M.C., 2008, Annu. Rev. Astron. Astrophys. 46, 339

[71] Yakovlev, D. G., & Pethick, C. J.,2004, Annu. Rev. Astron. Astrophys., 42, 169-210.

[72] Zel'Dovich, Y. B.,1964, Soviet Astronomy, 8, 13.

[73] Zeldovich, Ya.B. & Novikov, I.D., 1967, Sov.Astron.A.J.

[74] Boué, G. (2010). Rotation à long terme des planètes, application au basculement dUranus (Doctoral dissertation, Observatoire de Paris).

[75] Armitage PJ. 2007a. Lecture notes on the formation and early evolution of planetary systems. arXiv:astroph/0701485v1.

[76] Chambers J E. 2004. Planetary accretion in the inner solar system. Earth Planet. Sci.Lett.223:24152.

[77] Raymond, S. N., Izidoro, A., & Morbidelli, A. (2020). Solar system formation in the context of extrasolar planets. Planetary Astrobiology, 287-324.

[78] Armitage, P. J. (2011). Dynamics of protoplanetary disks. Annual Review of Astronomy and Astrophysic5, 49, 195-236.

[79] Sanchez, M A (2021). A Study of Protoplanetary Disk Evolution in Infrared CO.

[80] Armitage, P.J. 2010. Astrophysics of Planet Formation, Cambridge, UK: Cambridge University Press. 294pp.

[81] Draine. Interstellar Dust Grains. ARA & A, 41:241-289, 2003.

[82] Pollack, J. B., Hollenbach, D., Beckwith, S., Simonelli, D. P., Roush, T., & Fong, W. (1994). Composition and radiative properties of grains in molecular clouds and accretion

disks. Astrophysical Journal, Part 1 (ISSN 0004-637X), vol. 421, no. 2, p. 615-639, 421, 615-639.

[83] Kallenbach, W. Benz, and G.W. Lugmair. From dust to terrestrial planets introduction. Space Science Reviews, 92:1-10, 2000.

[84] Pericaud, J. (2016). Des disques proto-planétaires aux disques de débris: étude des disques hybrides: observations dans le domaine millimérrique (Doctoral dissertation, Bordeaux).

[85] Cossou, C. (2013). Effet de la structure du disque sur la formation et la migration des planètes (Doctoral dissertation, Université Sciences et Technologies-Bordeaux I).

[86] Qaddah, B. (2020). Modélisation mumérique de la dynamique et de lévolution thernique dume goutte métallique en chute libre dans un milien visqueux (Doctoral dissertation, Aix-Marseille).

[87] Stevenson, D. J. (1982). Fommation of the giant planets. Planetary and Space Science, 30(8), 755-764.

[88] Dutrey, A 2008, Protoplanetary Disks as seen by Interferometrys, The Power of Optical/IR Interferometry: Recent Scientific Results and 2nd Generation Instrumentation, Eso Astrophysics Symposia, p. 217-226.

[89] ontmerle, T. ; Angereau, J. -C. ; Chaussidon, M ; Gounelle, M. ; Marty, B. ; Morbidelli, A 2006, iFrom Suns to Life: A Chronological Approach to the History of Life on Earth 3. Solar System Formation and Early Evolution: the First 100 Million Yearsn, Earth Moon and Planets 98, p. $39 - 95$.

[90] Papaloizou, J. C. B.; Nelson, R. P.; Kley, W. ; Masset, F. S. ; Artymowicz, P. 2007, wisk-Planet Interactions During Planet Formations in B. Reipurth, D. Jemitt, and K. Keil (eds.), Protostars and Planets V, University of Arizona Press, p. 655-668.

[91] Gomes, $\mathbb{R}$; Levison, H. F.; Tsiganis, K; Morbidelli, A. 2005, Origin of the cataclysmic Late Heavy Bombardment period of the terrestrial planetsn, Nanure, 435, p. $466 - 469$

[92] Tsiganis, K. ; Gomes, R. ; Morbidelli, A. ; Lerison, H. F. 2005, $\approx$ Origin of the orbital architecture of the giant planets of the Solar Systems, Nature, 435, p. 459-461.

[93] Tanaka, T. (2011). Exact time-dependent solutions for the thin accretion disc equation: boundary conditions at finite radius. Monthly Notices of the Royal Astronomical Society, 410(2), 1007-1017

[94] Haisch KE Jr., Lada EA, Lada CJ 2001. Ap. J. Lett. 553:153

[95] R. Kallenbach, W. Benz, and G.W. Lugmair. From dust to terrestrial planets introduction. Space Science Reriews, 92:1-10, 2000.

[96] Weidenschilling, S. J. (2000). Formation of planetesimals and accretion of the terrestrial planets. Space Science Reviews, 92(1-2), 295-310.

[97] Chambers, J. (2010). Terrestrial planet formation. Exoplanets, 1, 297-317.

[98] Rubie, D. C., Nimmo, F., & Melosh, H. J. (2007). Treatise on geophysics. Formation of Earth's Core, 9, 51-90.

[99] Laibe, G., Gonzalez, J. F., Fouchet, L., & Maddison, S. T. (2008). SPH simulations of grain growth in protoplanetary disks. Astronomy & Astrophysics, 487(1), 265-270.

[100] Kokubo, E., & Ida, S. (1995). Orbital evolution of protoplanets embedded in a swarm of planetesimals. Icarus, 114(2), 247-257.

[101] Wetherill, G. W., & Stewart, G. R. (1993). Formation of planetary embryos: Effects of fragmentation, low relative velocity, and independent variation of eccentricity and inclination. Icarus, 106(1), 190-209.

[102] Agnor, C. B., Canup, R. M., & Levison, H. F. (1999). On the character and consequences of large impacts in the late stage of terrestrial planet formation. Icarus, 142(1), 219-237.

[103] Kokubo, E., & Genda, H. (2010). Formation of terrestrial planets from protoplanets under a realistic accretion condition. The Astrophysical Journal Letters, 714(1), L21.

[104] Chambers, J. E., & Wetherill, G. W. (1998). Making the terrestrial planets: N-body integrations of planetary embryos in three dimensions. Icarus, 136(2), 304-327.

[105] Qaddah, J. Monteux, V. Clesi, A.Bouhifd, and M. Le Bars. Dynamics and stability of an iron drop falling in a magma ocean. Phys. Earth Planet. Int., 289:75 - 89, 2019.

[106] Guillot, T., Stevenson, D. J., Hubbard, W. B., & Saumon, D., 2004, Jupiter. The Planet, Satellites and Magnetosphere, 35

List of publications and communications

Publications

1. Belghitar, E. B., Meftah, M. T., and **Malki, Z**. 2021, Ukrainian Journal of Physics, 66(11), 921.

2. Malki, Z.,Meftah, M. T.,Belghitar, E. B.,Korichi, Z., & Benkrima, Y.(2023). Angular momentum transport at a planet in the gaseous protoplanetary disk: a new version of an old model. Tobacco Regulatory Science (TRS), 3320-3330.

Communications

1. **Z**, Malki, E, B, Belghitar , M, T,. Meftah. **Study Planetary migration in protoplanetary disks**. International Seminar on Material Sciences (Physics and Chemistry) online (webinar), organized by Algerian Journal of Engineering, Architecture and Urbanism (AJEAU), period of September 17 and 18, 2021, University of USTO, Bir Djir, Oran Algeria.

2. **Z**, Malki, E, B, Belghitar , M, T,. Meftah. **Study the evolution of the accretion disk: the black hole** . International Seminar on Material Sciences (Physics and Chemistry) online (webinar), organized by Algerian Journal of Engineering, Architecture and Urbanism (AJEAU), period of January 22, 2021, University of USTO, Bir Djir, Oran Algeria.

3. **Z**, Malki, E, B, Belghitar , M, T,. Meftah. .Contribution to study the migration of the protoplanet float in protoplanetary disk. 1st International Conference on Sustainable Energy and Advanced Materials IC-SEAM21 April 21-22, 2021, Ouargla, Algeria.

4. **Z**, Malki, E, B, Belghitar.explosions in binary systems:(a black hole orbiting a secondary star).1st- International conference on Materials Sciences and Applications (ICMSA-2023) 8-9 February 2023, Khenchela, Algeria.

دراسة نظرية لظواهر فيزيائية حول القرص الكوكبي الأولي

ملخص

التراكم هو إحدى العمليات المسؤولة إلى حد كبير عن ظهور معظم الأشياء في الكون. تقريبًا جميع الأجسام الفلكية، من الكواكب والنجوم إلى المجرات بأكملها تشكلت من خلال هذه العملية. بشكل عام، تشكل المادة المتراكمة قرصًا حول جسم مركزي بسبب الحفاظ على الزخم الزاوي للمادة. الهدف الأول من هذا العمل هو دراسة أقراص التراكم وبشكل رئيسي أقراص الكواكب الأولية لأنها تسمح بدراسة عدد كبير من العمليات الفيزيائية التي تحدد تطوره، ويتطور أيضا بسبب اللزوجة وانتقال الزخم الزاوي بواسطة النجم المركزي. والهدف الثاني الرئيسي هو الحصول على الحلول التحليلية لمعادلة تطور قرص كوكبي أولي وكوكب، ومعرفة تأثير الزخم الزاوي على توزيع كثافة السطح دون استخدام أي تقديرات تقريبية له، إنطلاقا من المعادلات الأساسية التي تحكم التطور الزمني للكثافة السطحية لقرص التراكم، وبناءا كذلك على معادلة التطور المشترك للكوكب والقرص الكوكبي الأولي الناتجة عن هجرة الكواكب بسبب تفاعل المد والجزر مع القرص، ويخضع القرص أيضا لعزم دوران المد والجزر من الكوكب. يحتوي الحد الثاني من هذه المعادلة على معدل نقل الزخم الزاوي لكل وحدة كتلة من الكوكب الى القرص. وبتطبيق شروط وتقريبات تحدد سلوك الكثافة السطحية بشكل أوضح بالطريقتين في كل منطقة، نتحصل على الحلول التحليلية للمعادلة تطور قرص كوكبي اولي وكوكب، وكانت النتائج موافقة لنتائج سابقة.

الكلمات المفتاحية: التراكم، القرص الكوكبي الأولي، الكثافة السطحية، الزخم الزاوي.

Etude théorique des phénomènes physiques autour d'un disque proto-planétaire

Résumé

L'accrétion est l'un des processus en grande partie responsables de l'émergence de la plupart des choses dans l'univers. Presque tous les objets astronomiques, des planètes et étoiles aux galaxies entières, ont été formés grâce à ce processus. En général, la matière qui s'accrète forme un disque autour d'un corps central en raison de la conservation du moment cinétique de la matière. Le premier objectif de ce travail est d'étudier les disques d'accrétion, principalement les disques protoplanétaires, car ils permettent d'étudier un grand nombre de processus physiques qui déterminent leur développement, et ils se développent également en raison de la viscosité et du transfert de moment cinétique par l'étoile centrale. Le deuxième objectif principal est d'obtenir des solutions analytiques à l'équation de l'évolution d'un disque protoplanétaire et d'une planète, et de connaître l'effet du moment cinétique sur la distribution de la densité de surface sans utiliser aucune approximation, sur la base des équations de base qui régissent l'évolution temporelle de la densité surfacique du disque d'accrétion, et également basée sur l'équation de la co-évolution de la planète et du disque. Formation protoplanétaire résultant de la migration des planètes due à l'interaction des marées avec le disque, et le disque est également soumis au couple de marée de la planète. Le deuxième terme de cette équation contient le taux de transfert du moment cinétique par unité de masse de la planète au disque. En appliquant des conditions et des approximations qui déterminent plus clairement le comportement de la densité de surface dans les deux méthodes dans chaque région, nous obtenons des solutions analytiques à l'équation de l'évolution d'un disque protoplanétaire et d'une planète, et les résultats étaient cohérents avec les résultats précédents.

Mots-clés : accrétion, disque protoplanétaire, densité surfacique, moment cinétique.